2004

Alternating current potential drop and eddy current methods for nondestructive evaluation of case depth

Yongqiang Huang
Iowa State University

Alternating current potential drop and eddy current methods for nondestructive evaluation of case depth

by

Yongqiang Huang

A dissertation submitted to the graduate faculty

in partial fulfillment of the requirements for the degree of

DOCTOR OF PHILOSOPHY

Major: Electrical Engineering (Electromagnetics)

Program of Study Committee:
John Bowler, Major Professor
Nicola Bowler
Douglas Jacobson
Marcus Johnson
Ronald Roberts
Jiming Song

Iowa State University

Ames, Iowa

2004

Graduate College
Iowa State University

This is to certify that the doctoral dissertation of

Yongqiang Huang

has met the dissertation requirements of Iowa State University

Signature was redacted for privacy.

Major Professor

Signature was redacted for privacy.

For the Major Program

TABLE OF CONTENTS

LIST OF TABLES

LIST OF FIGURES

ABSTRACT

Case hardening treatments offer a means of enhancing the strength and wear properties of parts made from steels. Generally applied to near-finished components, the processes impart a high-hardness wear-resistant surface which, with sufficient depth, can also improve fatigue strength. Applications range from simple mild steel pressings to heavy-duty alloy-steel transmission components. The characteristics of case hardening are the surface hardness, effective case depth, and depth profile of the residual stress. The specified case depth varies for different applications. It is useful to be able to measure the case depth nondestructively to ensure the specification is met.

In the work outlined in this dissertation, the aim is to evaluate the properties of case hardened parts nondestructively. The case hardening process produces a change in the electromagnetic properties of the steel components in the near surface region. Consequently, the electrical conductivity and magnetic permeability have different values near the surface compared with those of the substrate. It is assumed that the conductivity and permeability variation with depth is indicative of the hardness profile allowing the case depth to be estimated from electromagnetic measurements. A two-layer model is adopted to approximate the case hardened steel parts as a homogeneous substrate layer surrounded by a homogeneous surface layer with uniform thickness. Alternating current potential drop (ACPD) theoretical calculations have been performed and compared with experimental measurements for both case hardened cylindrical rods and homogeneous metal plates. Driver and pick-up coils have been used for eddy current induction measurements on the cylindrical rod specimens. The multi-frequency measurement data are used to estimate the case depth by model-based inversion. The measured case depth is in reasonable agreement with the effective case depth from the measured hardness profile.

Excellent agreement is observed between the measurement data and the theoretical calculation on homogeneous metal plates.

CHAPTER 1. INTRODUCTION OF CASE DEPTH

1.1 Case Hardening Treatment

What is case hardening? The American Heritage Dictionary of the English Language (Fourth Edition, 2000) gives the following definition "To harden the surface or case of iron or steel by high-temperature shallow infusion of carbon followed by quenching". Carbon and/or other elements are added to the surface of low-carbon steels or iron so that upon quenching a hardened case or surface is obtained. The center of the steel remains soft or ductile throughout the hardening process.

Case hardening processes include carburizing, nitriding, carbonitriding, cyaniding, induction and flame hardening. For each of these methods, chemical composition, mechanical properties, or both are changed.

Carburizing is a case hardening process in which carbon is dissolved in the surface layers of a low-carbon steel part at a temperature (850 to 950 C) sufficient to render the steel austenitic, followed by quenching and tempering to form a martensitic microstructure. The resulting gradient in carbon content below the surface of the part causes a gradient in hardness, producing a strong, wear-resistant surface layer on a material, usually low-carbon steel, which is readily fabricated into parts. Carburizing steels for case hardening usually have base carbon contents of about 0.2%, with the carbon content of the carburized layer generally being controlled at between 0.8 and 1%. However, surface carbon is often limited to 0.9% because too high a carbon content can result in retained austenite and brittle martensite.

Nitriding is a surface-hardening heat treatment that introduces nitrogen into the surface of steel at a temperature range (500 to 550 C), while it is in the ferrite condition. Nitriding is similar to carburizing in that surface composition is altered, but different in that nitrogen is added

into ferrite instead of austenite. Because nitriding does not involve heating into the austenite phase field and a subsequent quench to form martensite, nitriding can be accomplished with a minimum of distortion and with excellent dimensional control.

Carbonitriding is a modified form of gas carburizing, rather than a form of nitriding. The modification consists of introducing ammonia into the gas carburizing atmosphere to add nitrogen to the carburized case as it is being produced. Nascent nitrogen forms at the work surface by the dissociation of ammonia in the furnace atmosphere; the nitrogen diffuses into the steel simultaneously with carbon. Typically, carbonitriding is carried out at a lower temperature and for a shorter time than is gas carburizing, producing a shallower case than is usual in production carburizing.

Cyaniding process heats ferrous materials above the transformation temperature in a molten salt bath containing cyanide. The absorption of both carbon and nitrogen at the surface also produces a gradient in from the surface. Subsequent cooling is specified to produce the required hard, wear-resistant properties. The cyaniding method is being replaced by carbonitriding for two reasons. The first reason is that disposal of cyanide salts is difficult. The second reason is that it is difficult to remove residual salts from cyanide-hardened workpieces, especially those of intricate design.

Induction hardening is a widely used process for the surface hardening of steel. The components are heated by means of an alternating magnetic field to a temperature within or above the transformation range followed by immediate quenching. The core of the component remains unaffected by the treatment and its physical properties are those of the bar from which it was machined, whilst the hardness of the case can be within the range 37–58 HRC. Carbon and alloy steels with a carbon content in the range 0.40–0.45% are most suitable for this process.

Flame hardening is a surface hardening process in which heat is applied by a high temperature flame followed by quenching jets of water. It is usually applied to medium to large size components such as large gears, sprockets, slide ways of machine tools, bearing surfaces of shafts and axles, etc. Steels most suited have a carbon content within the range 0.40–0.55%.

It should be noted that maximum hardness of a case hardened part is not maintained

throughout the full depth of the case. Part-way through the case, hardness begins to reduce progressively until it reaches the core hardness. It is therefore important not to grind a case hardened part excessively, otherwise the resulting surface hardness and strength will be significantly diminished.

1.2 Case Depth Measurement

Precise estimation of case depth is essential for quality control of the case hardening process and for evaluation of parts for conformance with specifications.

It is necessary to distinguish between effective case depth and total case depth. Effective case depth is the perpendicular distance from the surface of a hardened case to the deepest point at which a specified level of hardness is reached. The hardness criterion, except when otherwise specified in the Table 1.1, is 50 HRC [1]. The Rockwell hardness number is followed by the symbol HR and the scale designation. 50 HRC represents a Rockwell hardness number of 50 on the Rockwell C scale. The Rockwell hardness test is one of several common indentation hardness tests used today. To accommodate the testing of diverse products, several different indenter types were developed for the Rockwell hardness test to be used in conjunction with a range of standard force levels. Each combination of indenter type and applied force levels has been designated as a distinct Rockwell hardness scale. The ASTM defines thirty different Rockwell scales [5]. Total case depth is the perpendicular distance from the surface of a hardened case to the point at which differences in chemical or physical properties of the case and core can no longer be distinguished. The effective case depth is typically about two-thirds to three-quarters the total case depth.

Table 1.1 Effective case depth hardness criterion

Carbon Content	Effective Case Depth Hardness
0.28–0.32% C	35 HRC
0.33–0.42% C	40 HRC
0.43–0.52% C	45 HRC
0.53% and over	50 HRC

The methods used for measuring case depth are chemical, mechanical, visual, and nondestructive. Among the various methods for measuring case depth, each procedure has its own primary application area, and no single method is good for all purposes. The variation in case depth as determined by the different methods can be extensive. Some of the factors that affect case depth measurement are case characteristics, steel composition, and quenching conditions. The chemical method is considered to be the most accurate method of measuring total case depth. The mechanical method is the most widely used and is considered the most accurate method of measuring effective case depth. [1–5].

1.3 Problem Statement

Thermal processing is a major part of manufacturing process in a wide range of industries, including automotive, power generation and aerospace, to improve part properties such as wear resistance and fracture toughness. Metal surfaces, such as those on gears, cams and axels, wear in service when they rub against other hard surfaces. Surface hardening improves strength and resistance to wear and extends part life. Often, only specific areas need to be hardened. Surface hardening, such as case hardening, produces a hard surface to certain depth, while the core remains softer.

One of the testing methods used to determine whether a part has been properly heat treated is the hardness test, which can be destructive in nature if a part has to be sectioned to measure hardness or if it cannot tolerate any surface imperfections; i. e. , the indentation from the hardness test. Hardness tests also can be time consuming with respect to testing in the lab and providing feedback of the results. A test that is fast, cheap and nondestructive is preferable.

Estimates of case depth can be made using ultrasonic time-of-flight measurements [27–35]. These rely on reflections from the transition zone between the case hardened layer and the core. Multi-frequency eddy current methods have also been used to determine case depth and, in addition, they can give estimates of hardness [46–52]. The usual technique relies on measuring eddy current probe signals first on a sample batch with known properties whose

pretreatment properties are similar to those of the test samples. The batch data is used to establish a statistical correlation between eddy current signals and the post treatment material properties. These are then used to estimate the properties of an unknown sample.

This work presently being conducted here attempts to get around the need for a sample batch of known properties by matching probe signal measurements with model predictions and deducing the material parameters directly.

1.4 Scope of the Dissertation

This dissertation deals with the nondestructive evaluation of case depth using alternating current potential drop and eddy current methods. Chapter 2 introduces the different potential drop methods and reviews some existing nondestructive evaluation methods of case depth measurement. Chapter 3 discusses the alternating current potential drop (ACPD) method on case hardened cylindrical steel rods. Chapter 4 shows some eddy current measurements on case hardened cylindrical steel rods. Chapter 5 presents the ACPD method on homogeneous metal plates. Chapter 6 gives some concluding remarks and identifies some areas for future research activity.

CHAPTER 2. REVIEW OF POTENTIAL DROP METHODS AND NDE OF CASE DEPTH

Nondestructive methods of measuring case depth make use of the changing mechanical and/or electrical and magnetic properties of the material through the depth of a case hardened part. These property changes come from the differences of material microstructure, hardness and/or chemical components within the case hardened piece. Eddy current and ultrasonic tests are the most frequently used nondestructive tests. Potential drop methods are usually applied on crack problem. Extensive research on surface crack problem using potential drop were done in the past twenty years. Its application to case depth measurement is completely new.

2.1 Potential Drop Methods

Potential drop techniques are based on the measurement of voltage (potential drop) along the surface of a metallic conductor which has an electrical current passing through it. The potential drop measurement depends upon the electrical resistance between the measuring points. The electrical resistance is determined by the specimen conductivity, permeability, geometry, dimensions and the working frequency. Sometimes the term "potential difference" is used instead of "potential drop".

As metallic materials have low electrical resistance, some variants of the technique need to employ relatively high currents (up to 30–40 amps) and even with these, the resultant potentials may be only in the nanovolt region. In this case, preamplification is required. However the absolute values of the current and potential are not generally used. In which case the relative changes in the potential drop are more relevant.

The two most popular potential drop methods are the direct current potential drop (DCPD) and alternating current potential drop (ACPD). Both of them have gained wide acceptance as reliable, economic and precise crack measurement methods. Alternating current field measurement (ACFM) is the non-contact form of ACPD.

2.1.1 Direct Current Potential Drop

Direct current potential drop [6, 7] is the traditional method, which uses a high DC current (30–50 amps). It has the advantage of being relatively simple, but requires heavy cabling and contacts, and results in specimen heating due to the large current. The latter requires compensation when conducting high temperature tests (which is not difficult as specimen thermocouples can be used to control furnace temperature), but sometimes precludes its use for ambient temperature test.

2.1.2 Pulsed Direct Current Potential Drop

Pulsed direct current potential drop [8, 9] is very similar to the direct current potential drop method, but the current is only applied when a potential measurement is being taken. This means that there is no specimen heating problem and this method gives an improved noise performance over continuous direct current measurement.

2.1.3 Alternating Current Potential Drop

The Alternating current potential drop method [10–13] is based on the 'skin effect', a characteristic of high frequency current flowing in a conductive material, whereby the majority of the current is confined to a thin skin at the surface of the material. The skin depth δ is shown in equation (2.1).

$$\delta = \frac{1}{\sqrt{\pi f \sigma \mu_r \mu_0}} \tag{2.1}$$

where σ is the electrical conductivity of the material, μ_r is its relative permeability, μ_0 is the permeability of free space, and f is the frequency of the applied alternating current. Materials

of high permeability or conductivity have relatively small skin depths. For the same material, its skin depth will decrease when the working frequency increases.

The alternating current potential drop method has some disadvantages but many advantages over direct current potential drop method. The current is confined to the surface layers of the specimen (the so-called 'skin effect'), which means that a much lower current (typically one amp) is required. The sensitivity is greater than with the direct current method. Different working frequencies (which affects the skin depth) can be selected for different materials.

The disadvantages are that it is a far more complex piece of equipment than the traditional direct current apparatus and does suffer from inductive pick up (which direct current does not). This means that great care must be taken in positioning the current input and measurement leads. Connections must be robust, as movement of connections during a test may change the results. Other precautions include twisting together the input and output leads of each pair of current and potential drop measurement cables, and minimizing the loop area enclosed by both the current and voltage leads, to reduce the magnitude of any inductive pick up.

2.1.4 Alternating Current Field Measurement

The alternating current field measurement (ACFM) [10–14] technique was developed during the 1980s from the ACPD technique to combine the ability of ACPD to size without calibration with the ability of eddy current techniques to work without electrical contact. This is achieved by inducing a locally uniform AC field in the target material and measuring the magnetic fields above the specimen. The uniform current flow can be modelled analytically, thus making the field response predictable and allowing characterization and sizing of defects. ACFM technique measures the magnetic field perturbations associated with the electrical field perturbations induced by the presence of a flaw. ACFM technique is easier to deploy than ACPD but the signals are something harder to interpret.

2.1.5 ACPD Method on Crack Problem

The alternating current potential drop method was used extensively to detect and characterize surface cracks [15–25]. Suppose an infinite plate contains an infinitely long surface crack of uniform depth. The current connections are placed across the crack and the current flow is perpendicular to the plane of the crack. The probe is aligned to the line connecting the two current connection points. If the distance between the two current connection points is large compared with the crack depth and the measurement area dimensions, the potential gradient is constant within the measurement area. The measured voltage is solely dependent on the path length between the probe tips. The crack depth can be estimated by comparing the voltage measured off and on the crack. The calculation equation for the crack depth is very simple:

$$\frac{V_0}{l} = \frac{V_1}{l + 2d} \tag{2.2}$$

or

$$d = \left(\frac{V_1}{V_0} - 1\right)\frac{l}{2} \tag{2.3}$$

where l is the distance between the two probe tips, d is the crack depth, V_0 and V_1 are the voltage measured off and on the crack. This method is shown in Figure 2.1.

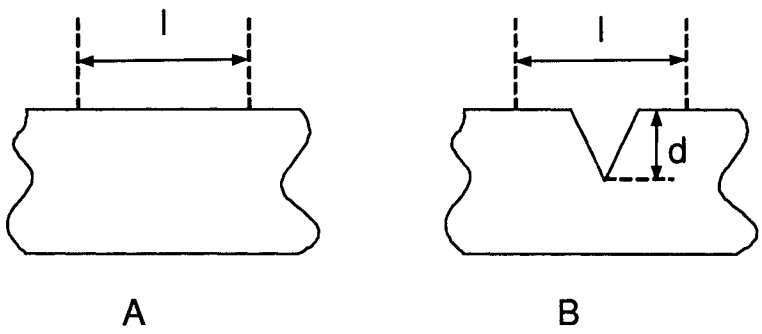

Figure 2.1 The ACPD method on crack measurement. Part A is uncracked body. Part B is cracked body.

This method does not require any prior calibration. It has four points in the measurement system, two points for the alternating current connection, two points for the voltage mea-

surement probe. It is most important in practice to arrange for the field to be as uniform as possible.

Commercial instrument from Matelect is available for ACPD crack measurement [26]. The Matprobe-2 is an advanced crack depth measurement probe comprising a brass and stainless steel body that contains all the necessary contacts to pass both the current and monitor the resultant ACPD. Four spring loaded pins form the contacts. Its principle of operation is exactly what is described above. In order to obtain a meaningful value of crack depth it is necessary to obtain both a value of the ACPD on a non cracked area and the value over a crack. It is assumed that the AC current is largely confined to the surface of the specimen, then the ACPD measured will be proportional to the path length between the probes. Cracks act to increase the path length and a simple subtraction of the two results obtained will yield a value proportional to the crack depth.

2.2 NDE of Case Depth

Case hardening improves both the wear resistance and the fatigue strength of parts under dynamic and/or thermal stresses. The characteristics of case hardening are primarily determined by surface hardness, the effective case depth, and the depth profile of the residual stress.

Case depth, or the thickness of the case hardened layer, is an essential quality attribute of the case hardening process. Using destructive testing methods [1, 3], the quality of the case hardening process can only be evaluated by random sampling, which are expensive and time consuming. It is preferable that a test is fast, cheap and nondestructive. This is not a completely new problem. There are some NDE methods for case depth measurement and some commercial equipment is available as discussed below.

2.2.1 Ultrasonic Method

The ultrasonic backscattering method [27–30] is used to monitor and analyze the effective depth of hardening results. The backscattered ultrasonic amplitude depends on the actual gradient of the microstructure. In the transition area, grain boundaries, grain size, and second

phases are areas where the acoustic impedance value is changed discontinuously, depending on the ultrasonic frequency. If case hardening changes the grain and secondary phase structure, different backscattering signals in the hardened and the bulk material occur. These amplitude characteristics can be used to evaluate the case depth by using simple time-of-flight measurements.

The Ultrasonic Microstructural Analyzer (UMA) made by Sonix Inc. uses a high frequency (10MHz to 25MHz) ultrasonic wave to nondestructively analyze the subsurface microstructure of a component to measure hardness depth of heat treated steel components or particle distribution uniformly of metal matrix composites. It makes measurements without the need for surface preparation and performs the test on induction hardened cylindrically shaped steel parts [31–35]. In 1994 the UMA was chosen as one of the world's top 100 technologies by R&D magazine.

2.2.2 Electromagnetic Methods

Electromagnetic nondestructive evaluation of case depth is based on variations in electrical and magnetic properties in the case hardened workpiece. The electromagnetic properties include electrical conductivity and magnetic permeability, and are related to the structural and mechanical properties of the materials. The case depth can be assessed from electromagnetic measurements results [36].

When a ferromagnetic material is subjected to a varying magnetic field, the discrete changes in the magnetic flux density induce voltage pulses in a pick up coil. This phenomenon, called magnetic Barkhausen emission (MBE), is attributed to the irreversible movement of magnetic domain walls overcoming the obstacles in their path during magnetization [36]. MBE is highly sensitive to microstructurual variations. It is used to measure case depth [37–39].

3MA instruments (Micromagnetic, Multiparameter, Microstructure and Stress Analyzer) [30] measure elastic, electrical and magnetic material properties with one sensor in an industrial environment. It makes use of eddy current, Barkhausen noise, time signal of tangential magnetic field strength and incremental permeability. These multi-parameter characteristics

allow intelligent signal processing. Multi-parameter least square analysis is applied to achieve the best correlation between 3MA parameters and material properties. The method requires a preparatory calibration procedure on parts with known hardness and case depth. Quantitative hardness and case depth values can be got very quickly.

With the magneto-inductive method, it is possible to investigate the core and surface selectively by varying the frequency. The magneto-inductive response depends on the electrical and magnetic properties of the tested material. The magneto-inductive test method was used for nondestructive identification checking, control of case depth, tensile strength or hardness [40, 41]. The MAGNATEST $S3.625$ from Foerster Instruments is one commercial instrument in the field of magneto-inductive testing [42].

2.2.3 Eddy Current Method

Eddy current testing is one of the techniques used to perform electromagnetic inspection. Eddy current testing is used to inspect a wide range of ferrous and non-ferrous material for defects or deterioration without damaging the material [43–45]. The eddy current testing technique is based on inducing electron flow (eddy currents) in electrically conductive material. Any defect in the material such as cracks, pitting, wall loss, or other discontinuities disrupts the flow of the eddy currents. Higher frequency signals are used to detect near-surface flaws; lower frequencies are used when deeper, subsurface flaw detection is required.

Eddy current testing uses the change in magnetic permeability and electrical conductivity as the basis for producing a measurable output and so any part characteristic that depends on these quantities can be identified. Eddy current testing can be used to detect surface and near surface flaws, differences in metal chemical composition and heat treatment, hardness, case hardness depth and residual stress. Other testing techniques can be used to measure these characteristics individually. Eddy current testing can be used to measure all of them.

Eddy current systems are commonly used for case depth measurements and are known to be reliable for many applications [46–52]. Commercial eddy current testing instruments for case depth measurements are available from Verimation Technology [53], SmartEddy Systems

[54], Zetec [55] and Magnetic Inspection Laboratory [56].

In Dr. John Bowler's research group, eddy current method was used to measure case depth of cylindrical steel rods [57, 58]. Alternating current potential drop method is also used to make case depth measurements. It is the main topic of this dissertation.

CHAPTER 3. ACPD METHOD ON CASE HARDENED CYLINDRICAL STEEL RODS

3.1 Introduction

Steel components are often subjected to the case hardening process in order to improve their resistance to wear. The case hardened layer depth varies for different applications, and it is useful to measure the thickness of this layer nondestructively to ensure the specification is met.

The ACPD method is based on the 'skin effect', a characteristic of high frequency current flowing in a ferromagnetic material, whereby the majority of the current is confined to a thin skin at the surface of the material. The skin depth is calculated using equation (2.1). For low frequency AC current, the skin depth is bigger than the case hardened layer depth, such that the measured potential drop is dependent on both case hardened layer and substrate layer parameters. When the frequency is high, its skin depth is smaller than case hardened layer depth. The measured potential drop is then mainly dependent on the surface layer properties.

3.2 Theoretical Model

The case hardening process produces a change in the electromagnetic properties of the steel rod in the near surface region. Consequently, the electrical conductivity and magnetic permeability have different values near the surface compared with those of the substrate. It is assumed that the conductivity and permeability variation with depth is indicative of the hardness profile allowing the depth of the case hardened region to be estimated from electromagnetic measurements. The material properties can be evaluated by data fitting between

experimental measurement data and the predictions from an appropriate theoretical model.

It is assumed that the cylindrical rod is uniform in the axial direction. The cross section of the steel rod is shown in Figure 3.1. The outside ring (region 3) is the case hardened layer. The inside area (region 1) is the core layer. The middle ring (region 2) is located between the case hardened layer and the core layer. It is the transition layer. It should be noted that maximum hardness of a case hardened part is not maintained throughout the full depth of the case. Part way through the case, hardness begins to reduce progressively until it reaches the core hardness (Figure 3.2) [59]. The thickness of the transition layer is dependent on the hardness profile. It is thick if the hardness changes slowly. It is thin if the hardness changes very quickly.

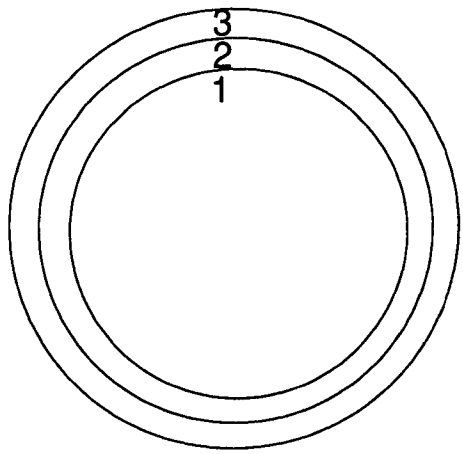

Figure 3.1 Cross section of the cylindrical steel rod

In the hardness measurements, the effective case depth of the case hardened layer is determined from the hardness profile (Figure 3.2). Considering the carbon content of the steel rod, one hardness number is selected to calculate the case depth. Usually this point is located on the transition region in the hardness profile.

Obviously the theory models are simple if the component has an elementary geometry and simplifying assumptions are made concerning the nature of the case hardened layer. It is assumed that surface case hardened layer is homogeneous and has uniform thickness in the

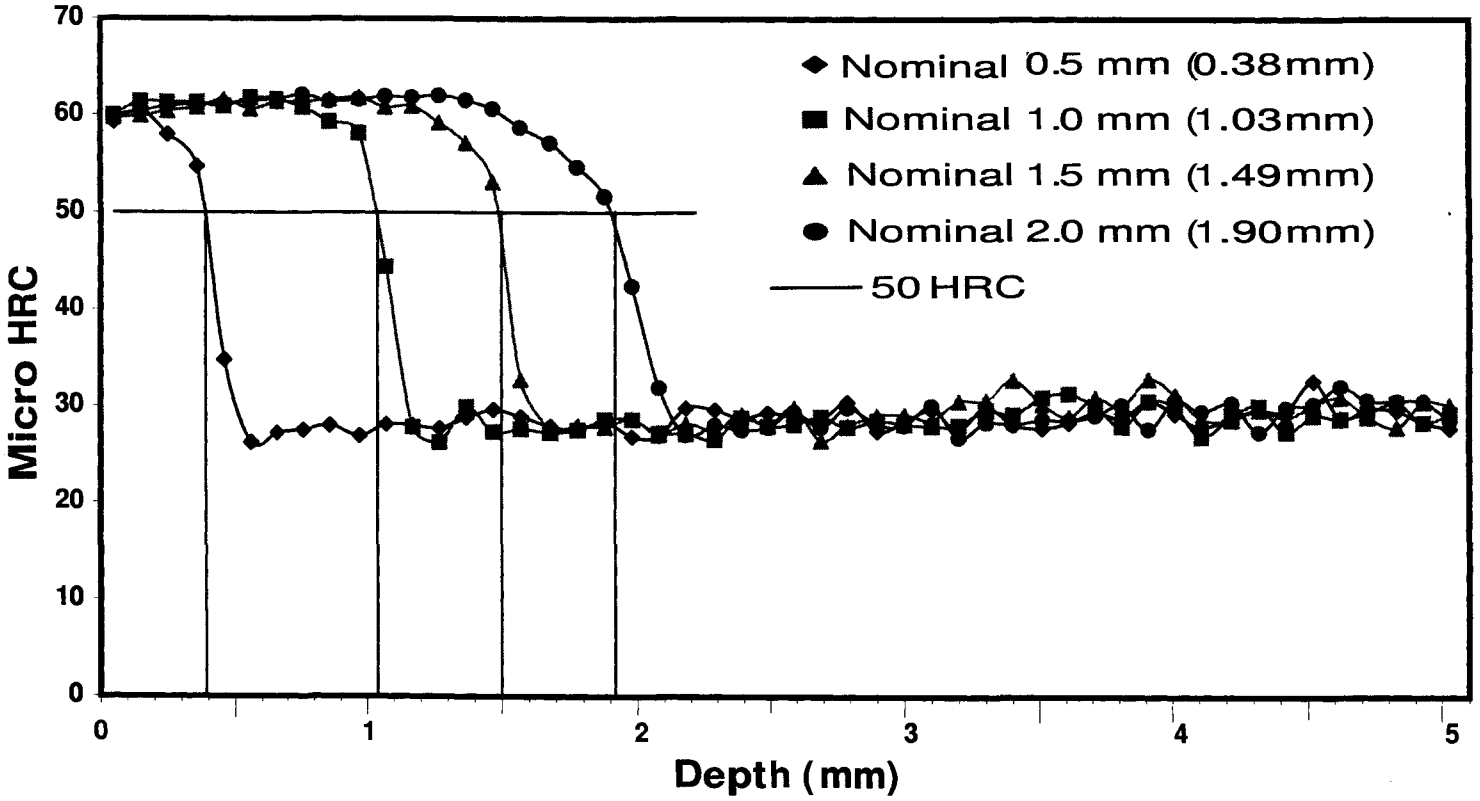
Micro HRC
70
60
50
40
30
20
10
0
0
1
2
3
4
5
Depth (mm)
Nominal 0.5 mm (0.38mm)
Nominal 1.0 mm (1.03mm)
Nominal 1.5 mm (1.49mm)
Nominal 2.0 mm (1.90mm)
50 HRC

radial direction. The core layer is homogeneous. There is no transition zone between these two layers (Figure 3.3). There are five unknown rod parameters for this model: the substrate

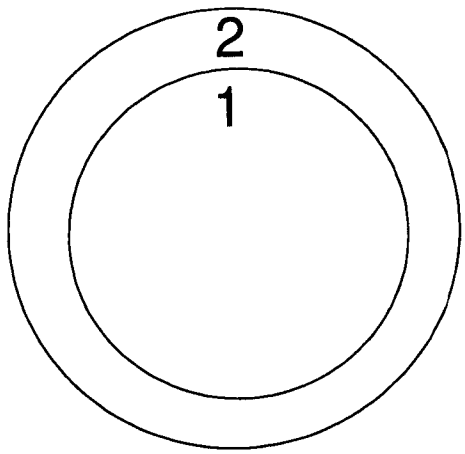

Figure 3.3 Cross section of the idealized case hardened cylindrical steel rod

layer conductivity σ_1 and relative permeability μ_1, the surface layer conductivity σ_2 and relative permeability μ_2 and its layer depth d. By using this idealized case hardened rod, the objective is to estimate the five unknown model parameters from alternating current potential drop measurements. These five unknown parameters are determined using model-based inversion.

It is assumed that the process of case hardening does not modify the material properties below the case hardened layer. In other words, the conductivity σ_1 and permeability μ_1 of the substrate layer of a case harden treated steel rod are the same as those of an untreated steel rod. These five unknown model parameters are determined separately in two steps. The substrate layer conductivity σ_1 and permeability μ_1 are found from the untreated steel rod measurements. The surface layer conductivity σ_2, permeability μ_2 and its layer depth d are then estimated from case hardened steel rod measurements.

3.3 Theory

ACPD theory has been developed for the cylindrical rods [60]. A homogeneous cylindrical rod is considered first. Its results are extended to the case hardened steel rods. The theory for

cylindrical rod is described in detail in the Appendix C.

3.4 Experiment

3.4.1 ACPD Rod Measurement System Description

A schematic diagram of the experimental arrangement for ACPD measurements on the cylindrical steel rods is shown in Figure 3.4.

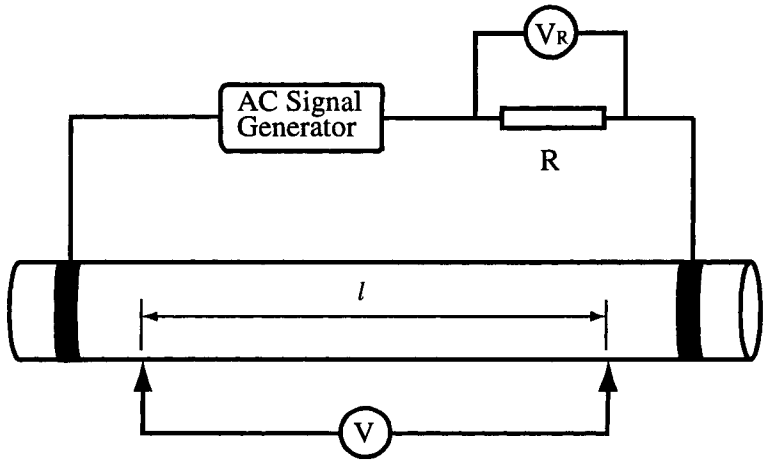

Figure 3.4 Schematic diagram of the ACPD measurement system

The alternating current is injected into the cylindrical rod by the AC signal generator. It is one KEPCO bipolar operational power supply/amplifier. Its model number is BOP 36-12M. The working frequency and amplitude of the AC current is controlled by an AC signal generator. This AC signal comes from the internal function generator inside the SR830 DSP lock-in amplifier. The control sinusoidal signal is connected to the current programming input of the power supply. The amplitude of this AC source signal controls the output current magnitude from the power supply. The output current has the same frequency and phase as the AC input signal. The power supply works as a current drive source. It provides constant current to the cylindrical rod. From the measurement data, the current is almost kept constant for the majority of the working frequencies but decreases at high frequencies.

The current is injected into the cylindrical rod through one copper loop. One end of the rod is slid into the copper loop. Then the copper loop is kept in tight contact with the rod surface by using one hose clip. Another copper loop is used to take the current out from the rod at the other end. The copper loops are used for current injection and extraction for the purpose of full surface contact with the cylindrical rods. It is to make the current distribution uniform and symmetric in the axial direction.

A high precision resistor is connected to the rod AC circuit serially to monitor the current. This resistor has 1% accuracy resistance value within the whole ACPD measurement frequency range. By measuring the voltage across the resistor, the current can be detected. The high precision resistor is designed specially for current detection with the four connection pins. Two current connection pins are located outside. Two voltage measurement pins are located inside. The voltage is measured by the SR830 DSP lock-in amplifier.

Two GSS-8-7-G probes from Interconnect Devices Inc. are used to get potential drop along the cylindrical rod. The probe is spring loaded. Its plunger is made of beryllium copper, gold plated over nickel. The probes keep point contact with the measurement rod. Very thin (36 AWG, American Wire Gauge standard, 0.13 mm diameter) copper wire is soldered to the head of the probe. Two copper wires are used to connect the two probes separately. They are drawn to the middle point of the two probe head points then are twisted together. The gap between the thin copper wire and the cylindrical rod surface is very small. This kind of arrangement is designed to keep the self inductance of the potential drop measurement circuit as small as possible. The potential drop between these two probes is measured by the SR830 DSP lock-in amplifier. Lock-in amplifiers are used to detect and measure very small AC signals (all the way down to a few nanovolts). Lock-in amplifiers use a technique known as phase-sensitive detection to single out the component of the signal at specific reference frequency and phase. Noise signals at frequencies other than the reference frequency are rejected and do not affect the measurement.

A simple rod holder system has been designed and made for the ACPD rod measurement. It is made of plexiglas. It is completely transparent in one direction. The potential drop probes

are held in the bottom horizontal plastic stripe. The bottom stripe is fixed to the two vertical support stripes of the holder system. The wire connection for the potential drop probes is also fixed to the bottom horizontal stripe. The top horizontal plastic stripe is mounted to the two vertical support stripes. The top stripe is flexible to open and close. It is very easy and convenient to change the measured rod by taking off the top stripe. Plastic machine screws are used to put four stripes (one top, one bottom and two sides) together. The two current injection and extraction copper loops are kept outside of the rod holder system. The measured rod is a little bit longer than the rod holder system. So the two ends of the rod are extended to the outside of the holder system. In such way the system dimension parameters are unchanged from one rod to other rod measurement.

There is one lock-in amplifier, but two voltage signals must be measured. One simple computer controlled switch is used to solve this problem. It is put just before the signal input connectors of the lock-in amplifier. For one fixed frequency, the voltage across the precision resistor is measured first. Then the switch changes its connection so that the potential drop voltage along the rod can be measured. The working frequency and all other system conditions are kept unchanged when the switch changes its connection from one voltage signal to the other. The control signal to the switch circuit is from the auxiliary analog output of the lock-in amplifier. Its output voltage can be from -10 to 10 Volt. The maximum current output is 10 mA. The working current of the electrical relay is about 75 mA. So a simple transistor amplifier circuit is used to drive the relay. A separate DC power supply is used to provide the working current to the relay.

The sinusoidal signal is from the internal function generator of the lock-in amplifier. It can provide sinusoidal output with variable amplitude and frequency. The frequency range is from 0.001 Hz to 102 kHz. The actual ACPD measurement frequency is from 1 Hz to 10 kHz. Measurements are made at logarithmic frequency increments.

A computer program is developed to control the lock-in amplifier and control ACPD measurements automatically. A GPIB bus is used to connect the lock-in amplifier to the computer. The control program sends commands to the lock-in amplifier to set the desired AC signal out-

put from the internal function generator. Its frequency, phase and amplitude are set to the expected value. Then the two voltage signals are measured by the lock-in amplifier. The measured data are sent back to the control program. All the measurement parameters of the lock-in amplifier are set by the control program, including time constant and sensitivity. The control program also set the right auxiliary analog output for the switch circuit in the ACPD measurement system. A specified number of data set can be measured sequentially for one rod. The average of these measured data will be used for data analysis.

3.4.2 ACPD Rod Impedance

The homogeneous rod impedance Z is the potential drop V divided by the current I in equation (C.12).

$$Z = \frac{V(\omega)}{I} = \frac{klJ_0(ka)}{2\pi\sigma a J_1(ka)} \tag{3.1}$$

where $k^2 = -j\omega\mu\sigma$ and the root with a positive real part is taken. The measured potential drop includes a contribution from the electromotive force (emf) induced in the potential drop measurement circuit due to the changing of magnetic flux linking this circuit. Expressing the induced emf in terms of the self inductance L, the total impedance measured across a length l of the rod is

$$Z = \frac{klJ_0(ka)}{2\pi\sigma a J_1(ka)} + j\omega L \tag{3.2}$$

where the self inductance L is found from experimental data by fitting predictions of equation (3.2) to the high frequency ACPD measurements. It is obvious that the self inductance L has influence only on the imaginary part of the rod impedance. At high frequency the contribution from the self inductance is comparable to the rod impedance from the theory model. It is important that the self inductance L is kept as small as possible and constant for multi-frequency measurements.

3.4.3 Cylindrical Copper Rod

The accuracy of the ACPD measurement system is tested by measuring the conductivity of a pure copper rod. The conductivity is commonly based on the International Annealed Copper

Standard (IACS). In this system, the conductivity of annealed, unalloyed copper is the standard and arbitrarily rated at 100%. The conductivity of other metals and alloys is expressed as a percentage of the standard. Ratings can also be expressed as MegaSiemens/meter (MS/m). The conductivity of the test copper rod is supposed to be very close to 100% IACS, or 58 MS/m. The MIZ-21A eddy current instrument from Zetec Inc is used to measure the conductivity of this pure copper rod. The measured conductivity is 98.9% IACS. The relative permeability μ of the copper rod is known to be 1. Only the conductivity σ is unknown in the rod impedance equation (3.1).

Multi-frequency ACPD rod impedance measurements on the copper rod give the conductivity to be 100.70% IACS, or 58.4 MS/m, indicating that the measurement system is accurate to within 2%. The measured ACPD rod impedance variation with frequency on the copper rod is shown in Figure 3.5 and 3.6.

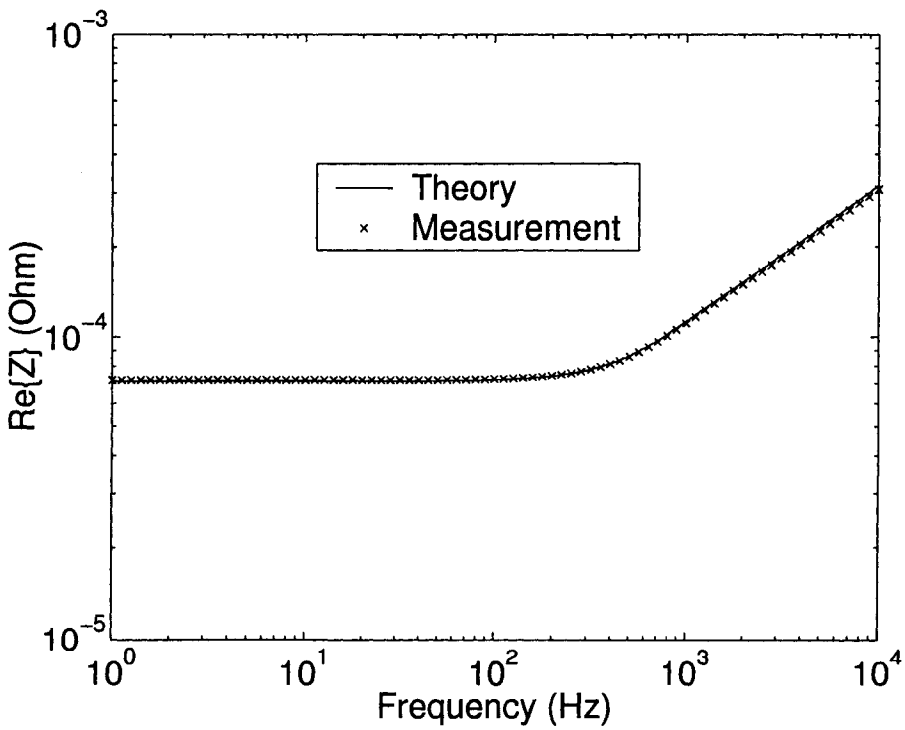

Figure 3.5 Real part of the ACPD rod impedance measurements on copper rod

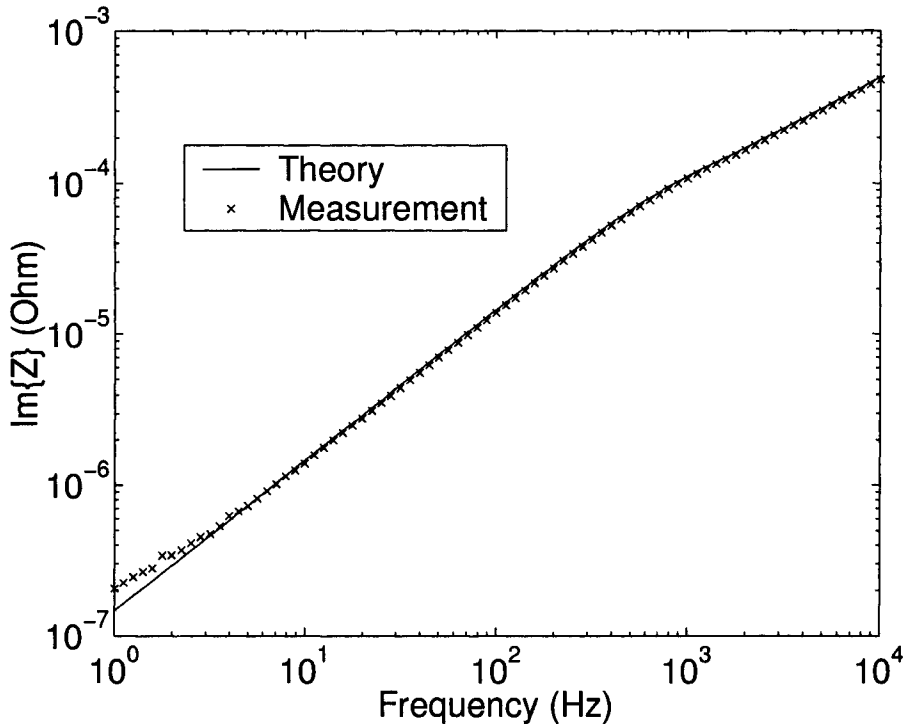

Figure 3.6 Imaginary part of the ACPD rod impedance measurements on copper rod

3.4.4 Untreated Cylindrical Steel Rod

The untreated cylindrical steel rod is assumed to be homogeneous. It is is assumed to be uniform in the axial direction. It has only two unknown parameters, conductivity σ and relative permeability μ_r.

The ACPD rod impedance Z in equation (3.1) is used to estimate both the conductivity and permeability of the untreated steel rod from multi-frequency measurements. The measured rod impedance is normalized by the theoretical rod impedance from the fitted parameters. To minimized the influence from the distributed self inductance on the ACPD rod impedance, only the real part is used for data fitting.

The measured ACPD rod impedance variation with frequency on the untreated steel rod is shown in Figure 3.7 and 3.8.

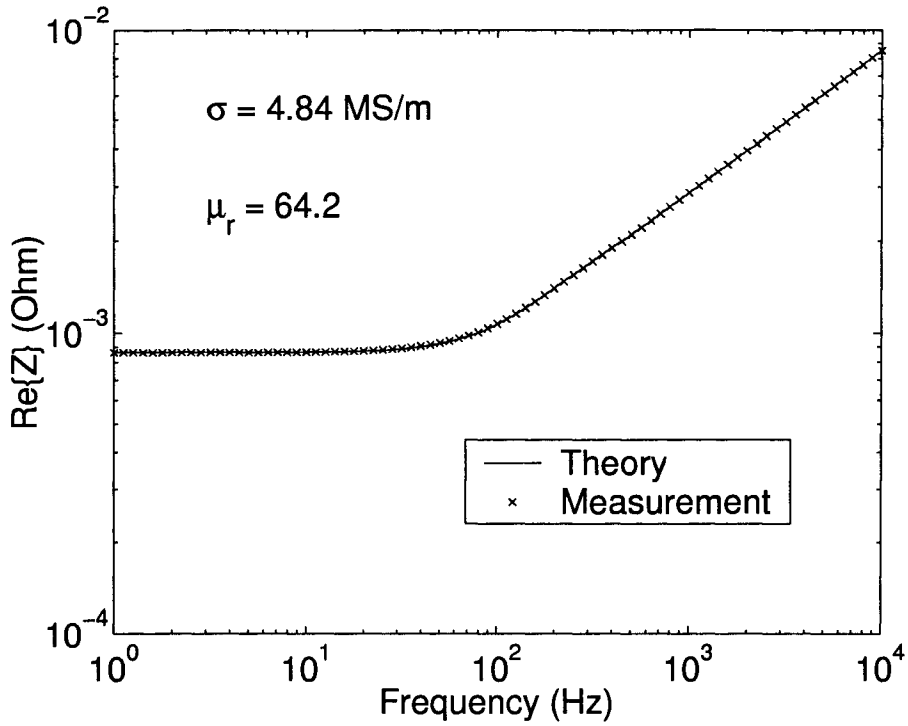

Figure 3.7 Real part of the ACPD rod impedance measurements on untreated steel rod

3.4.5 Case Hardened Cylindrical Steel Rod

In the idealized case hardened cylindrical steel rod, the rod is uniform in the axial direction. It has a homogeneous substrate surrounded by a homogeneous surface layer of uniform thickness.

The rod impedance Z for the case hardened steel rod is the potential drop V divided by the current I in equation (C.39). It is used to estimate the three unknown parameters for the case hardened layer, conductivity σ_2, permeability μ_2 and case depth d. The conductivity σ_1 and permeability μ_1 for the substrate layer is estimated by using rod impedance in equation (3.1) from untreated cylindrical steel rod measurements.

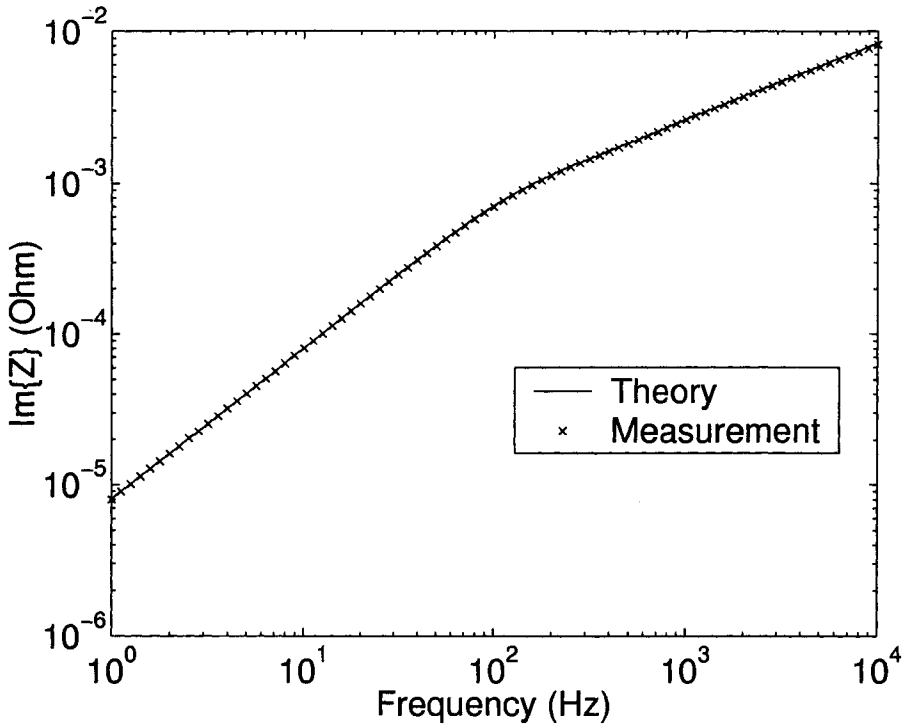

Figure 3.8 Imaginary part of the ACPD rod impedance measurements on untreated steel rod

3.5 Results

One set of six cylindrical rod specimens are used in the ACPD rod impedance measurements. There are one pure copper rod and five steel rods. The five steel rods are common grade 1045 carbon steel rods from McMaster-Carr that meets ASTM A108 standard. One is not heat treated, the other four are heat treated by induction hardening [59]. Their dimensions are shown in Table 3.1.

The ACPD rod impedance on those case hardened cylindrical steel rods is normalized by the rod impedance on the untreated rod.

$$Z_n = \frac{Z}{Z_0} \tag{3.3}$$

Where Z is the measured rod impedance in equation (3.2) due to the case hardened steel rod, Z_0 is the theoretical rod impedance in equation (3.2) due to an artificial homogeneous

Table 3.1 Measured dimensions of six cylindrical rods

Rod Specimens	Length (mm)	Diameter (mm)
copper rod	509	11.06
untreated rod	503	11.02
0.5 mm case	502	11.00
1.0 mm case	503	11.02
1.5 mm case	502	11.02
2.0 mm case	501	11.02

rod. It has the same dimension as the case hardened rod, but has the same measured electrical conductivity and magnetic permeability of the untreated steel rod. Data fitting between ACPD measurements data and the theoretical model prediction is based on the normalized rod impedance. The rod impedance is a complex number: it has real and imaginary parts. Only the real part of the normalized rod impedance in equation (3.4) is used for data fitting. The imaginary part is calculated using equation (3.5). The self inductance L in the ACPD measurement system has no contribution to the real part of the rod impedance in equation (3.2).

$$R_n = \frac{Re\{Z\}}{Re\{Z_0\}} \tag{3.4}$$

$$X_n = \frac{Im\{Z\}}{Im\{Z_0\}} \tag{3.5}$$

The real and imaginary part of the normalized rod impedance measured on case hardened steel rods are shown in Figure 3.9 and 3.10 respectively.

The fitted five unknown parameters of each specimen are shown in Table 3.2. They are substrate layer conductivity σ_1 and relative permeability μ_1, case hardened surface layer case depth d, conductivity σ_2 and relative permeability μ_2. Data fitting error is the summation of the squared difference between the real part of the normalized rod impedance data and theoretical calculation over frequency.

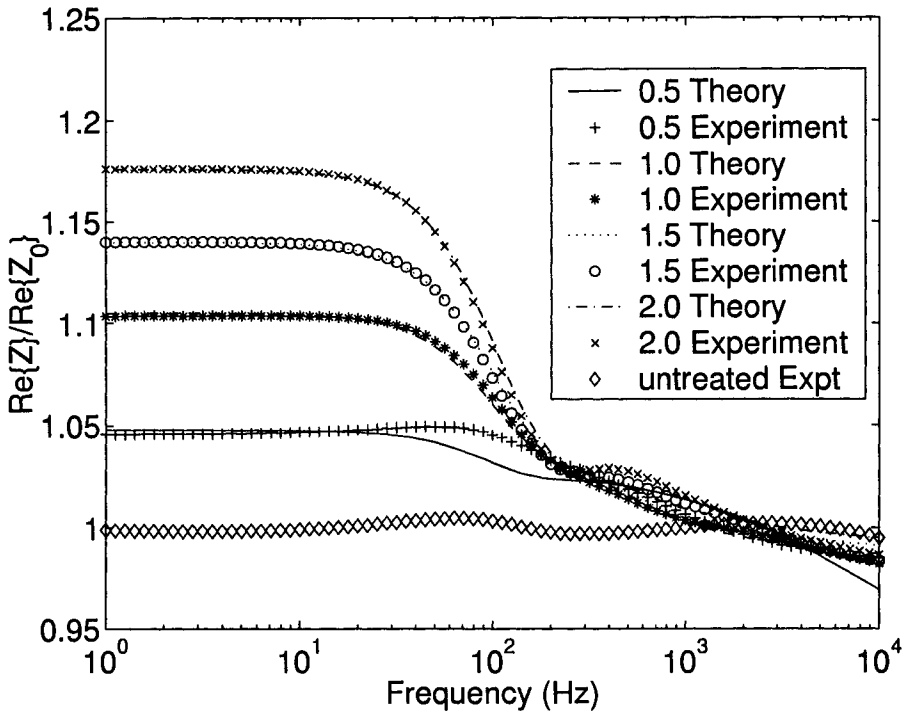

Figure 3.9 Real part of the ACPD rod impedance measurements on case hardened cylindrical steel rods. The impedance data are normalized by the theoretical rod impedance on the untreated rod. Numbers in the legend are the nominal case depth in mm.

3.6 Experiment on One-inch Diameter Rods

Two set of one-inch diameter steel rods are used on ACPD rod impedance measurements. Their dimensions are shown in Table 3.3. These two set of one-inch steel rods are common grade 1045 carbon steel rods from McMaster-Carr that meets ASTM A108 standard. Number 10 and 20 rods are not heat treated, the other rods are heat treated by induction hardening [59]. Number 10 to 17 rods belong to one set, number 20 to 27 rods belong to the other set. Number 11 and 21 rods get the same induction hardening treatment. Number 12 and 22 rods get the same induction hardening treatment, number 17 and 27 rods get the same induction hardening treatment. They are supposed to have the same hardness profile respectively. The hardness profile is shown in Figure 3.11. For example, the hardness profile of number 15 and

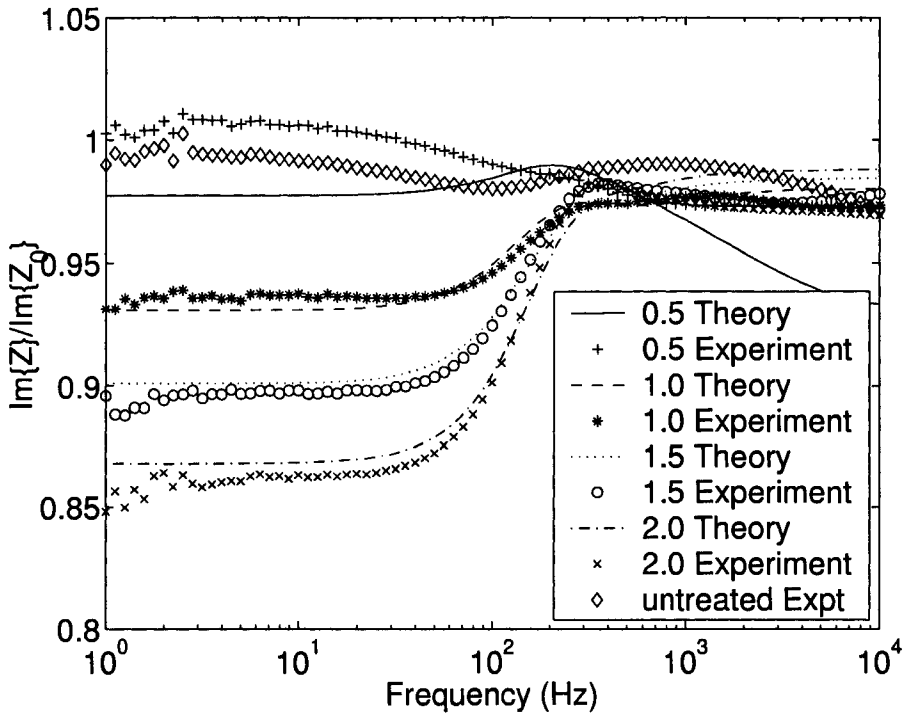

Figure 3.10 Imaginary part of the ACPD rod impedance measurements on case hardened cylindrical steel rods. The impedance data are normalized by the theoretical rod impedance on the untreated rod. Numbers in the legend are the nominal case depth in mm.

25 rods is shown in Figure 3.11 with curve 15.

3.6.1 One-inch Diameter Copper Rod

The accuracy of the ACPD measurement system on one-inch diameter rods is tested by measuring the conductivity of a pure copper rod. It is alloy 101, 99.99% pure copper rod. The conductivity value from the manufacturer is 101% IACS for this copper rod. The MIZ-21A eddy current instrument from Zetec Inc. is used to measure its conductivity. The measured conductivity is 101.1% IACS.

Multi-frequency ACPD rod impedance measurements on this copper rod give the conductivity to be 101.3% IACS, or 58.7 MS/m, indicating that the measurement system is accurate to within 1%. The measured ACPD rod impedance variation with frequency on this copper

Table 3.2 The results shown are surface layer and substrate parameters found by data fitting between ACPD measurements and the theoretical model prediction. Effective case depth data are from the hardness profile in Figure 3.2

Rods	substrate layer		case hardened layer			Data fitting error	case depth (mm)
	μ_1	σ_1(MS/m)	μ_2	σ_2(MS/m)	d(mm)		
Copper	1.0	58.4	N/A	N/A	N/A	1.38×10^{-3}	N/A
untreated	64.2	4.84	N/A	N/A	N/A	4.22×10^{-4}	N/A
0.5 case	64.2	4.84	37.1	3.14	0.37	3.67×10^{-3}	0.38
1.0 case	64.2	4.84	50.0	3.92	1.62	3.04×10^{-4}	1.03
1.5 case	64.2	4.84	50.6	3.93	2.27	8.88×10^{-4}	1.49
2.0 case	64.2	4.84	50.7	3.90	2.92	1.20×10^{-3}	1.90

rod is shown in Figure 3.12 and 3.13.

3.6.2 One-inch Diameter Untreated Rods

The measured ACPD rod impedance variation with frequency on the untreated steel rod #10 is shown in Figure 3.14 and 3.15. Before it is annealed, the data fitting results show that its conductivity is 4.5996 MS/m, its relative permeability is 61.9079. There is big variation when the data is shown in normalized way in Figure 3.14. After it is annealed, the variation is cut by half. The data fitting results show that its conductivity is 4.8918 MS/m, its relative permeability is 65.3251. It is customary to stress relieve carbon the steel parts at a temperature of 650 C for 2 hours [61]. Since the variation is cut by half after the rod is annealed for 2 hours, maybe the variation can be further reduced by extending its anneal time. So the #20 untreated rod is annealed for 6 hours to see the difference.

The measured ACPD rod impedance variation with frequency on the untreated steel rod #20 is shown in Figure 3.16 and 3.17. Before it is annealed, the data fitting results show that its conductivity is 4.5999 MS/m, its relative permeability is 61.2728. There is big variation when the data is shown in normalized way in Figure 3.16. After it is annealed for 6 hours, the variation is cut by half. It seems that the variation can not be reduced any more by extending the anneal time. The data fitting results show that its conductivity is 5.0542 MS/m, its relative

Table 3.3 Measured dimensions of the one-inch diameter cylindrical rods

Rod Specimens	Length (mm)	Diameter (mm)
Copper rod	912.4	25.389
Steel #10	410.9	25.388
Steel #11	411.3	25.382
Steel #12	410.9	25.382
Steel #13	411.2	25.382
Steel #14	410.6	25.383
Steel #15	410.1	25.381
Steel #16	411.2	25.375
Steel #17	411.1	25.364
Steel #20	411.2	25.387
Steel #21	411.9	25.389
Steel #22	410.0	25.381
Steel #23	409.7	25.381
Steel #24	410.9	25.375
Steel #25	410.2	25.384
Steel #26	411.9	25.373
Steel #27	411.9	25.372

permeability is 66.1478.

From the ACPD measurements on these two untreated steel rods, it is shown that the cold finished carbon steel rods should be annealed before they are used for the ACPD measurements.

3.6.3 One-inch Diameter Induction Hardened Rods

There are 14 induction hardened steel rods in total. It is very difficult to see clearly if they are shown in one diagram. It is not necessary to show diagrams here for all those rods one by one. So only the measurement data on #27 rod are shown here. It is shown in absolute terms in Figure 3.18 and 3.19. It is shown in normalized way in Figure 3.20 and 3.21.

3.6.4 Results on One-inch Diameter Rods

The data fitting results for these one-inch diameter rods are shown in Table 3.4. Comparison of case depth from ACPD measurements and hardness profile is shown in Figure 3.22.

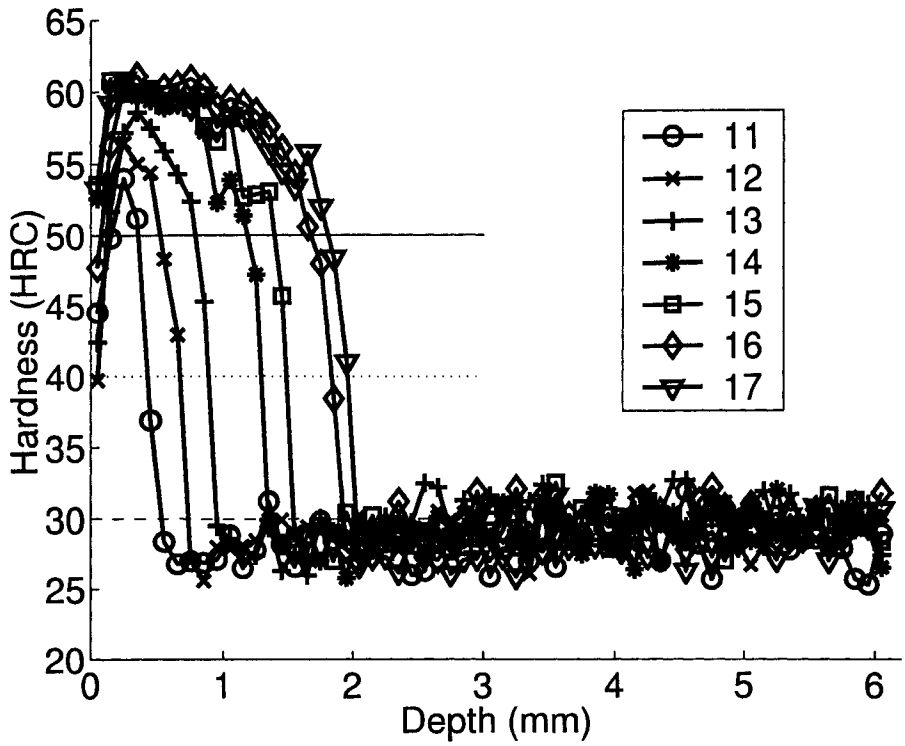

Figure 3.11 Hardness profile for one-inch diameter steel rods. Effective case depth is measured at 50 HRC hardness. Steel rods and hardness profile are provided by Dr. Douglas Rebinsky from Caterpillar Inc.

3.7 Discussion

The surface layer and substrate parameters found by data fitting between ACPD measurements and the theoretical model prediction are shown in Table 3.2. The measured case hardened surface layer depth is in reasonable agreement with the effective case depth from the hardness profile. Several factors have influence upon the agreement between them as discussed below.

3.7.1 Effective Case Depth

Usually the effective case depth is used to indicate the case hardened layer depth (Figure 3.2). The effective depth is an important quality in case hardening. It is known that

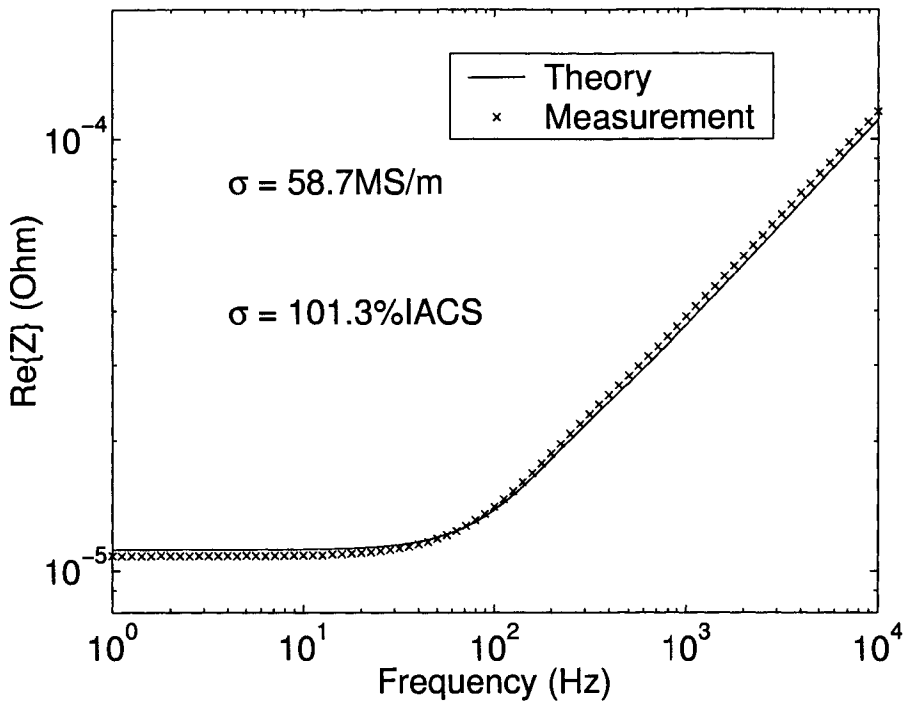

Figure 3.12 Real part of the ACPD rod impedance measurements on one-inch diameter copper rod

maximum hardness of a case hardened part is not maintained throughout the full depth of the case. Part-way through the case, hardness begins to reduce progressively until it reaches the core hardness.

Effective case depth is the perpendicular distance from the surface of a hardened case to the deepest point at which a specified level of hardness is reached. The hardness criterion is shown in the Table 1.1. It is one industry standard. In some way it is arbitrary defined.

Beside the specified hardness criterion, effective case depth also depends on how (rate of change) the transition zone changed between the case hardened steel and the softer base material. It is reasonable that the accuracy of the ACPD measurement method is also dependent on how the actual transition zone changes between the case hardened surface layer and the substrate layer, though there is no transition zone in the idealized case hardened rod model. The accuracy of the ACPD measurements system is indicated by the agreement between the effective depth and the ACPD measurements result. It is expected that the ACPD measurements

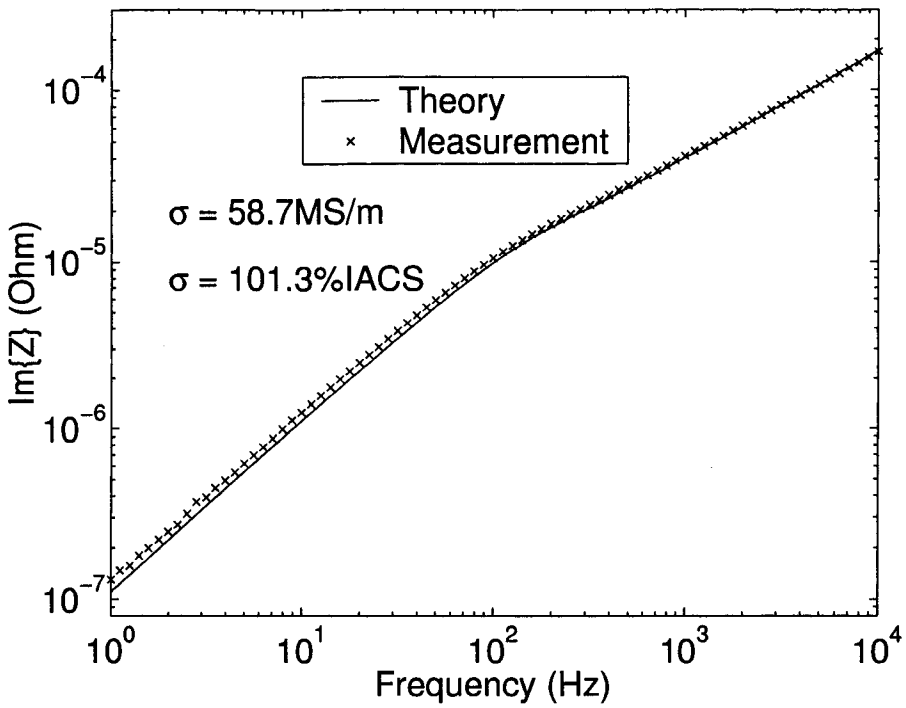

Figure 3.13 Imaginary part of the ACPD rod impedance measurements on one-inch diameter copper rod

result is more accurate if the hardness changes very quickly.

3.7.2 Measurements Errors

In the ACPD measurements system, the measured potential drop includes a contribution from the electromotive force (emf) induced in the potential drop measurement circuit due to the changing of magnetic flux linking this circuit (see equation (C.13) and (C.39)). It is one disadvantage of ACPD method. Great care is taken in positioning the current and potential drop measurement probes. Each pair of current and potential drop measurement cables are twisted together, the loop area enclosed by both the current and voltage leads is minimized to reduce the magnitude of any inductive pick up.

One cause of the measurements error is that the cylindrical rod is not exactly uniform in the axial direction. From the dimension measurements, it is found that the diameter at one end of the steel rod is not the same as the diameter at the other end. One possible reason

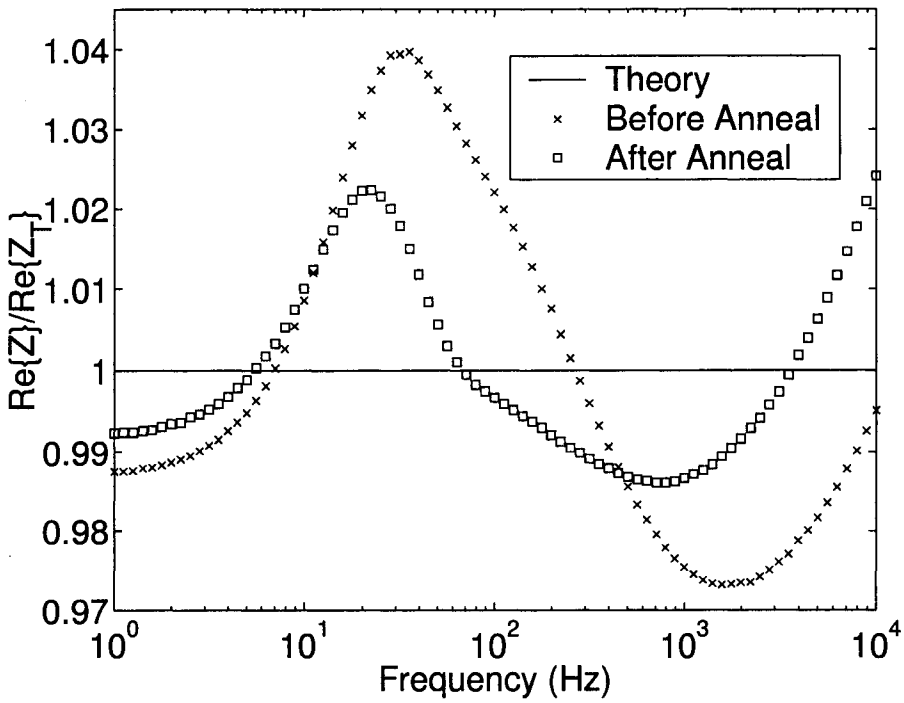

Figure 3.14 Real part of the ACPD rod impedance measurements on #10 untreated steel rod. The experiment data is normalized to the theoretical calculation value. The measurements are done before and after the rod is annealed for 2 hours.

is that the steel rod is not exactly uniform when it is manufactured, especially when it is very long compared with its diameter. Another possible reason is the distortion caused by the case hardening process. Changes in size or shape can arise in case hardened components from a variety of causes, some inherent in these high-temperature rapid-cool processes, some attributable to component design shortcomings, and others relating to earlier manufacturing steps (for example, thermal relief of stresses introduced by prior forming). Close-tolerance components must be ground (with care) after treatment. The case depth specification must allow for this.

Some other measurements errors include the steel rod dimension measurement errors, voltage across the resistor and potential drop measurement error, measurement error for the resistance value of the high precision resistor and its variation with frequency.

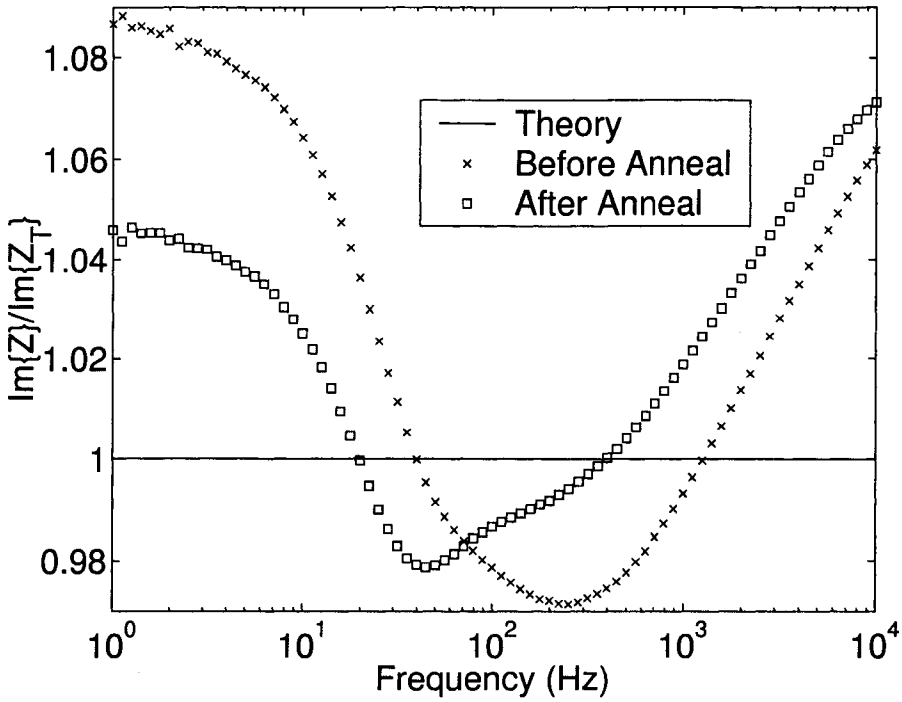

Figure 3.15 Imaginary part of the ACPD rod impedance measurements on #10 untreated steel rod. The experiment data is normalized to the theoretical calculation value. The measurements are done before and after the rod is annealed for 2 hours.

Digital caliper is used to measure the steel rod diameter. The digital caliper has an accuracy of 0.01 mm. Compared with the actual rod diameter, the relative measured error is less than 0.02%. A ruler is used to measure the distance between the two potential drop probes (because it is too long for digital caliper). The minimal scale is 0.2 mm. If the rod length is fallen between two scale labels, it is judged by human eye. The measurement error is about 0.1 mm. Compared with the actual distance between the two potential probes, its relative measurement error is less than 0.05%. The high precision resistor is measured by using Agilent 4294A precision impedance analyzer from 40 Hz to 40 kHz. The resistance variation with frequency is less than 1%. SR830 DSP lock-in amplifier is used to measure the potential drop along the rod and voltage across the precision resistor.

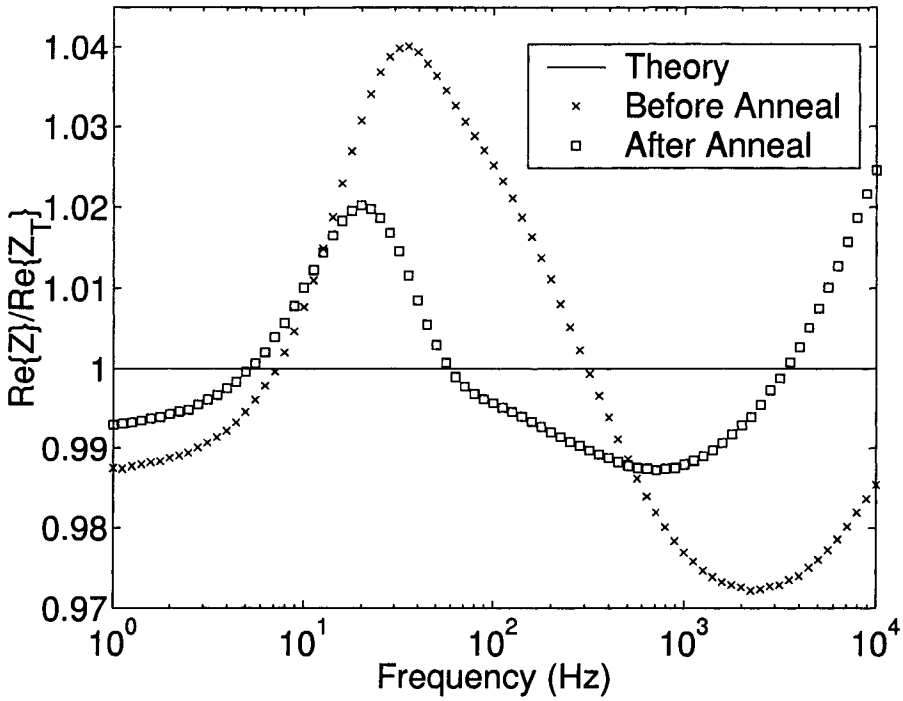

Figure 3.16 Real part of the ACPD rod impedance measurements on #20 untreated steel rod. The experiment data is normalized to the theoretical calculation value. The measurements are done before and after the rod is annealed for 6 hours.

3.7.3 End Effect

In the ACPD cylindrical rod measurements system, the current is injected into the cylindrical rod through a copper loop at one end. Another copper loop is used to take the AC current out from the rod at the other end. The two potential drop probes are located about 2 cm from the copper loop. This arrangement is designed to make the potential drop values big. If the electric field is fixed at one frequency, the measured potential drop value is proportional to the distance between the two potential drop probes (see equation (C.39)). If the measured signal value is very small, then the signal to noise ratio will be big.

For the time being it is unknown if there is some end effect on the measured potential drop. The ACPD theory on the cylindrical rod does not give attention to the end effect. It is assumed that the cylindrical rod is infinite long. At present no experiments have been done to

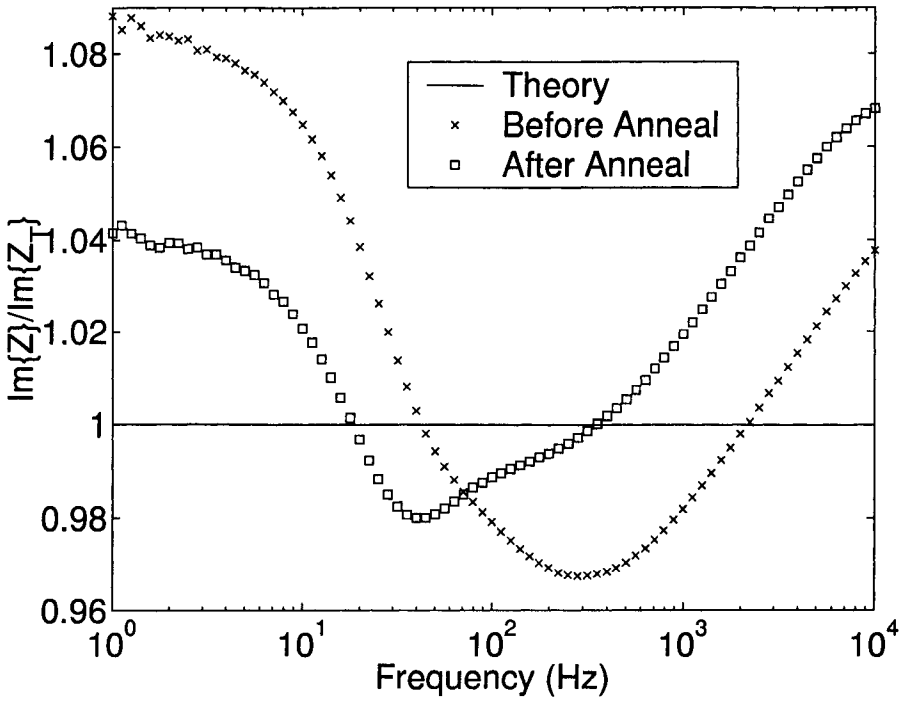

Figure 3.17 Imaginary part of the ACPD rod impedance measurements on #20 untreated steel rod. The experiment data is normalized to the theoretical calculation value. The measurements are done before and after the rod is annealed for 6 hours.

resolve this issue although it is straightforward to check if the end effects are significant. The distance between the two potential drop probes can be made smaller. Then the potential drop can be measured on different positions along the rod. To check the end effect, two different positions are enough. At the first position, the two potential drop probes stay at the center of the rod. At the second position, one can move the potential drop probes as close to the current injection or extraction copper loop as possible. The AC current and work frequency should be kept unchanged for these two positions measurements. Comparison of these two measured potential drop values can show the end effect.

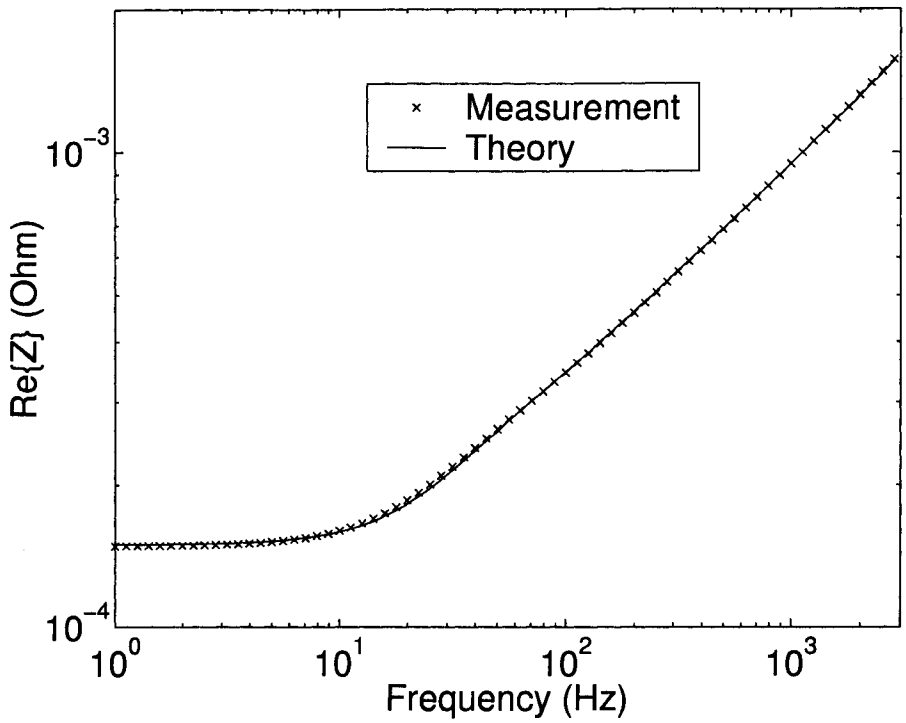

Figure 3.18 Real part of the ACPD rod impedance measurements on #27 induction hardened steel rod.

3.7.4 Anneal and Demagnetize the Steel Rod

The five steel rods are common grade 1045 carbon steel rods from McMaster-Carr that meets ASTM A108 standard. They are cold processed from the manufacturer. When they are shipped to Iowa State University for research, one is not heat treated, the other four are heat treated by induction hardening [59].

It is known that the presence of residual stress in the parts caused by cold working, drawing, extrusion, forging, welding or maching operations greatly increases the tendency of distortion. And the residual stress also have effect on electromagnetic parameters measurement. Stress reduction is necessary to avoid distortion during hardening and to avoid cracking resulting from the combination of residual stress and the thermal stress produced during heating to the hardening temperature. In order to get accurate conductivity and permeability from the steel rod, it should be annealed and demagnetized.

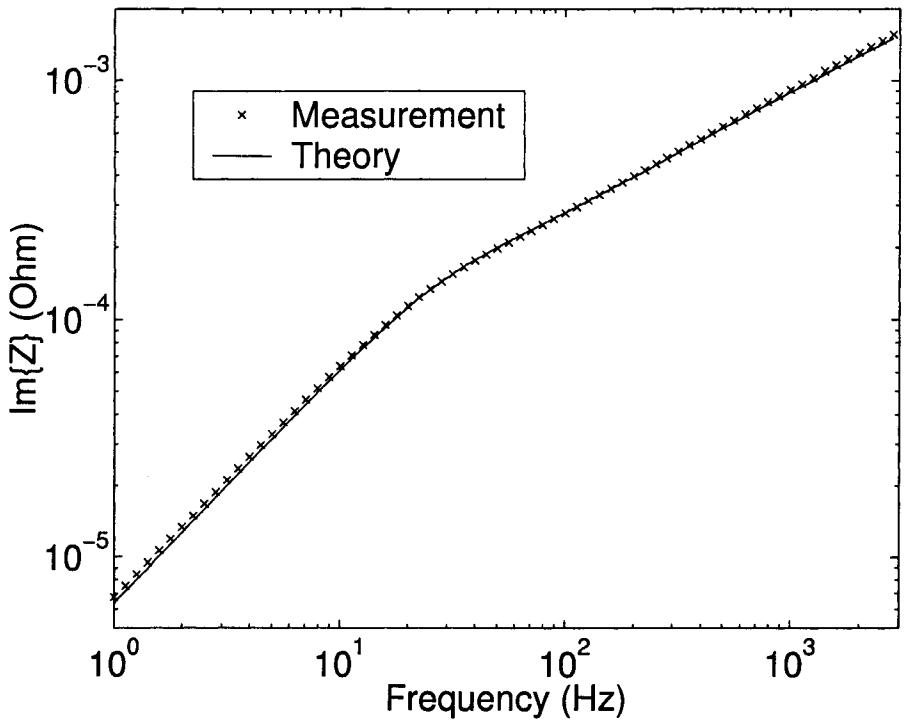

Figure 3.19 Imaginary part of the ACPD rod impedance measurements on #27 induction hardened steel rod.

All the five steel rods have been demagnetized in Iowa State University. But it is not clear whether they are been annealed or not. For the untreated rod, there may be some measurement error in the conductivity and permeability if it is not annealed. Since the electromagnetic properties of the substrate layer of case hardened rod is assumed to be the same as the untreated rod in the two-layer model, it will also cause some error to case depth measurement if the substrate layer changes in the treatment. Of course, some measurement errors may arise for non-annealed case hardened rods.

It is found the the original diameter of these steel rods is half inch, or 12.7 mm, and now they are about 11 mm diameter. The rods have been ground to the current size from half inch [59]. It is to remove the surface defects and distortion. This kind of heavy grinding has some drawbacks: possible elimination of most, if not all, of the hardened case of the carburized and hardened part; and the danger of burning and crack formation on the surface layers. It is

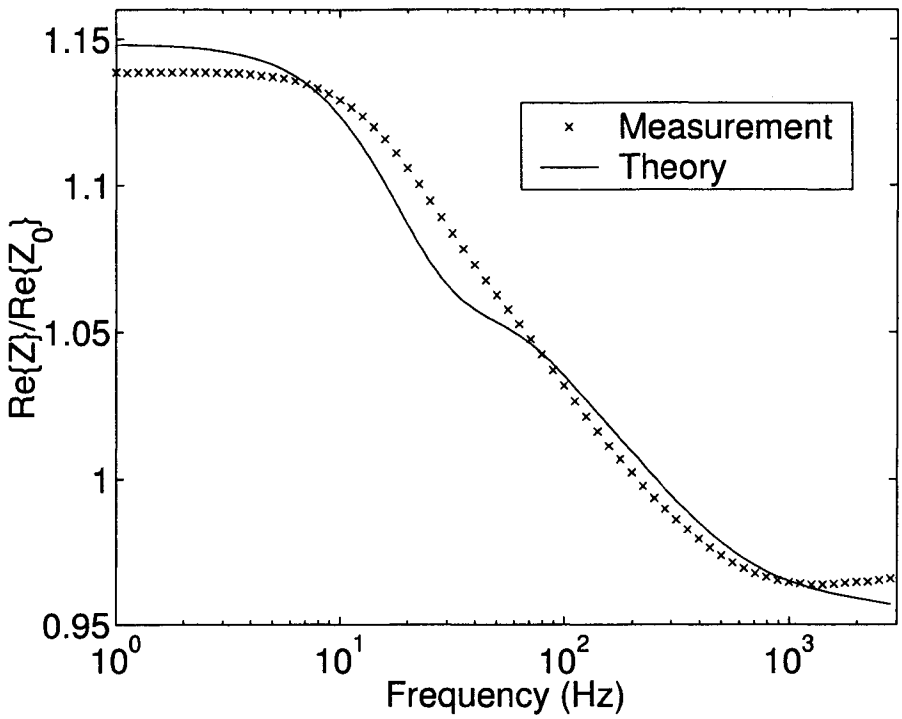

Figure 3.20 Real part of the ACPD rod impedance measurements on #27 induction hardened steel rod. The experiment data is normalized to the theoretical calculation value.

possible that this grinding will affect the electromagnetic properties measurements.

3.7.5 Hardness and Conductivity and Permeability Profiles

It is assumed that the steel rod is uniform in the axial direction. It is assumed that the conductivity and permeability variation with depth is indicative of the hardness profile allowing the depth of the case hardened layer to be estimated from electromagnetic measurements. It is also assumed that the hardness, electrical conductivity and magnetic permeability are symmetrical in the radial direction. It is assumed that the conductivity and permeability parameters track the hardness profile.

The hardness profile is found from the hardness measurements made on the end of the steel rod. It is assumed that the hardness is uniform along the axial direction. The rod is not been cut in the middle way to do the hardness measurement destructively.

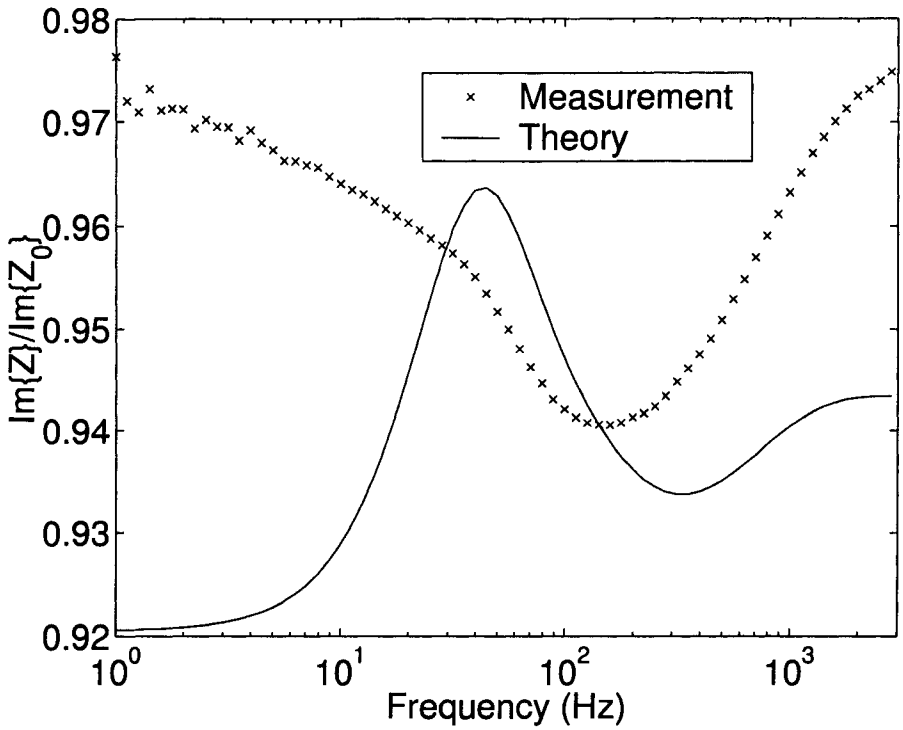

Figure 3.21 Imaginary part of the ACPD rod impedance measurements on #27 induction hardened steel rod. The experiment data is normalized to the theoretical calculation value.

It is assumed that the substrate layer of the case hardened steel rod has the same physical and electromagnetic properties as those values of the untreated rod. No experiment is done to verify this assumption. It is difficult and complicated to measure the electromagnetic properties of the substrate layer. It is possible that substrate layer may have different electrical conductivity and magnetic permeability from the untreated rod.

Analysis of conductivity and permeability profiles in induction hardened steel rod is made by Dr. Marcus Johnson [64]. The hardness, conductivity and permeability profiles are measured on a big (50 mm diameter) induction hardened steel rod. It is very straightforward that the hardness of the surface layer is bigger than the value of substrate layer. It is found that the electrical conductivity of the surface layer is smaller than the value of the substrate layer. It is also found that the magnetic permeability of the surface layer is smaller than the value of

Table 3.4 The results shown are surface layer and substrate parameters found by data fitting between ACPD measurements and the theoretical model prediction for one-inch diameter rods. Effective case depth data are from the hardness profile in Figure 3.11

	substrate layer		case hardened layer			Data fitting	case depth
Rods	μ_1	σ_1(MS/m)	μ_2	σ_2(MS/m)	d(mm)	error	(mm)
Copper	1.0	58.73	N/A	N/A	N/A	9.91×10^{-2}	N/A
#10	65.33	4.89	N/A	N/A	N/A	9.93×10^{-3}	N/A
#11	65.33	4.89	46.15	3.49	0.499	1.01×10^{-1}	0.358
#12	65.33	4.89	44.44	3.54	0.512	8.80×10^{-2}	0.524
#13	65.33	4.89	34.52	2.94	1.319	2.97×10^{-2}	0.784
#14	65.33	4.89	34.13	2.89	1.526	1.16×10^{-2}	1.183
#15	65.33	4.89	38.09	3.28	1.581	1.16×10^{-2}	1.392
#16	65.33	4.89	38.10	3.20	2.028	9.42×10^{-3}	1.674
#17	65.33	4.89	41.38	3.52	2.149	6.57×10^{-3}	1.806
#20	66.15	5.05	N/A	N/A	N/A	8.61×10^{-3}	N/A
#21	66.15	5.05	41.11	3.24	0.538	1.27×10^{-1}	0.358
#22	66.15	5.05	43.13	3.51	0.498	1.77×10^{-1}	0.524
#23	66.15	5.05	27.38	2.39	1.446	5.30×10^{-2}	0.784
#24	66.15	5.05	32.74	2.88	1.598	1.18×10^{-2}	1.183
#25	66.15	5.05	34.59	3.06	1.803	8.77×10^{-3}	1.392
#26	66.15	5.05	37.58	3.28	2.192	6.07×10^{-3}	1.674
#27	66.15	5.05	37.31	3.20	2.476	5.64×10^{-3}	1.806

the substrate layer. From this point of view the data fitting results (see Table 3.2) are in the right direction.

It is observed that electrical conductivity values align fairly well with hardness values. But the hysteresis loss and initial permeability measurements show a significant lag with respect to actual hardness profiles. This will lead a potential over prediction by the two-layer model-based measurement method. Some anomalous values for surface conductivity and coercivity are observed. It is certain that high surface values of conductivity will impact the model-based inversion method in some way.

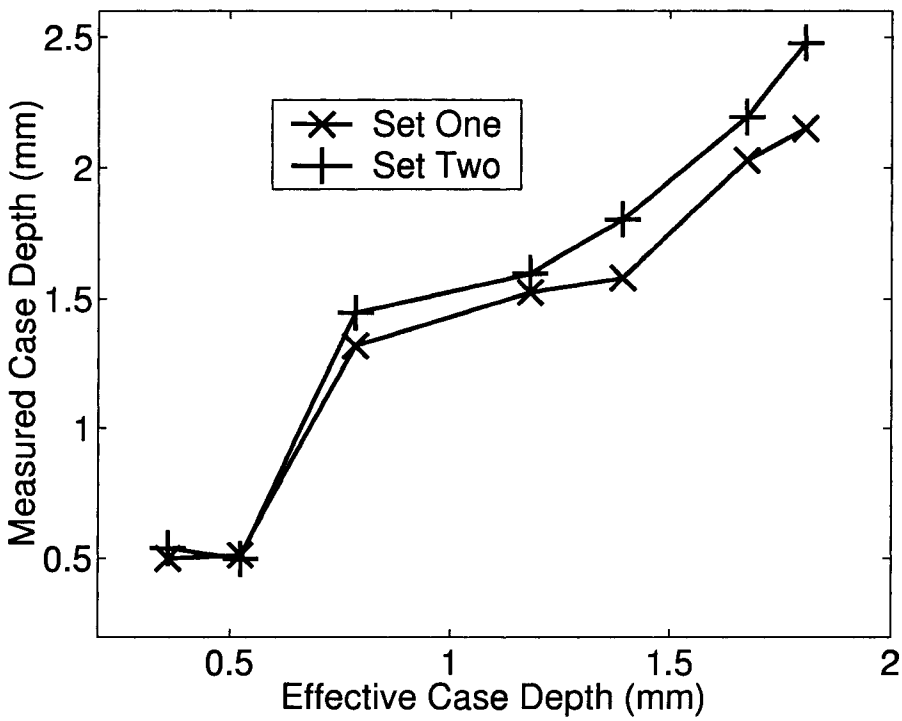

Figure 3.22 Comparison of the case depth from ACPD measurements and effective case depth for the one-inch diameter rods. Set one includes #11 to #17 rods. Set two includes #21 to #27 rods. Two sets of induction hardened rods are supposed to have the same hardness profile. The effective case depth is got from hardness profile which is shown Figure 3.11.

CHAPTER 4. EDDY CURRENT MEASUREMENTS ON CASE HARDENED CYLINDRICAL STEEL RODS

4.1 Introduction

Eddy current testing is one of the techniques used to perform electromagnetic inspection. Eddy current testing is used to inspect a wide range of ferrous and non-ferrous material for defects or deterioration without damaging the material. The eddy current testing technique is based on inducing electron flow (eddy currents) in electrically conductive material. Any defect in the material such as cracks, pitting, wall loss, or other discontinuities disrupts the flow of the eddy currents. Eddy current testing uses the change in magnetic permeability and electrical conductivity as the basis for producing a measurable output and so any part characteristic that depends on these quantities can be identified. Higher frequency signals are used to detect near-surface flaws; lower frequencies are used when deeper, subsurface flaw detection is required.

4.2 Theoretical Model

The same idealized case hardened cylindrical steel rod model in Chapter 3, Figure 3.3 is used here as the hypothesis. It is assumed that the cylindrical rod is uniform in the axial direction. It has a homogeneous substrate surrounded by a homogeneous surface layer of uniform thickness. There is no transition zone between these two layers. There are five unknown rod parameters for this model: the substrate layer conductivity σ_1 and relative permeability μ_1, the surface layer conductivity σ_2 and relative permeability μ_2 and its layer depth d.

Eddy current impedance measurements are sensitive to variations in conductivity and per-

meability with depth in cylindrical steel rods. The material properties can be evaluated by comparing experiment measurements of eddy current coaxial driver and pickup coils mutual impedance with predictions from an appropriate theoretical model and by adjusting the model parameters until good data fitting is achieved. The model parameters are then assumed to represent the actual parameters of the physical system.

4.3 Theory

For an idealized case hardened cylindrical steel rod, the eddy current mutual impedance between the coaxial driver and pickup coils is given by a closed form analytical expression in [62, equation 65 and 66]. A very brief description is given here.

The general configuration is an axially symmetric driving coil located coaxially with an arbitrary number of cylindrical conductors with arbitrary thickness, permeability, permittivity, and conductivity. All media are assumed to be linear, isotropic, and homogeneous. These cylindrical conductors are infinitely long in the axial direction. The driving current is time harmonic with angular frequency ω. Then, the current density J and vector potential A will have only azimuthal components in cylindrical coordinates.

A delta-function coil is considered first. This delta-function coil is coaxial with an arbitrary number of cylindrical conductors both inside and outside the coil. The vector potential in any region for these multiple concentric conductors in the presence of a delta-function coil is determined. A coil with rectangular cross-section is then represented by the superposition of a number of delta-function coils. The vector potential due to a finite cross section coil can also be determined by the superposition of the vector potential due to the delta-function coil.

Once the vector potential has been obtained, it can be used to calculate the self impedance of single coil and mutual impedance of a pair of coaxial coils.

These general derivations have been very useful in the design of solutions to induction problems. For the case hardened cylindrical steel rods, it is just one simplified special case of these general solutions. Here there are two coils which are coaxial with two cylindrical conductors. From the idealized case hardened cylindrical steel rod model, the rod consists of

a case hardened surface layer and substrate core layer. These two layers can be treated as two coaxial cylindrical conductors. The pickup coil is inside of the driver coil. The case hardened rod is inside the pickup coil. The mutual impedance between the driver and pickup coils in the presence of the case hardened cylindrical steel rod is investigated in the eddy current measurements.

The mutual impedance between coils 1 and 2 is the voltage induced in one coil by a unit current in the other. By the reciprocity theorem, the mutual impedance between coils 1 and 2 is equal to the the mutual impedance between coils 2 and 1.

4.4 Experiment

4.4.1 Drive and Pickup Coil Preparation

Polyetherimide (Ultem) is used to make the coil former for the driver and pickup coils. Polyetherimide is an amorphous thermoplastic that maintain its strength and rigidity at elevated temperatures. Its excellent electrical properties are consistent over temperature and frequency ranges. Exceptional flame retardance supports aircraft / aerospace applications. Ultem is a registered trademark of General Electric company.

The cylindrical rod must slide into the pickup coil former and the coil former should be able to hold the rod. Between the coil former and the cylindrical rod, no gap should be left to minimize the coil lift off and to make the rod coaxial with the coil. In practice the inside diameter of the coil former should be almost the same of the rod diameter. But if these two diameters are the same, the rod can not slide into the coil former. The inside diameter of the pickup coil former is made to be just 100 to 200 micro meter bigger than the rod diameter. The outside diameter of the coil former should be very close to the inside diameter to minimize the coil lift off. Of course the coil former can not be zero thickness. The excellent mechanical properties of Ultem make it possible to produce a former with 1 mm wall thickness. Great care must be taken during the maching process. After the coil former is ready, specified AWG copper wire is used to wind the coil. Great care must be taken when winding the wire onto the coil. Some pressure must be added to the thin copper wire during the winding so that neat

wire turns can be distributed almost uniformly along the whole coil former. At the same time the copper wire can not be too tight as it is very fragile and easily broken. In addition, the coil former may be distorted or damaged if the copper wire turns are too tight. After the coil is completely wound the coil former will not be discarded but left with the coil. In such way, if the coil former is distorted, it will be very difficult to slide the rod into the central hole of the coil former.

The pickup coil with its former will slide into the cental hole of the drive coil former. The same consideration and great care must be given to the driver coil former and its winding service. The drive coil former is also made of Ultem material, again a wall thickness of just 1 mm is made.

A black box was designed to hold the drive coil former, pickup coil former and the cylindrical rod. The box will provide protection to the two coil formers and support to cylindrical rod. The pickup coil is mounted into the center hole of the drive coil. The drive coil is put into the black box. Plastic machine screws are used to fix these two coil formers to the black box. Both ends of drive coil formers are mounted. Both ends of the pickup coil former are also mounted. In such a way these two coils are coaxial. Their axial length are designed to be same so that no offset exists in the axial direction. The black box also provides support to the cylindrical rod at two end points of the coil former. The cylindrical rod is slid into the center hole of the pickup coil former. The rod is coaxial with the two coils, but it does not apply pressure on the pickup coil former. The length of the cylindrical rod is much bigger than the drive and pickup coil length. The connection wires for the two coils come out at the center of the top box surface. For the round coil it can roll easily and fall to the ground by itself. The coils are mounted into the cubic box and the box can stay stable on the experiment desk.

Special consideration is given to choose the right size copper wire for two coils. For the drive coil, actual AC current will flow through the coil. For the pickup coil, no current will flow through the coil, only the induced voltage will be measured. So the wire for the drive coil should be thicker than the wire for the pickup coil. In practice, 32 AWG, 0.20 mm diameter wire is used to wind the drive coil. 38 AWG, 0.10 mm diameter wire is used to wind the

pickup coil. For a graduate student without professional training, layer winding is not possible in practice to wind the coil with such kind of tiny wire by hand. Random winding is used. The exact number of wire turns is very important to the experiment system. High priority is given to get the exact coil turns very accurately. Since the pickup coil will slide into the cental hole of the drive coil former, the wound wire of the pickup coil can not extend past the former's diameter. In practice there is some spare space left on the pickup coil former. The spare space can provide protection to the coil wire. Considering the drive coil will slide into the black box, the wounded wire of the drive coil can not be full of its former, either.

The outer diameter of the driver and pickup coils can be measured directly by using digital calipers, which are found to be 29.86 mm and 16.92 mm respectively. An effective value of the outer radius of the coil is determined by measuring the low frequency reactance in free space and fitting the experimental data to the predicted data based on the theory of Dodd and Deeds [63, 64]. The fitted values are given in Table 4.1. Low frequency reactance is measured and self inductance versus frequency is plotted. Below a certain frequency the measurements become inaccurate. The correct DC value for the self inductance can be found by extrapolating back from the linear portion of the curve. The Dodd and Deeds theory model is run and values of the outer radius updated until the predicted self inductance match up with that which is measured. The low frequency inductance measurement for driver coil is shown in Figure 4.1. An accurate value for the DC free space self inductance of the driver coil is estimated to be 87.8 mH by extrapolation of the data shown in Figure 4.1. A value of 14.330 mm for the outer radius of driver coil is obtained in this way. The low frequency measurement for pickup coil is shown in Figure 4.2. An accurate value for the DC free space self inductance of the pickup coil is estimated to be 181.7 mH by extrapolation in Figure 4.2. The outer radius of pickup coil is fit to be 7.9725 mm[1].

[1]Data and graphics for the driver and pickup coils are provided by Dr. Marcus Johnson.

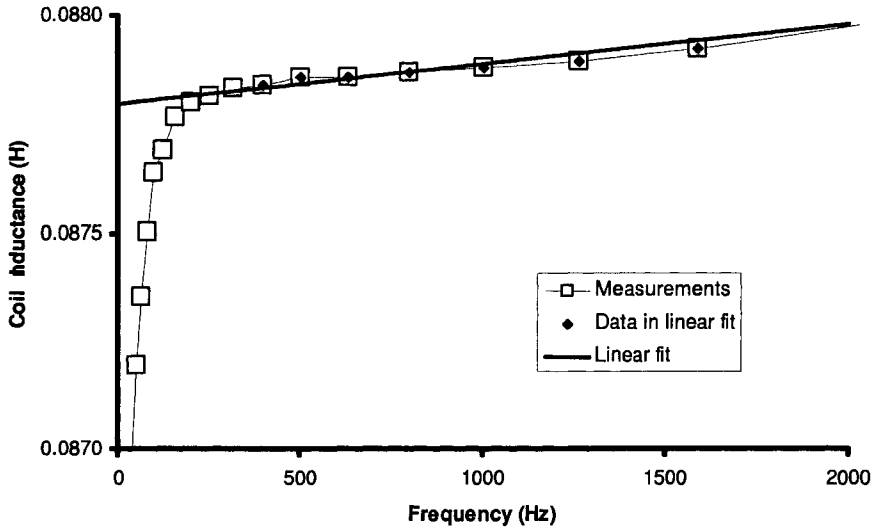

Figure 4.1 Low frequency inductance measurements for driver coil in free space. Data linear fit equation is $L = (9 \times 10^{-8} f + 0.0878)\, H$, where f is the frequency.

4.4.2 Induction Measurement System Description

The two coils, driver and pickup coils having the same axial length, are used to make mutual impedance (equation (4.1)) measurements on the cylindrical rod samples. The driver coil, pickup coil and cylindrical rod are coaxial. The pickup coil is mounted inside the driver coil. The rod is been slid into the pickup coil. A schematic diagram of the coaxial driver pickup coils mutual impedance measurements system is shown in Figure 4.3. Parameters for the two coils are shown in Table 4.1.

Table 4.1 Dimensions of the driver and pickup coils

Parameters	Driver coil	Pickup coil
Number of turns	2300	5000
Inner radius (mm)	10.40	6.60
Outer radius (mm)	14.330	7.9725
Axial Length (mm)	19.96	19.96

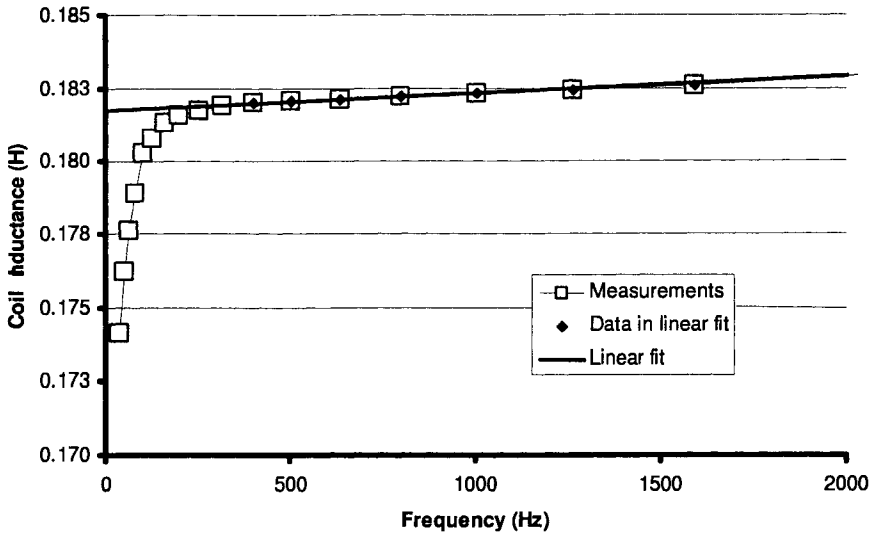

Figure 4.2 Low frequency inductance measurements for pickup coil in free space. Data linear fit equation is $L = (6 \times 10^{-7} f + 0.1817)\, H$, where f is the frequency.

The alternating current is injected into the drive coil by the internal function generator of the SR830 DSP lock-in amplifier. No outside power supply or amplifier is used between the internal function generator and the driver coil. It is found that much noise is introduced to the measurement system if additional outside power supply and amplifier circuit are used.

A high precision resistor is connected in series with the drive coil in order to monitor the current. This resistor has 1% accuracy resistance value within the whole measurement frequency range. By measuring the voltage across the resistor, the current can be determined. The resistance of the high precision resistor is much bigger than the amplitude of the impedance of the drive coil. The coil impedance is changed with the working frequency. The current is roughly kept constant since the high precision resistor dominates the drive coil measurement circuit. The voltage across the resistor is measured by the SR830 DSP lock-in amplifier. The induced voltage from the pickup coil is also measured by the lock-in amplifier.

There is one lock-in amplifier, but two voltage signals are needed to be measured. One simple switch is used to solve this problem. It is put just before the signal input connectors

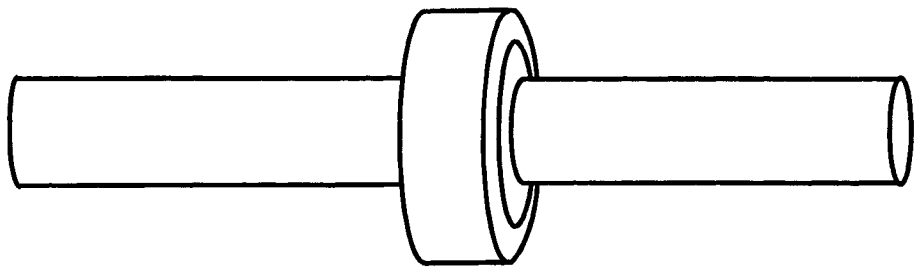

Figure 4.3 Diagram of the coaxial driver pickup coils with cylindrical rod

of the lock-in amplifier. For one fixed frequency, the voltage across the precision resistor is measured first. Then the switch changes its connection so that the induced voltage from the pickup coil can be measured. The working frequency and all other system conditions are kept unchanged when the switch changes its connection from one voltage signal to the other. The control signal to the switch circuit is from the auxiliary analog output of the lock-in amplifier. The switch is almost the same as the switch used in ACPD rod measurement system as described in Chapter 3.

The AC sinusoidal signal is from the internal function generator of the lock-in amplifier. It can provide AC sinusoidal output with different amplitude and frequency. The amplitude can vary from 0 to 5 Volt. The frequency range is from 0.001 Hz to 102 kHz. The actual eddy current induction measurement frequency is from 1 Hz to 10 kHz. Measurements are made at logarithmic frequency increments.

A computer program is developed to control the lock-in amplifier and make eddy current induction measurements automatic. The GPIB bus is used to connect the lock-in amplifier to the computer. The control program sends commands to the lock-in amplifier to set the desired AC signal output from the internal function generator. Its frequency, phase and amplitude are set to the expected value. Then the two voltage signals are measured by the lock-in amplifier. The measured data are sent back to the control program. All the measurement parameters of the lock-in amplifier are set by the control program, including time constant and sensitivity. The control program also set the right auxiliary analog output for the switch circuit. A specified

number of data set can be measured sequentially. The average of these measured data will be used for data analysis.

The same set of cylindrical rod specimens from ACPD measurements are used in the eddy current induction measurements. The length of six cylindrical rod specimens (Table 3.1) is about 50 cm. The cylindrical rod is infinite long in the theoretical model. The cylindrical rod cannot be infinite long in reality. The rods are much longer than the drive and pickup coils in the experimental system. End effects are expected to be negligible.

The mutual impedance between the driver and pickup coils in the presence of measurement rod is defined as the voltage induced in the pickup coil due to unit current through the driver coil. It is a complex number.

$$Z = \frac{V_2}{I_1} \tag{4.1}$$

where V_2 is the voltage induced in pickup coil, I_1 is the current through the drive coil. The mutual impedance change due to the rod is given by

$$\Delta Z = Z - Z_0 \tag{4.2}$$

where $Z = R + jX$ and $Z_0 = R_0 + jX_0$, R is the real part of the impedance, X is the imaginary part of the impedance. Z is the mutual impedance in the presence of the measurement cylindrical rod, Z_0 is the mutual impedance between the driver and pickup coils in free space.

$$\Delta R = R - R_0 \tag{4.3}$$

$$\Delta X = X - X_0 \tag{4.4}$$

4.4.3 Cylindrical Copper Rod

The accuracy of the driver pickup coils mutual impedance measurement system is tested by measuring the conductivity of a pure copper rod. It is the same copper rod as used in ACPD measurements. Its conductivity is supposed to be very close to 100% IACS. Its conductivity measured by MIZ-21A eddy current instrument from Zetec Inc is 98.9% IACS. The relative permeability μ of the copper rod is known to be 1. Only the conductivity σ is unknown in the mutual impedance equation.

Multi-frequency eddy current mutual impedance measurements on the copper rod give the conductivity to be 99.9% IACS, or 57.9 MS/m, indicating that the measurement system is accurate to within 2%. The measured driver pickup mutual impedance variation with frequency on a copper rod is shown in Figure 4.4 and 4.5.

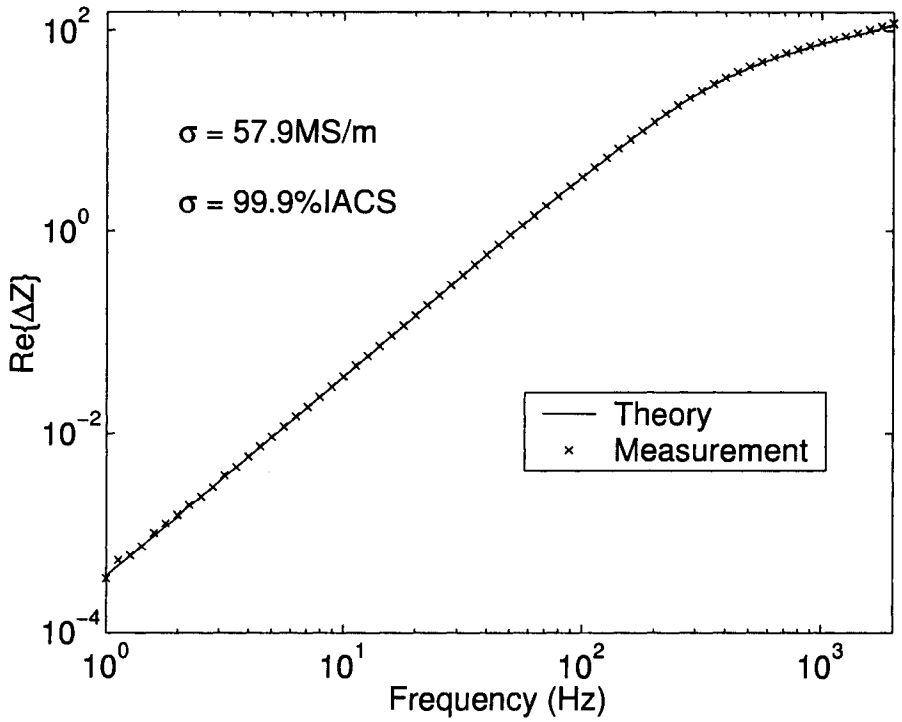

Figure 4.4 Real part of the eddy current driver pickup coils mutual impedance measurements on copper rod.

4.4.4 Untreated Cylindrical Steel Rod

The untreated cylindrical steel rod is assumed to be homogeneous. It is assumed to be uniform in the axial direction. It has only two unknown parameters, conductivity σ and relative permeability μ_r.

The driver pickup coils mutual impedance is used to estimate both the conductivity and permeability of the untreated steel rod from multi-frequency measurements. The change of mutual impedance measured on untreated steel rod is normalized by the theoretical change

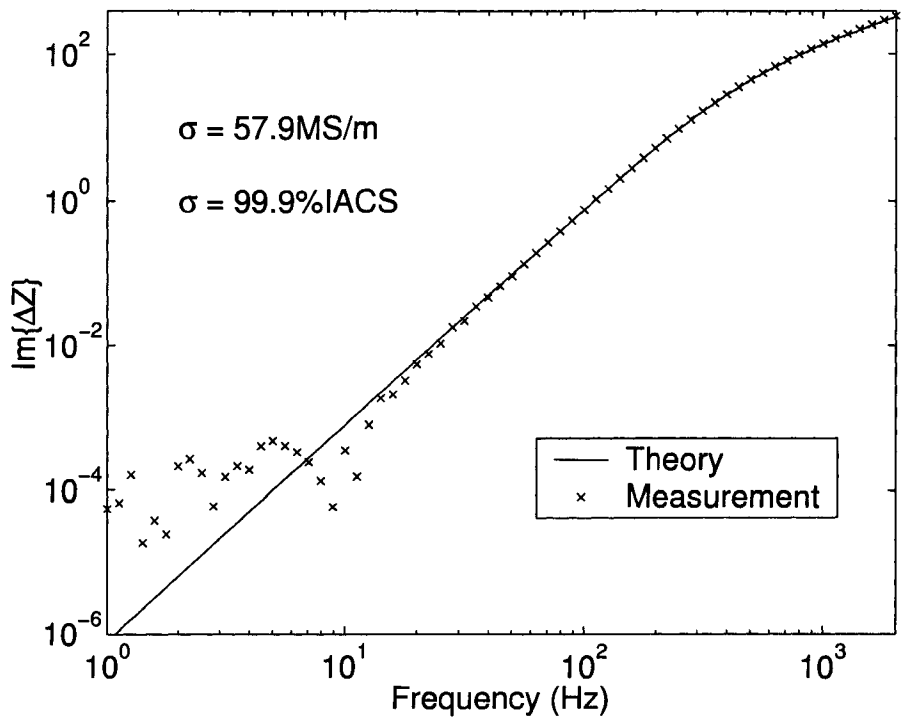

Figure 4.5 Imaginary part of the eddy current driver pickup coils mutual impedance measurements on copper rod.

of mutual impedance from the fitted parameters. Only the imaginary part is used for data fitting.

The measured eddy current mutual impedance variation with frequency on the untreated steel rod is shown in Figure 4.6 and 4.7.

4.4.5 Case Hardened Cylindrical Steel Rod

In the idealized case hardened cylindrical steel rod, the rod is uniform in the axial direction. It has a homogeneous substrate surrounded by a homogeneous surface layer of uniform thickness.

The driver pickup coils mutual impedance is used to estimate the three unknown parameters for the case hardened layer, conductivity σ_2, permeability μ_2 and thickness d. The conductivity σ_1 and permeability μ_1 for the substrate layer is estimated by using mutual impedance

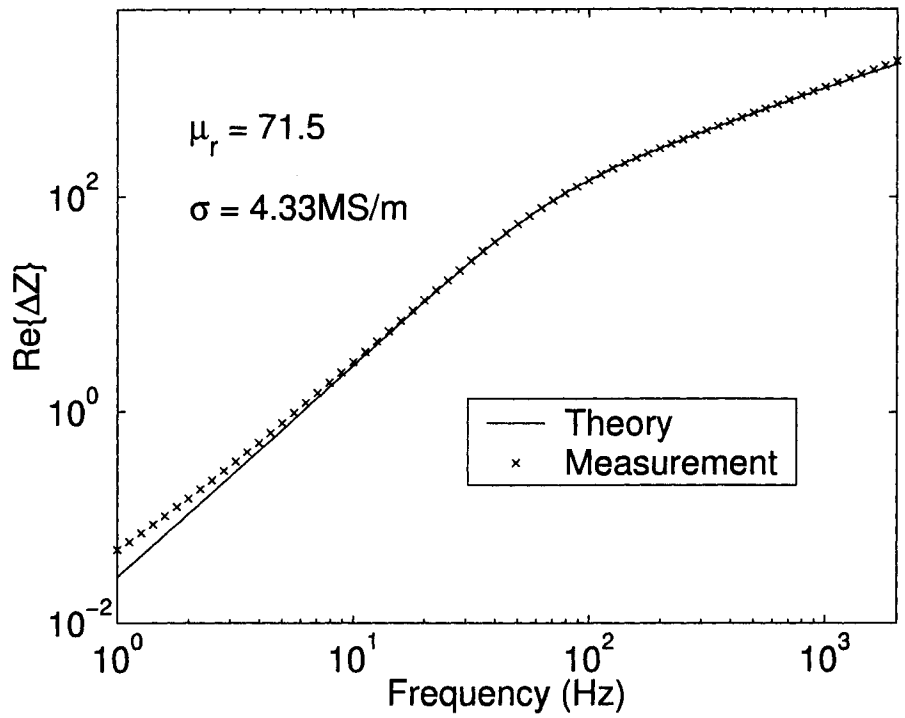

Figure 4.6 Real part of the eddy current driver pickup coils mutual impedance measurements on untreated steel rod

measurements on untreated steel rod.

4.5 Results

The same set of six cylindrical rod specimens from ACPD measurements are used in the eddy current driver pickup coils mutual impedance measurements. Their dimensions are shown in Table 3.1.

The driver pickup coils mutual impedance change ΔZ due to those case hardened cylindrical steel rods are normalized by the mutual impedance change ΔZ_0 due to the untreated rod.

$$Z_n = \frac{\Delta Z}{\Delta Z_0} \tag{4.5}$$

$$X_n = \frac{Im\{\Delta Z\}}{Im\{\Delta Z_0\}} = \frac{\Delta X}{\Delta X_0} \tag{4.6}$$

$$R_n = \frac{Re\{\Delta Z\}}{Re\{\Delta Z_0\}} = \frac{\Delta R}{\Delta R_0} \tag{4.7}$$

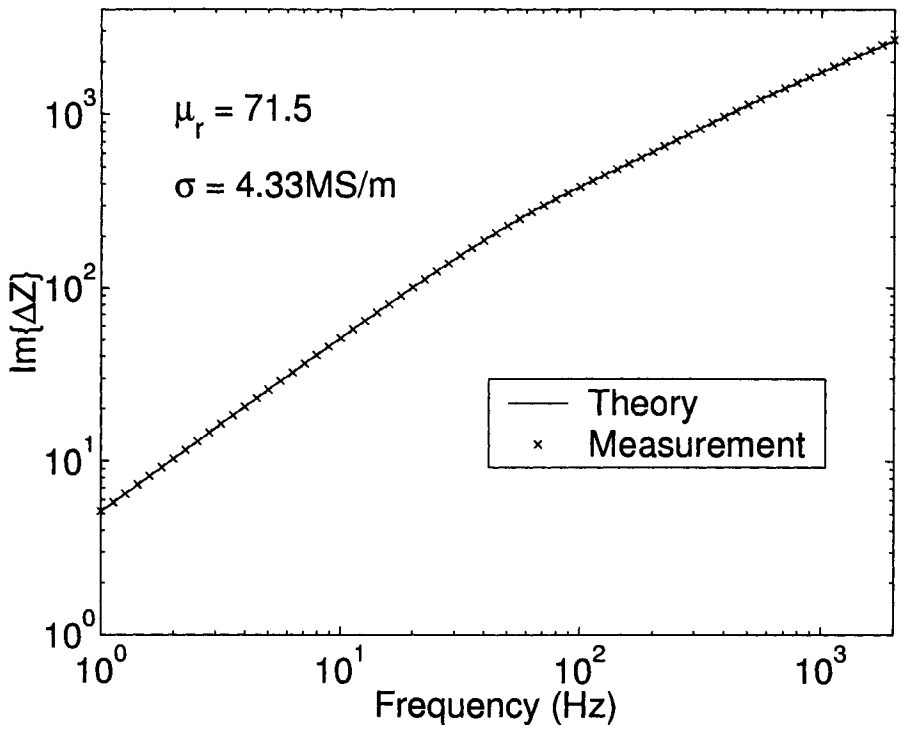

Figure 4.7 Imaginary part of the eddy current driver pickup coils mutual impedance measurements on untreated steel rod

Where ΔZ_0 is from equation (4.2) due to the untreated steel rod, ΔZ is from equation (4.2) due to the case hardened steel rod. Data fitting between driver pickup coils measurements data and the theoretical model prediction is based on the normalized mutual impedance change in equation (4.5). For the mutual impedance change, the amplitude of imaginary part is much bigger than the amplitude of the real part. In such way only the imaginary part of the normalized mutual impedance change is used for data fitting. It is described in equation (4.6). Data fitting diagram is shown in Figure 4.8. The real part of the normalized mutual impedance change in equation (4.7) is shown in Figure 4.9.

From Figure 4.8, the data fitting for the imaginary part is reasonably good. From Figure 4.9, there is some big variation in the low frequency part (from 1 Hz to 100 Hz) for the real part. It is because the mutual impedance change in low frequency part is very small. For example, when the working frequency is 10 kHz, the mutual impedance is about 5.57 kOhm

in free space, it is about 11.65 kOhm with steel rods. The mutual impedance change is about 5 kOhm. But when the working frequency is 1 Hz, the mutual impedance is about 0.45 Ohm in free space, it is about 5.29 Ohm with steel rods. The mutual impedance change is about 5 Ohm. It is very difficult to measure the impedance change very accurately at low frequency. This kind of low frequency error is hidden when the mutual impedance change is shown in absolute terms for the measured frequency range. It is visible when normalized data is shown.

The fitted five unknown parameters of each specimen are shown in Table 4.2. They are substrate layer conductivity σ_1 and relative permeability μ_1, surface layer thickness d, conductivity σ_2 and relative permeability μ_2. Data fitting error is the summation of the squared difference between the imaginary part of the normalized mutual impedance change data and theoretical calculation over frequency.

Table 4.2 The results shown are surface layer and substrate parameters found by data fitting between eddy current mutual impedance measurements and the theoretical model prediction. Effective case depth data are from the hardness profile in Figure 3.2

	substrate layer		case hardened layer			Data fitting	case depth
Rods	μ_1	σ_1(MS/m)	μ_2	σ_2(MS/m)	d(mm)	error	(mm)
Copper	1.0	57.9	N/A	N/A	N/A	2.62×10^{-4}	N/A
untreated	71.5	4.33	N/A	N/A	N/A	2.29×10^{-3}	N/A
0.5 case	71.5	4.33	44.2	3.19	0.31	4.23×10^{-4}	0.38
1.0 case	71.5	4.33	66.9	4.92	1.47	5.02×10^{-4}	1.03
1.5 case	71.5	4.33	65.1	4.82	2.21	1.77×10^{-3}	1.49
2.0 case	71.5	4.33	59.4	4.34	2.23	3.41×10^{-3}	1.90

4.6 Discussion

The surface layer and substrate parameters found by data fitting between eddy current driver pickup coils mutual impedance measurements and the theoretical model prediction are shown in Table 4.2. The measured case hardened surface layer depth is in reasonable agreement with the effective case depth from the hardness profile. Several factors have influence upon the agreement between them.

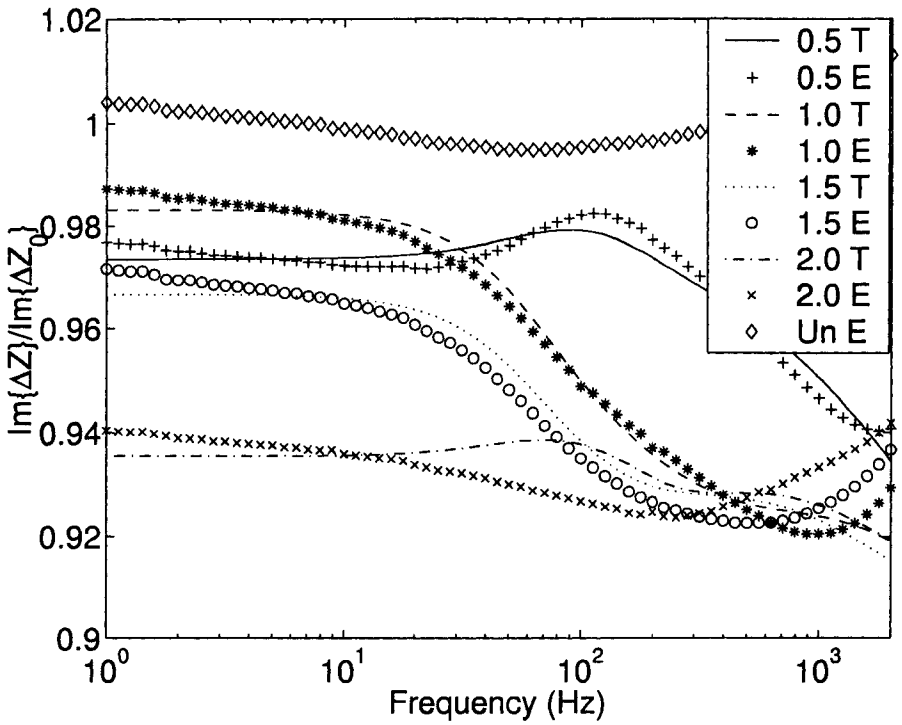

Figure 4.8 Imaginary part of the normalized eddy current driver pickup coils mutual impedance change on case hardened cylindrical steel rods. "T" stands for theoretical calculation results, "E" stands for experiment measurements data. "Un" is for untreated steel rod. Numbers in the legend are the nominal case depth in mm.

4.6.1 Effective Case Depth

As discussed in Chapter 3, effective case depth depends on the hardness criterion and how the transition zone changes between the case hardened steel and softer base material. It is reasonable that the accuracy of the eddy current driver pickup coils mutual impedance measurements system is also dependent on how the actual transition zone changes between case hardened surface layer and the substrate layer. It is expected that the eddy current measurements result is more accurate if the hardness changes very quickly.

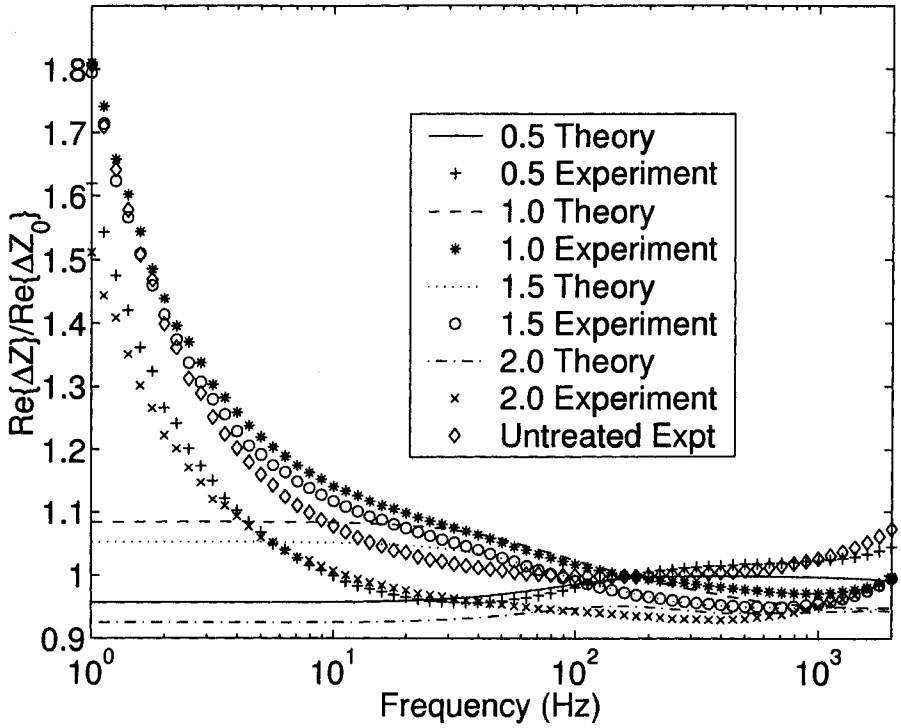

Figure 4.9 Real part of the normalized eddy current driver pickup coils mutual impedance change on case hardened cylindrical steel rods. Numbers in the legend are the nominal case depth in mm.

4.6.2 Measurements Errors

Possible measurements errors include the cylindrical rod dimensional size error, the induction voltage error from the pickup coil , the voltage error across the resistor, the resistance value error of the current monitor high precision resistor, driver and pickup coil dimensional size error, and the mutual impedance error between the driver and pickup coil in free space and with cylindrical rods.

Digital caliper is used to measure the cylindrical rod, driver and pickup coils dimensional sizes. The digital caliper has accuracy of 0.01 mm. Compared with the actual rod diameter, the relative measurement error is less than 0.02%. For the driver and pickup coils dimensions, the relative measurement error is less than 0.01%. The high precision resistor is measured by using Agilent 4294A precision impedance analyzer from 40 Hz to 40 kHz. The resistance

variation with frequency is less than 1%. SR830 DSP lock-in amplifier is used to measure the voltage values.

A big value (compared with the DC resistance value of the driver coil) resistor is connected into the driver coil circuit. The reason to use a big value resistor is to try to keep the driver current constant, or the current will not change very much during the whole multi-frequency measurements.

4.6.3 Comparison between the ACPD and Eddy Current Results

Compare the measured results from ACPD and eddy current method in Table 4.2 and Table 3.2. It is found that the case depth values from these two different methods are not exactly the same to each other. And the electric conductivity and permeability values are different. Take the conductivity and relative permeability for the untreated steel rod as the example. In the ACPD measurement results, the conductivity is 4.84 MS/m, the relative permeability is 64.2. In the eddy current driver pickup coils mutual impedance measurement results, the conductivity is 4.33 MS/m, the relative permeability is 71.5. There is about 10% difference between them. The conductivity from ACPD method is about 10% bigger than the value from the eddy current method. But the permeability from ACPD method is about 10% smaller than the value from the eddy current method. The case depth results from these two methods are close to each other within 10% difference. Take the nominal case depth 1.0 mm steel rod as the example. The case depth from ACPD method is 1.62 mm, it is 1.47 mm from the eddy current method. The difference between them is within 10%. Comparison of case depth from these two methods and hardness profile is shown in Figure 4.10.

It should be recognized that the relationship between case depths as determined by different methods can vary extensively. Factors affecting this relationship include case characteristics, parent steel composition, quenching conditions, and others [1].

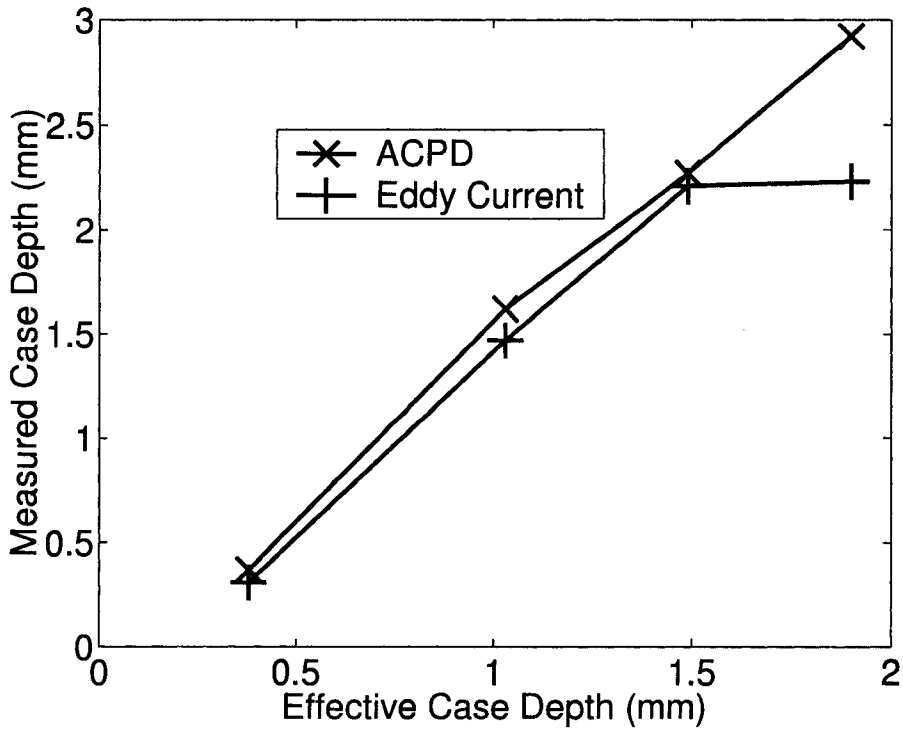

Figure 4.10 Comparison of the case depth from ACPD method and eddy current method. The effective case depth is got from hardness profile which is shown Figure 3.2.

4.6.4 End Effect

The cylindrical rod is infinite long in the theoretical model [62]. The cylindrical rod cannot be infinite long in reality. The length of six cylindrical rod specimens (see Table 3.1) is about 50 cm. The length of the drive and pickup coils is about 2 cm. The rods are much longer than the coils. In the eddy current induction measurement system, this assumption is approximately satisfied in some sense. For the actual measurement, the coils are always stay at the center of the cylindrical rods.

For the time being it is not clear whether there is some end effect on the measurement of induced voltage from the pickup coil and how big the end effect is if there is any. At present no experiment is done to check this issue. It should be pretty straightforward to check it. Since the coils length is much smaller than the rod length, it is not difficult to measure the induced

voltage on different positions along the rods.

To check the end effect, measurements should be made at a number of different positions. At the beginning, the drive and pickup coils stay at one end of the cylindrical rod. In practice the coils edge can be lined with the rod end. The AC current through the drive coil and its working frequency should be kept unchanged. All other system parameters should also be kept the same. Then the coils are moved to the other end of the rod step by step. Comparison of these measured induced voltage values can show the end effect. It is expected that the mutual impedance between the drive and pickup coils should be symmetrical with respect to the coils position on the rod.

To take care of the end effect, a new theory is developed on the finite length rod with coaxial encircling coil [66]. At this moment, no experiment data are available to check this theory. The new theory can handle both homogeneous rod and and multi-layer rod. This new theory will be used to analyze the mutual impedance change data on drive and pickup coils with cylindrical rod. The experiment system is under construction. It is very close to be completed at this time. Every effort is made to minimize all possible measurement errors on this new experimental system. Hopefully some good measurement data will be got in the near future. And better agreement will be observed between the results from ACPD method and the results from eddy current induction method.

CHAPTER 5. ACPD MEASUREMENTS ON METAL PLATE

5.1 Introduction

ACPD method is extended to the metal plate. It includes both half space plate and finite thickness plate. The AC current is injected into and extracted from the metal plate. The current inward/outward probes have point contact with the metal plate. Two additional point contact probes are used to get the potential drop between these two points on the plate surface. Measurement data are compared with theoretical calculation results and very good agreement is observed.

5.2 Basic Assumption

The metal plate is assumed to be homogeneous and isotropic. The width and length of the plate are assumed to be big enough so it can be treated as infinite plate. Its thickness is uniform for the whole plate. If the thickness of the plate is very big compared with the skin depth for the working frequency, it can be treated as half space plate. Otherwise it is treated as finite thickness plate. Skin depth is shown in equation (2.1). For specified metal material, the electrical conductivity and magnetic permeability are assumed to be constant within the whole measurement frequency. The skin depth decreases as the working frequency increases.

5.3 Theory

The ACPD theory on finite thickness metal plate is described in detail in the appendix A. The electric field is shown in equation (A.14) and (A.15). The potential drop along the metal plate is shown in equation (A.20). The electric field theory for a half space conductor with

alternating current injected & extracted by point contacts is published in [65].

5.4 Experiment

The ACPD measurements system on metal plate is very similar to the ACPD experiment system on cylindrical rod. The same KEPCO bipolar operational power supply/amplifier is used as the power supply. The AC sinusoidal signal from the internal function generator of the SR830 DSP lock-in amplifier is connected to the current programming input of the KEPCO power supply. The power supply works as a current drive source. It provides constant current to the metal plate. The same kind of high precision resistor is used to monitor the AC current to the metal plate. It has 1% accuracy resistance value within the whole ACPD measurements frequency range (from 1 Hz to 10 kHz). The voltage across the resistor is measured by the SR830 DSP lock-in amplifier. The same GSS-8-7-G probes are used to get potential drop between two points on the metal plate surface. The same kind of 36 AWG copper wire is used to connect the two potential drop probes. Two wires are used to connect the two probes separately. They are drawn to the middle point of the two probe head points then are twisted together. The gap between the tiny copper wire and the metal plate surface is very small but not negligible. This arrangement is adopted to keep the self inductance of the potential drop measurement circuit as small as possible. The potential drop between these two probes is also measured by the SR830 DSP lock-in amplifier. Again one simple switch is needed since two voltage signals are measured by one lock-in amplifier. This switch is almost the same as the switch in the ACPD rod measurement system. The control signal of this switch is from the auxiliary analog output of the lock-in amplifier.

The AC sinusoidal signal is from the internal function generator of the lock-in amplifier. The frequency range of the internal function generator is from 0.001 Hz to 102 kHz. The actual ACPD measurement frequency on metal plate is from 1 Hz to 10 kHz.

The gap between the tiny copper wire and the metal plate surface is very small. In the ACPD theory on metal plate, the distance between the metal plate surface and the potential drop connection wire is considered (see Figure A.1). The contribution from this small close cir-

cuit loop is added to the potential drop in theory. This small distance is not measured directly. It is got by data fitting between the measurement data and theoretical model computation.

Two SJ-0-B-5.5-DG-S probes from Interconnect Devices Inc. are used to inject current into and extract current from the metal plate. The probe is spring loaded. Its plunger is made of steel, gold plated over nickel. The probes keep point contact with the metal plate. Two current-carrying wires are soldered to the two current inward/outward probes. These two current probes and their connection wires are fixed in position by two separate plastic blocks. The plastic blocks have one through receptacle hole to hold the current probes. The probe is longer than the through hole such that the probe head extends beyond the block bottom surface by about 5 mm. The other end of the probe extends beyond the block top surface. The recommended travel distance of the current probe is about 5 mm. The plastic blocks are fixed to one position by PVC tape. When appropriate pressure is applied to the plastic block, the current probe head will trave about 5 mm distance and come to the block bottom surface, which is in tight contact with the metal plate surface. Two vertical wood sticks are used to apply some pressure to the plastic blocks. The probes and their wires are normal to the metal plate surface for as far as practically possible. In actual experimental system, it is about 40 cm. Two plastic tubes are used to guide the current connection wires such that the current is perpendicular to the plate surface. The effect of moving the wires beyond this distance is observed to have negligible influence on the potential drop measurements. It is very important to keep the current perpendicular to the metal plate surface. In such way the assumption in the ACPD theory on metal plate is approximately satisfied as well as possible.

The same GSS-8-7-G probes are used to get potential drop between two points on the metal plate surface. These two potential drop probes are mounted by one plastic block. The probe length is shorter than thickness of the plastic block. Two receptacle holes are drilled at the block bottom surface. The receptacle hole depth is a little bit shorter than the whole length of the probe when it is under no any pressure. So the probe head will come out a little bit from the block bottom surface if no pressure is applied to the probe. The probe is spring loaded. The probe head should travel the recommended distance to get best connection result. After

the probe head travels such distance, it will come to the block bottom surface exactly. Two 36 AWG copper wires are soldered to the two probes head. They are drawn to the middle point of the two probes and twisted together. They are guided out from the block bottom surface to the top surface via a center through hole. This plastic block is mounted to the stationary probe holder of the two dimensional scanning system. Plastic machine screws are used to mount the small probe block to the big probe holder.

In ACPD theory on metal plate, the two current probes are put in the x axis. The middle point between them is set to the coordinate origin. The two current probes are symmetrical to the coordinate origin. In the theory calculation, the two potential drop measurement points can be anyway on the plate surface. For example, it is not necessary that these two potential drop probes are symmetrical to the origin. And they can have different y position, of course. To simplify the experiment measurement, it is a good start point to set these two potential drop points with the same y coordinate because both of them are mounted to one plastic block.

The metal plate is mounted to the moving part of a two dimensional scanning system. The scanning system is from Parker Automation Daedal Division. The scanning system has very high movement resolution. The metal plate can move in two perpendicular directions. The two current inward/outward probes are kept fixed with the metal plate. When the metal plate moves, it will move the current probes with it because they are bound together. The two potential drop measurement probes are mounted to the stationary probe holder of the scanning system. The potential drop probes will not move. Two one-inch thick plastic plates with the same width and length as the metal plate sample are bound together. They are put between the metal plate and the moving support plate of the scanning system. Such kind of arrangement will help the ACPD measurement system on metal plate to avoid electromagnetic interference from the scanning system and its support desk which are made of metal material.

A computer program is developed to control the lock-in amplifier and control ACPD measurements automatically. A GPIB bus is used to connect the lock-in amplifier to the computer. This computer program also control the switch in the ACPD measurement system. At the same time this computer program control the movement of the two dimensional scanning system.

The control program sends commands to the lock-in amplifier via GPIB bus to set the right AC signal output from the internal function generator. The voltage value measured by the lock-in amplifier is sent back to the control program. The control program sends commands to the two dimensional scanning system via RS232 serial port to control the metal plate movement.

5.4.1 Brass Plate

A brass plate is used for the ACPD measurement on metal plate experiment. When it is ordered from the manufacturer, it is quarter inch thick, two feet long and two feet wide. It is found that too many scratches on its surface. The scratches can be treated as crack in practice. ACPD is established method to measure the crack depth. One tentative measurement is made on this raw brass plate. It is found that the data is very bad. So the brass plate is sent out to remove the surface scratch. Both side of the brass plate are precision ground. The surface scratches are removed. Of course the brass plate is thinner than before since some material must be removed.

The conductivity of the brass plate is measured by using MIZ-21A eddy current instrument from Zetec Inc. Its relative permeability is assumed to be one.

At the first step frequency measurement is made with stationary probes. The four probes (two current probes and two potential drop probes) are fixed on their own position on the plate surface. They are put in one straight line. The middle point between the two potential drop probes is the coordinate origin. The two current probes are also symmetrical to the coordinate origin. The working frequency of the AC current changes from 1 Hz to 10 kHz. It increases in the logarithmic scale. There are twenty different frequency points per decade.

Initial measurement results show that the measurement data are not stable from one measurement to the other. The two potential drop probes are connected to the two input ports of the lock-in amplifier. The lock-in amplifier is set to differential input mode. It is found that the common mode rejection errors exist for this kind of measurement arrangement. It is very common for the operational amplifier when it works in differential input mode if the two input signals are very close to each other. This is exact what happen to the ACPD measurement on

metal plate. The potential drop between the two potential drop probes are very small, usually it is about several microvolt. In other words, the potential of the two potential drop probes are very close to each other. It is found that the common mode rejection error is almost 50% of the potential drop signal. It is very important to remove the common mode rejection error from the measured potential drop value. A simple method is used to solve this problem. The principle is shown below.

Assume that two potential drop points are A and B. Their potential are V_A and V_B. Then the potential drop between points A and B is V_{AB}.

$$V_{AB} = V_A - V_B \tag{5.1}$$

The potential drop between points B and A is V_{BA}.

$$V_{BA} = V_B - V_A \tag{5.2}$$

Obviously these two potential drop should have the same amplitude and opposite sign if no other measurement error exists.

$$V_{BA} = -V_{AB} \tag{5.3}$$

From the measured data, these two potential drop have completely different amplitude. It is strong evidence that the actual measured potential drop includes some common mode rejection error V_{cmr}. Equation (5.1) and (5.2) are modified to include the common mode rejection error.

$$V_{AB} = V_A - V_B + V_{cmr} \tag{5.4}$$

$$V_{BA} = V_B - V_A + V_{cmr} \tag{5.5}$$

By subtract equation (5.5) from equation (5.4),

$$V_{AB} - V_{BA} = 2\,(V_A - V_B) \tag{5.6}$$

The true potential drop value is got from these two measurement values.

$$V_A - V_B = \frac{V_{AB} - V_{BA}}{2} \tag{5.7}$$

Table 5.1 Experimental parameters for brass plate. S is the half distance between two current probes. p and q are the two pickup probes position. l is the distance between the potential drop measurement circuit and the conductor plate surface.

brass plate		probes	
conductivity, σ (MSm^{-1})	16.2 ± 0.3	S (mm)	25.44 ± 0.3
permeability, μ_r	1	p (mm)	-10.15 ± 0.01
thickness, T (mm)	5.66 ± 0.01	q (mm)	10.15 ± 0.01
horizontal dimensions (mm)	615 × 616	l (mm)	0.15 (fitted value)

The common mode rejection error can also be got from these two measurement values.

$$V_{cmr} = \frac{V_{AB} + V_{BA}}{2} \tag{5.8}$$

The common mode rejection error is dependent on the two input signals potential value and their difference, the working frequency and the amplifier itself. The AC current is injected into the metal plate by one current probe. Then the AC current is extracted out of the metal plate by the other current probe. No AC current flows through the two potential drop probes. To measure the V_{AB} value, the two potential drop connection wires are connected to the switch in one direction. Then the two wires are connected to the switch in reverse direction to measure the V_{BA} value. All other measurement system conditions are unchanged. It is reasonable to assume that the two common mode rejection error items in equation (5.4) and (5.5) are the same because all other measurement system conditions are unchanged.

The geometry dimensions and conductivity for the brass plate are given in Table 5.1. ACPD frequency measurements are made with stationary probes on brass plate. The measured potential drop variation with frequency are compared with the theoretical calculation. The results are shown in Figure 5.1 and 5.2. Excellent agreement is observed between the measurement data and theoretical computation.

At the second step, ACPD scan measurement is made with fixed working frequency. The four probes (two current probes and two potential drop probes) stay in one straight line. They have the same y coordinate position. The two current probes are fixed on their own position on the plate surface. They are symmetrical to the coordinate original point. The two potential

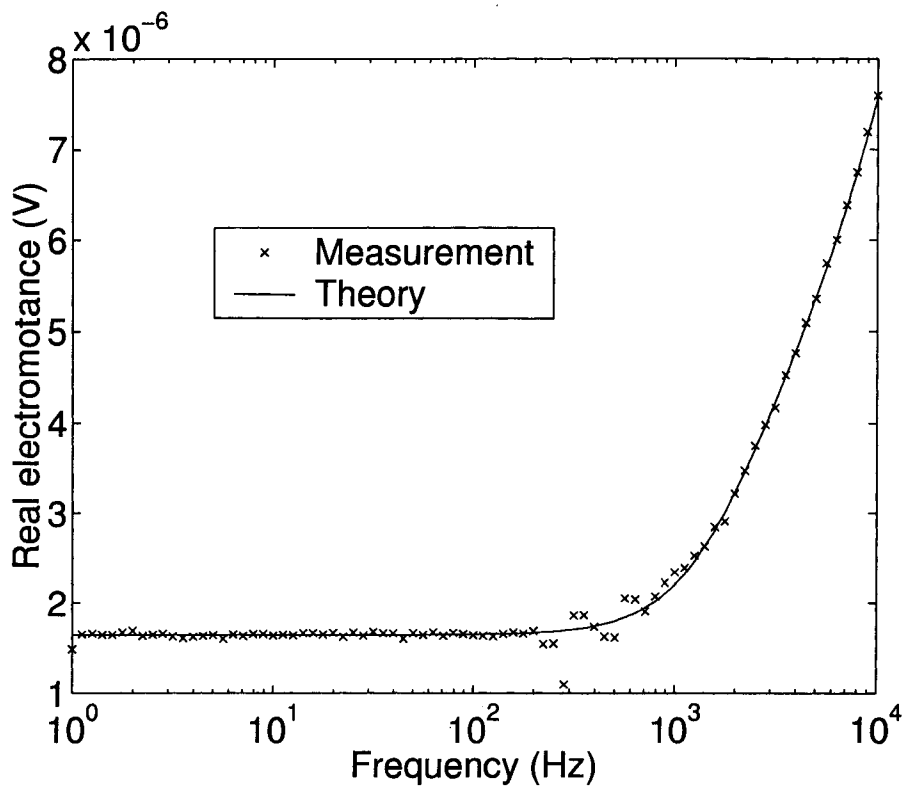

Figure 5.1 Real part of the ACPD frequency measurements on a brass plate. Measurement frequency is from 1 Hz to 10 kHz.

drop probes move between the two current probes from one side to the other. The plastic block that hold the two potential drop probes is moved very close to the plastic block that hold one current probe. The distance between the side surface of these two plastic blocks is very small such that the potential drop probe is moved as close to the current probe as possible in practice. Great care must be given that these two plastic blocks do not touch with each other. Otherwise the current probe will be pushed to change its position. The distance between the two current probes will be changed. Then the potential drop block moves to the other current probe step by step. The distance between the two potential drop probes is fixed during the scan movement because they are put into one support block. At each scan position, the working frequency of the AC current is set to 10 Hz first. The two voltage signals (voltage across the precision resistor and the potential drop voltage) are measured by the lock-in amplifier. Ten

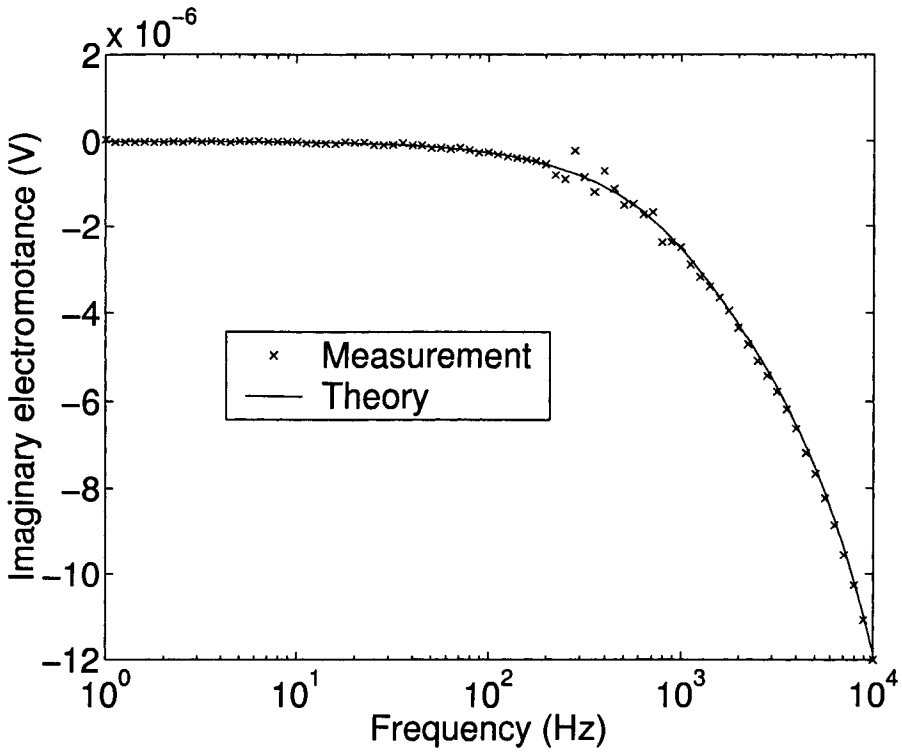

Figure 5.2 Imaginary part of the ACPD frequency measurements on a brass plate. Measurement frequency is from 1 Hz to 10 kHz.

sets of data are taken sequentially. Then the working frequency is set to 10 kHz. Ten sets of data on those two voltage signals are taken sequentially. After that, the scan system goes to the next scan point. The average of the ten measurement data sets is used for data analysis to reduce random error.

Great care is given to make scan measurement. The potential drop probe is very sharp at its head. It is kept point contact with the metal plate surface. Its plunger is made of beryllium copper, gold plated over nickel. When the metal plate moves, it is very easy for the potential drop probes to leave heavy scratch and then damage the metal plate surface. A special small hat is made of tin material. Tin is one kind of soft metal material. Its hardness is relative small. This tin hat is put on top of the probe head to protect the metal plate surface. Unfortunately it is found the tin head still leave scratch on the brass plate and its surface is damaged. It is found that one straight line scratch is left between the two current probe

blocks. Considering this kind of damage, no other two dimensional scan is made. For example, the two potential drop probes can have different y position from the two current probes. Or they can be anywhere on the metal plate surface in theory.

The measured potential drop variation with probe position are compared with the theoretical calculation. The results are shown in Figure 5.3, 5.4, 5.5 and 5.6. Very good agreement is observed between the measurement data and theoretical computation when the frequency is 10 kHz (Figure 5.5 and 5.6). For the 10 Hz measurement, the agreement between experiment and theory is remarkably good for the imaginary part (Figure 5.4), given that the magnitude is so small (about 10 nanovolt order). Poorer agreement for the real part is due to the fact that the theory is far-field (Figure 5.3). At 10 Hz, near field effects are observed. This part on theoretical calculation will added in the future.

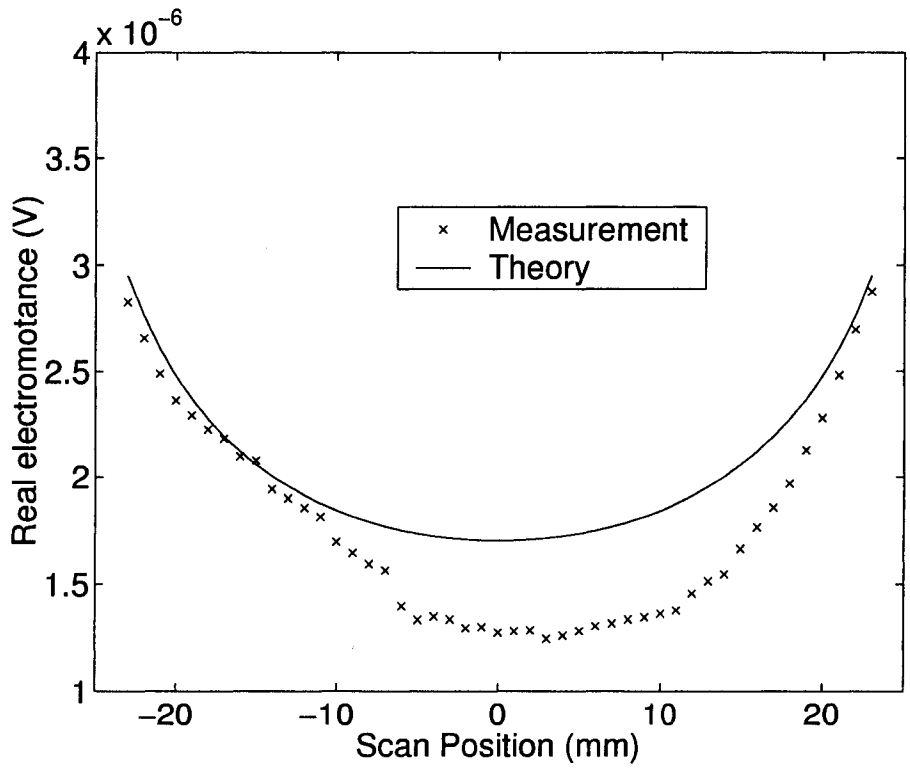

Figure 5.3 Real part of the ACPD scan measurements on a brass plate. Measurement frequency is 10 Hz.

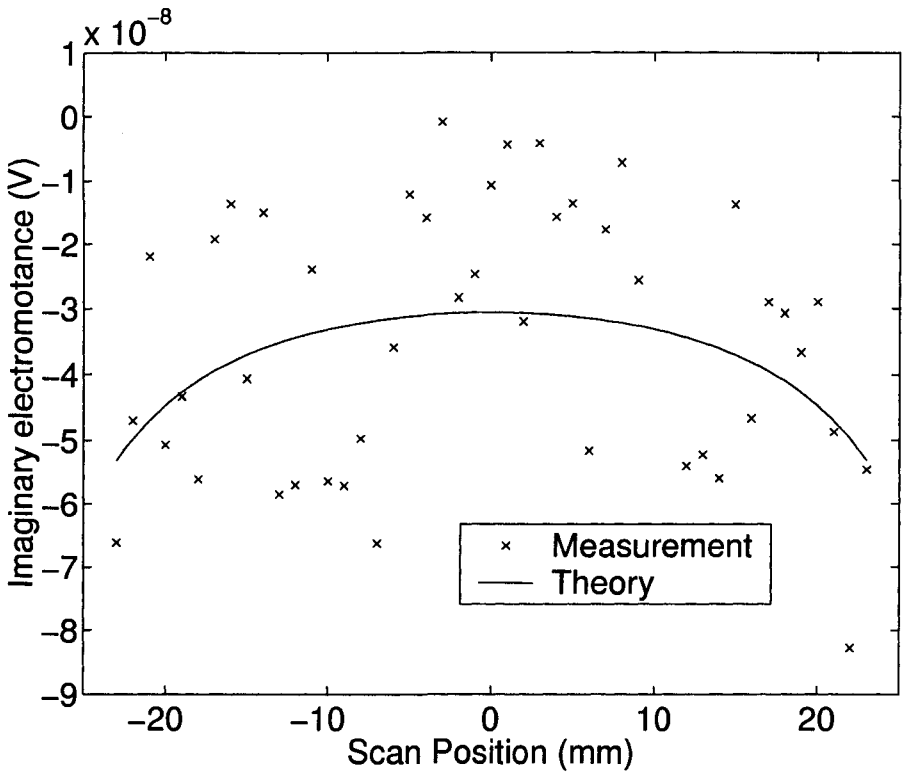

Figure 5.4 Imaginary part of the ACPD scan measurements on a brass plate. Measurement frequency is 10 Hz.

5.4.2 Aluminum Plate

ACPD measurements on metal plate are made on different metal material. An aluminum plate from McMaster-Carr is used for measurements. It is alloy 7075 aluminum (corrosion-resistant aircraft-grade). Exceptionally strong and still lightweight, this alloy is one of the hardest and strongest aluminum alloys and is perfect for high-stress parts. It is nonmagnetic. It is one inch thick, two feet wide and two feet long. It is precision ground at both sides.

The measurements on aluminum plate are almost the same as the measurements on brass plate. The two current probes are the same, but the distance between them is made a little bit shorter. The potential drop probes are the same. Other conditions are the same. Only frequency measurements are made on this aluminum plate. The common mode rejection errors are removed from the measurements data by the same method as applied on the brass plate.

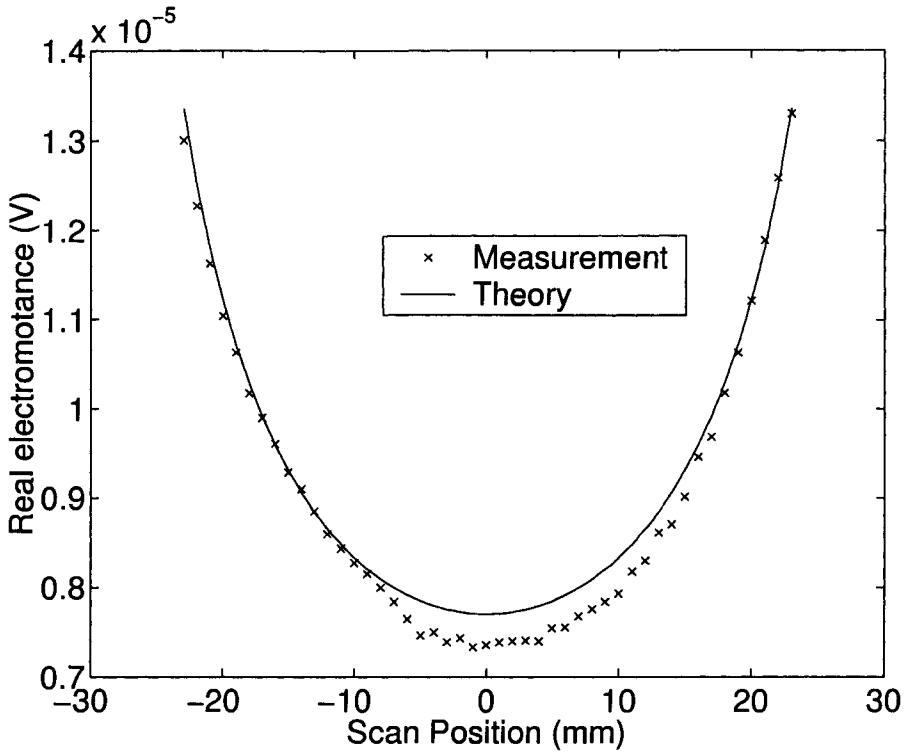

Figure 5.5 Real part of the ACPD scan measurements on a brass plate. Measurement frequency is 10 kHz.

The electrical conductivity of the aluminum plate is measured by using MIZ-21A eddy current instrument from Zetec Inc. Its relative permeability is assumed to be one. The geometry dimensions and conductivity for the aluminum plate are given in Table 5.2. ACPD frequency measurements are made with stationary probes on this aluminum plate. The measured potential drop variation with frequency are compared with the theoretical calculation. The results are shown in Figure 5.7 and 5.8. Very good agreement is observed between the measurement data and theoretical computation.

5.4.3 Carbon Steel Plate

A carbon steel plate from McMaster-Carr is used for ACPD measurements. It is grade C-1018 low-carbon steel. This fine-grained, vacuum-degassed steel has manganese so it is stronger and harder than other low-carbon steels. Easily machined, it has great weldability

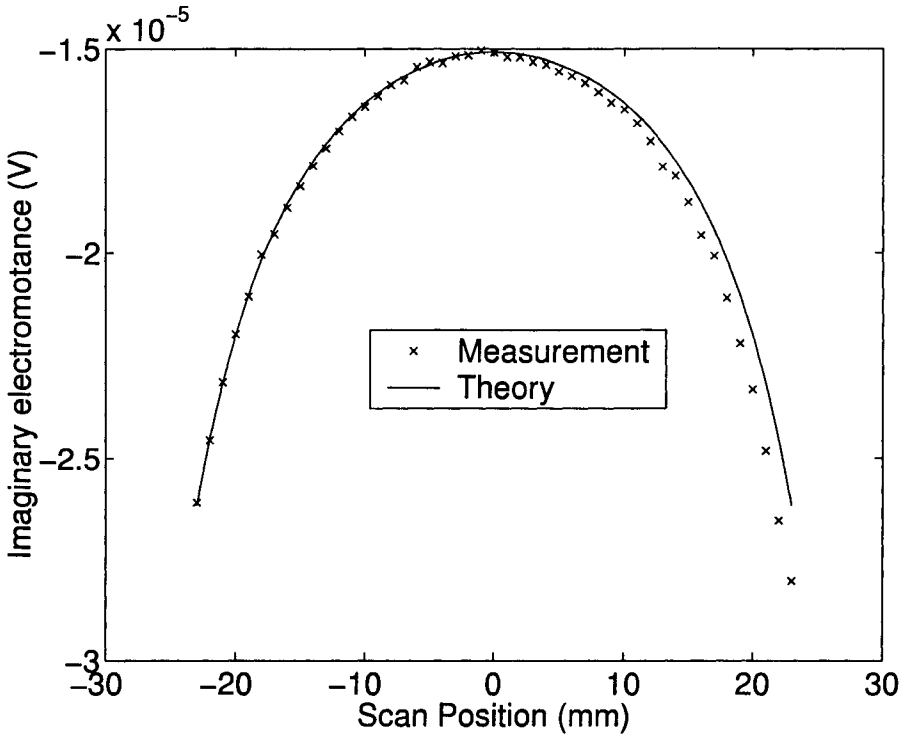

Figure 5.6 Imaginary part of the ACPD scan measurements on a brass plate. Measurement frequency is 10 kHz.

and a uniform response to case hardening. This plate is quarter inch thick, two feet wide and two feet long. It is precision ground at both sides. Only frequency measurements are made on this carbon steel plate.

The geometry dimensions and electromagnetic properties for the carbon steel plate are given in Table 5.3. ACPD frequency measurements are made with stationary probes on this carbon steel plate. The measured potential drop variation with frequency are shown in Figure 5.9 and 5.10.

The electric conductivity and magnetic permeability can not be measured directly because it is magnetic material. For the time being, the conductivity and permeability are got by data fitting. In the low frequency part, the potential drop calculation in theory is dependent on the plate conductivity, not on its permeability. The conductivity is chosen to fit the low frequency measurement data. This kind of data fitting is not very strictly accurate because it

Table 5.2 Experimental parameters for aluminum plate. S, p, q and l have the same meaning as in Table 5.1.

aluminum plate		probes	
conductivity, σ (MSm^{-1})	19.27 ± 0.3	S (mm)	25.44 ± 0.3
permeability, μ_r	1	p (mm)	-10.15 ± 0.01
thickness, T (mm)	25.37 ± 0.01	q (mm)	10.15 ± 0.01
horizontal dimensions (mm)	615 × 616	l (mm)	0.15 (fitted value)

Table 5.3 Experimental parameters for carbon steel plate. S, p, q and l have the same meaning as in Table 5.1.

carbon steel plate		probes	
conductivity, σ (MSm^{-1})	5.1 (fitted value)	S (mm)	25.44 ± 0.3
permeability, μ_r	110 (fitted value)	p (mm)	-10.15 ± 0.01
thickness, T (mm)	6.297 ± 0.01	q (mm)	10.15 ± 0.01
horizontal dimensions (mm)	615 × 619	l (mm)	0.15 (fitted value)

is judged by human eye on the data curve. In this step the conductivity value is changed to fit the measurement data. So the fitted conductivity is just one approximate value. In the high frequency part, the potential drop calculation is dependent on conductivity and permeability. Since the conductivity value is got by data fitting with low frequency data, only the permeability is unknown. It is got by data fitting with high frequency data. Again, the data fitting is not very strictly accurate because it is judged by human eye. The fitted conductivity and permeability value are shown in Table 5.3.

It is observed that the agreement between the experiment and theory on the carbon steel plate is not very good. Some possible reasons are explained here. As discussed above, the electric conductivity and magnetic permeability value are not very accurate. These two parameters are very important to theoretical calculation. This carbon steel plate is precision ground. The grinding service is cold finished. As discussed in chapter 3, it should be annealed and demagnetized before any measurement can be done. Because of its big size, it can not be annealed in Iowa State University. And the industry would not accept the process order for just one piece. It can not be demagnetized in one step because of its big size. One possible method is to demagnetize it locally at different points.

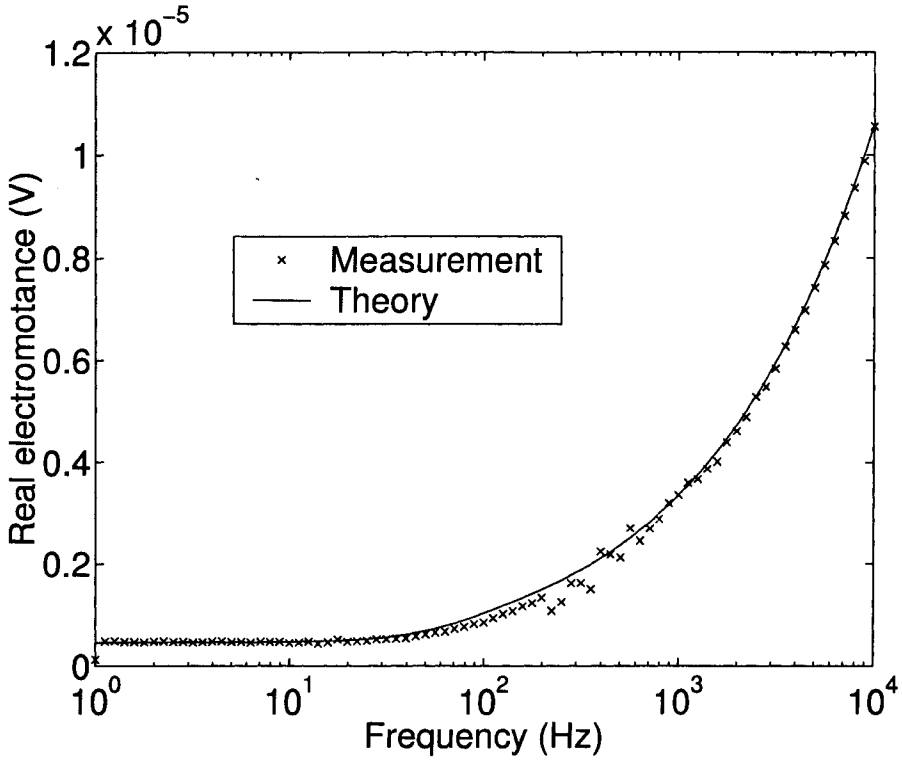

Figure 5.7 Real part of the ACPD frequency measurements on an aluminum plate. Measurement frequency is from 1 Hz to 10 kHz.

The ACPD frequency measurements with stationary probes on this carbon steel plate will be repeated after it is demagnetized locally. Hopefully the result will be something better.

5.4.4 Stainless Steel Plate

A stainless steel plate from Mcmaster-Carr is used for ACPD measurements. It is type 316 stainless steel. High nickel and molybdenum content can provide excellent resistance to corrosion and pitting. Type 316 has good weldability and higher strength then type 304 at elevated temperatures. Yield strength is $35 - 85$ ksi. Hardness is $160 - 235$ Brinell. It meets ASTM A240 specifications. It is quarter inch thick, eighteen inches wide and eighteen inches long. It is precision ground at both sides.

For this stainless steel plate, frequency measurements with stationary probes are made at the first step. At the second step ACPD position scan measurement with fixed working

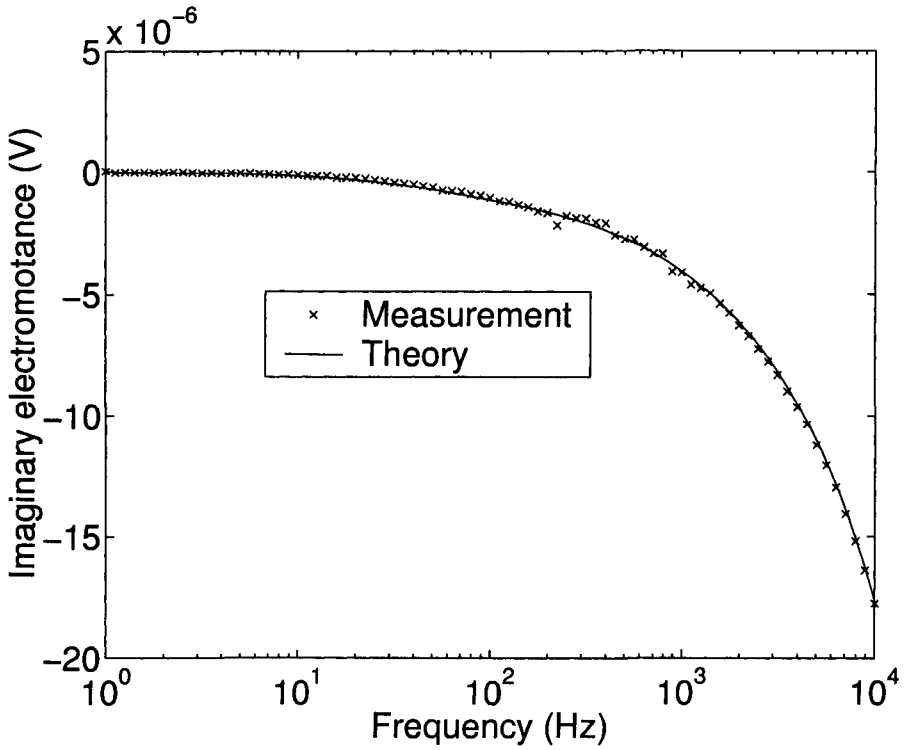

Figure 5.8 Imaginary part of the ACPD frequency measurements on an aluminum plate. Measurement frequency is from 1 Hz to 10 kHz.

frequency will be made in the near future.

The geometry dimensions and electrical conductivity and magnetic permeability for this stainless steel plate are given in Table 5.4. The electrical conductivity value is got by data fitting with coil impedance measurements on this stainless steel plate. Detailed description is shown in next part of this section.

The measured potential drop variation with frequency on stainless steel plate are shown in Figure 5.11 and 5.12. Very good agreement is observed between the measurement data and theoretical computation.

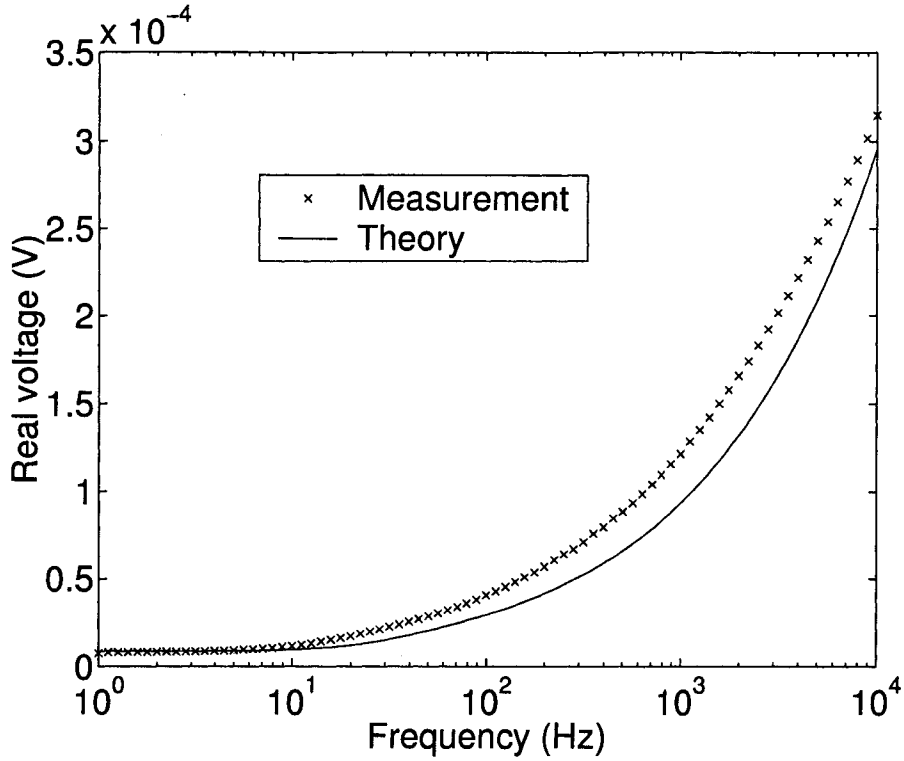

Figure 5.9 Real part of the ACPD frequency measurements on the low-carbon steel plate. Measurement frequency is from 1 Hz to 10 kHz.

5.4.5 Coil Impedance Measurements on Metal Plates

The electrical conductivity of the stainless steel plate can not be measured directly by using eddy current instrument. For the stainless plate, its relative magnetic permeability should be very small but is not exactly one. The measured conductivity from eddy current instrument is about 0.7 MS/m. If this value is put into theoretical calculation, the theory and experiment data give completely different potential drop. Obviously it is not right. An effective method to get the electrical conductivity and magnetic permeability of the stainless steel plate is to use the theory of Dodd and Deeds [63]. The impedance of an absolute coil is measured in free space and on the stainless steel plate. The experimental impedance change data of the coil are fitted to the predicted data based on the theory of Dodd and Deeds. The fitted values are given in Table 5.4. The parameters of the absolute coil are shown in Table 5.5. The data

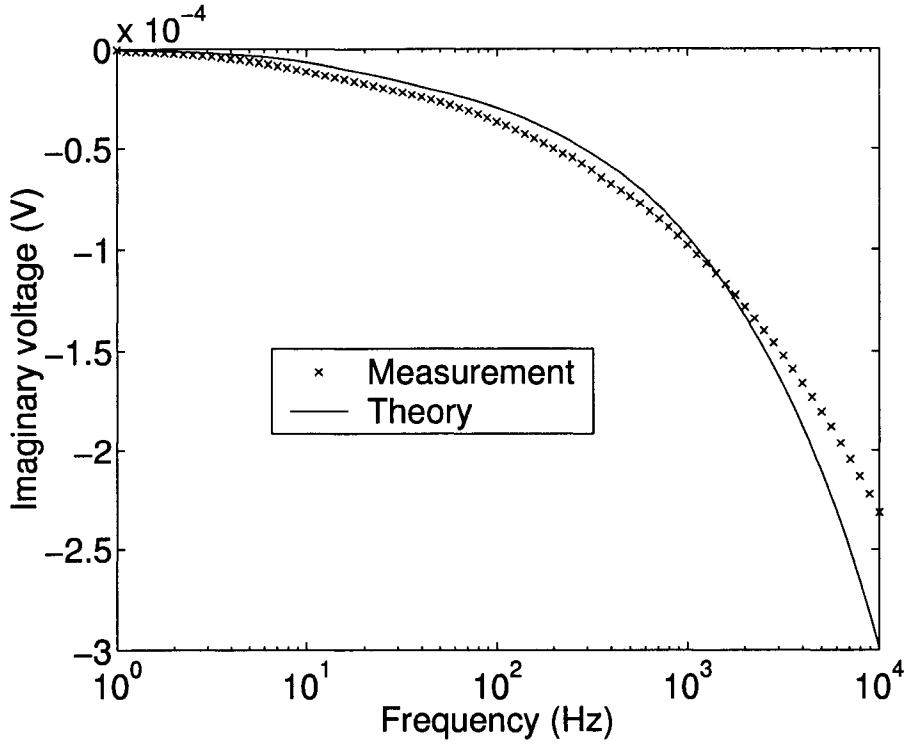

Figure 5.10 Imaginary part of the ACPD frequency measurements on the low-carbon steel plate. Measurement frequency is from 1 Hz to 10 kHz.

fitting of the coil impedance change are shown in Figure 5.13 and 5.14.

For the purpose of checking and comparison, the coil impedance measurements are also been made on the brass and aluminum plates. The same absolute coil is used for impedance measurement on brass and aluminum plates. Its parameters are shown in Table 5.5. The data fitting of the coil impedance change on the brass plate are shown in Figure 5.15 and 5.16. The data fitting of the coil impedance change on the aluminum plate are shown in Figure 5.17 and 5.18.

MIZ-21A eddy current instrument from Zetec Inc. is used to measure the electrical conductivity of the brass and aluminum plates. It is found that there is small difference between the conductivity value from Zetec eddy current instrument measurement and the fitted value from the coil impedance measurements. Calibration of the eddy current instrument need five

Table 5.4 Experimental parameters for stainless steel plate. S, p, q and l have the same meaning as in Table 5.1.

stainless steel plate		probes	
conductivity, σ (MSm^{-1})	1.36 (fitted value)	S (mm)	25.44 ± 0.3
permeability, μ_r	1 (assumed)	p (mm)	-10.15 ± 0.01
thickness, T (mm)	6.3618 ± 0.01	q (mm)	10.15 ± 0.01
horizontal dimensions (mm)	457 × 457	l (mm)	0.25 (fitted value)

Table 5.5 Parameters of the absolute coil. The coil is provided by Dr. Nicola Bowler.

Number of turns	1858
Inner radius (mm)	4.04
Outer radius (mm)	11.43
Axial Length (mm)	8.02
Stand off (mm)	1.08
Resonant frequency (kHz)	191.28
Self inductance (mH)	33.90

standard blocks with different conductivity. These five different conductivity values are fallen into five preset range. Unfortunately the standard blocks from Zetec Inc. is missing at this time. There is one other set of standard blocks. But only three of them have close conductivity value that are within the preset value range. So only three standard blocks are used for instrument calibration. This will affect the accuracy of the measured conductivity value.

5.5 Discussion

This chapter discuss the four-point ACPD measurements on homogeneous metal plate. Excellent agreement is observed between the experiment and theory. Some measurements errors have influence upon the agreement between them as discussed below.

5.5.1 Measurement Errors

The electrical conductivity of the brass plate is measured by using a MIZ-21A eddy current instrument from Zetec Inc. From the manufacturer's literature, this instrument is certified to

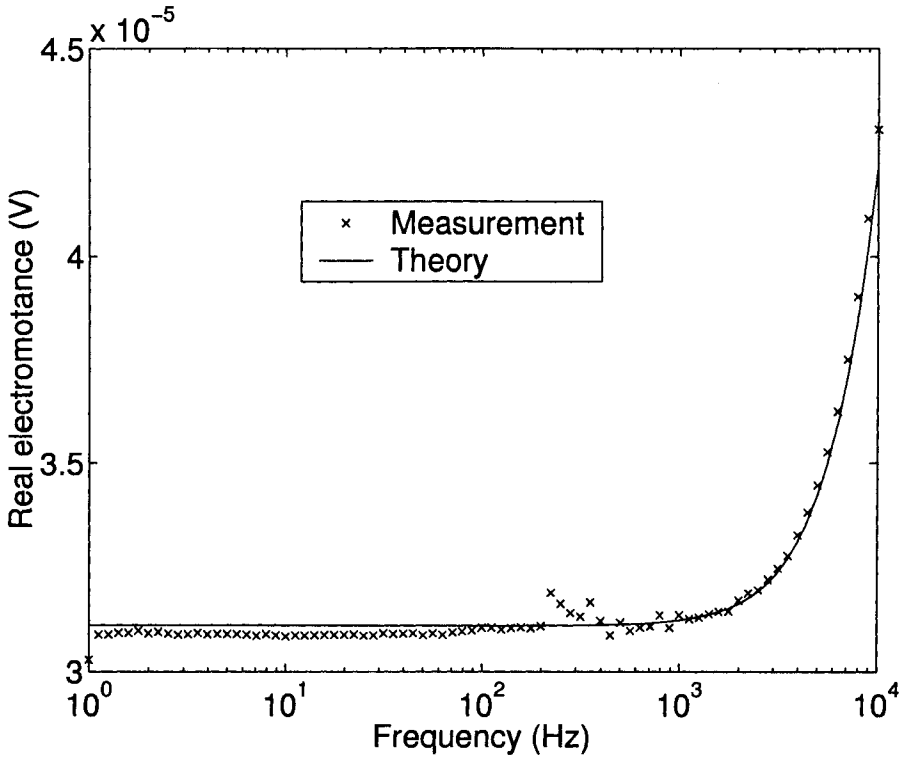

Figure 5.11 Real part of the ACPD frequency measurements on the stainless steel plate. Measurement frequency is from 1 Hz to 10 kHz.

have ±0.5% IACS accuracy when the material conductivity is between 16% and 60% IACS (9.5 and 35 MS/m). Combined instrument and standard, the accuracy is ±1% of value when the material conductivity is above 15% IACS, it is ±3% of value when the material conductivity is below 15% IACS.

Digital caliper is used to measure the metal plate thickness. All those metal plates are precision ground. It is assumed that the metal plate has uniform thickness for the whole plate. The thickness is measured at some points at plate edge. The average of these measured values is set to the thickness value. Common ruler is used to measure the plate width and length. The accuracy of the width and length measurements is not very important because they do not enter the theoretical calculation. In theory the plate is treated as infinite plate. It is all right as long as the plate width and length are big enough compared with the skin depth. In

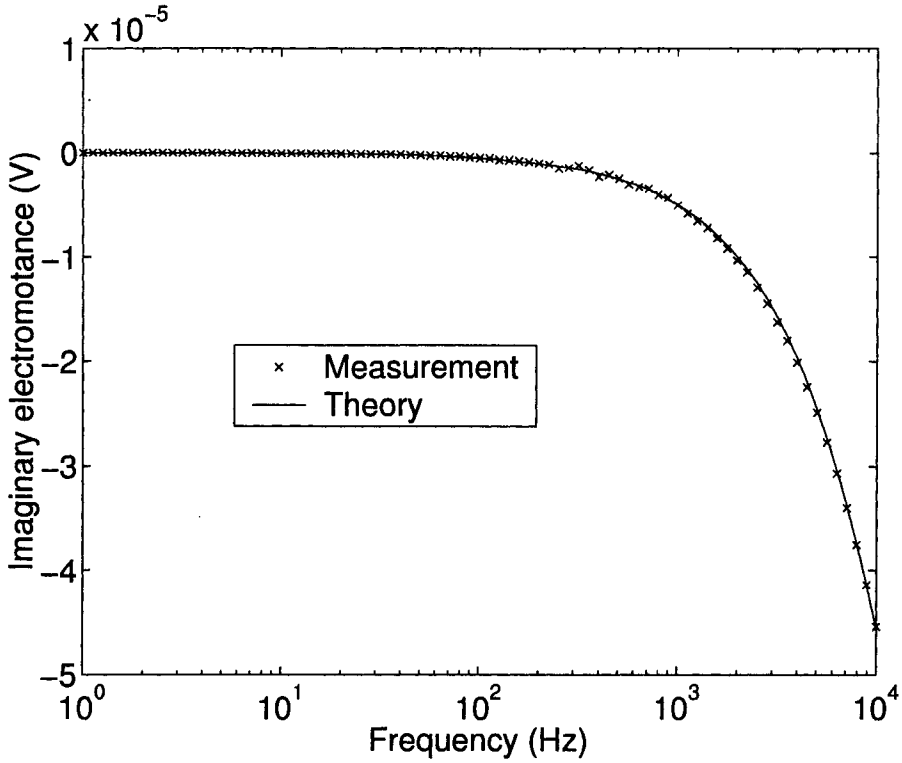

Figure 5.12 Imaginary part of the ACPD frequency measurements on the stainless steel plate. Measurement frequency is from 1 Hz to 10 kHz.

practice it can be treated as infinite plate when the width and length are 100 skin depth.

The distance between the two potential drop probes is measured by using digital caliper. The two potential drop probes are mounted on one plastic block. The distance between them will not be changed once they are mounted to their receptacles. The measured value is the distance between the head point of the two probes. The probes have very sharp head and have point contact with the metal plate.

The distance between the two current probes is measured by using common ruler. The two current probes are mounted on two separate plastic blocks. It is not possible to measure the distance between them before they are fixed on the metal plate. After they are fixed to position on the metal plate, it is very difficult to measure the distance between the two current probes directly. It is because there is some distance between the current probe and

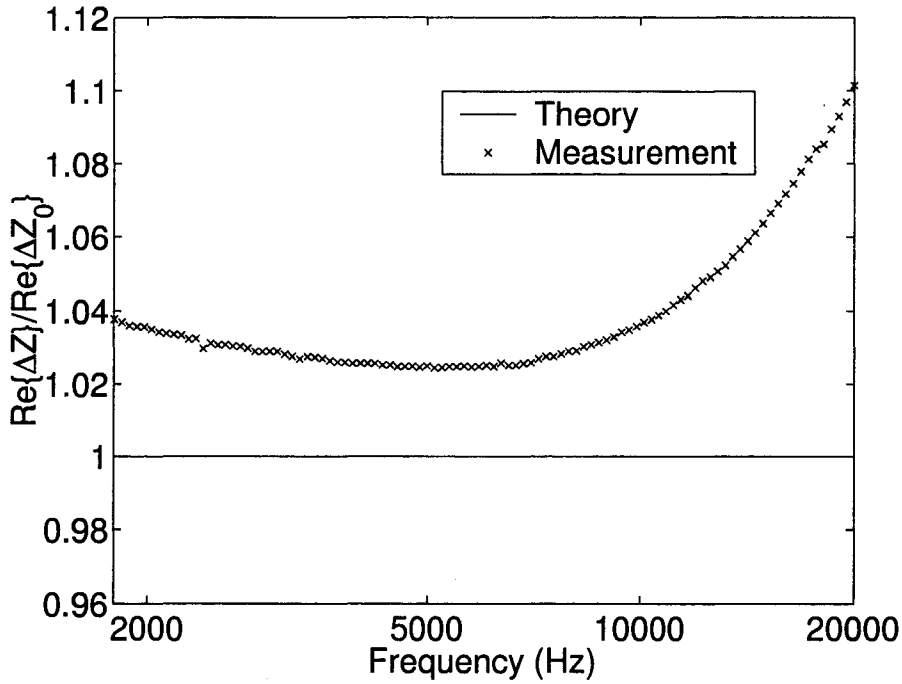

Figure 5.13 Real part of the impedance change of the absolute coil on the stainless steel plate and in free space. The experiment data are normalized to the theoretical calculation value. The real part data are not used for data fitting. The parameters of this coil are given in Table 5.5.

the edge of the support plastic block. The plastic block is not transparent when it is seen from the side surface. The distance between the two neighboring edges of these two blocks can be measured. Then the distance between the probe and the block edge must be added to get the total distance. The accuracy is dependent on these three distance measurements. Another possible option is to put the two current probes to two preset points on the metal plate. The distance between the two preset points is measured before it is occupied by the current probe blocks. The accuracy is dependent on how accurately the current probes are put on the two preset points, and how these two preset points are marked on the metal plate surface.

At the beginning of the ACPD measurement, all four probes are supposed to stay on a straight line and the middle point between the two current probes is assumed to be exactly the same middle point between the two potential drop probes. Great care is taken to make

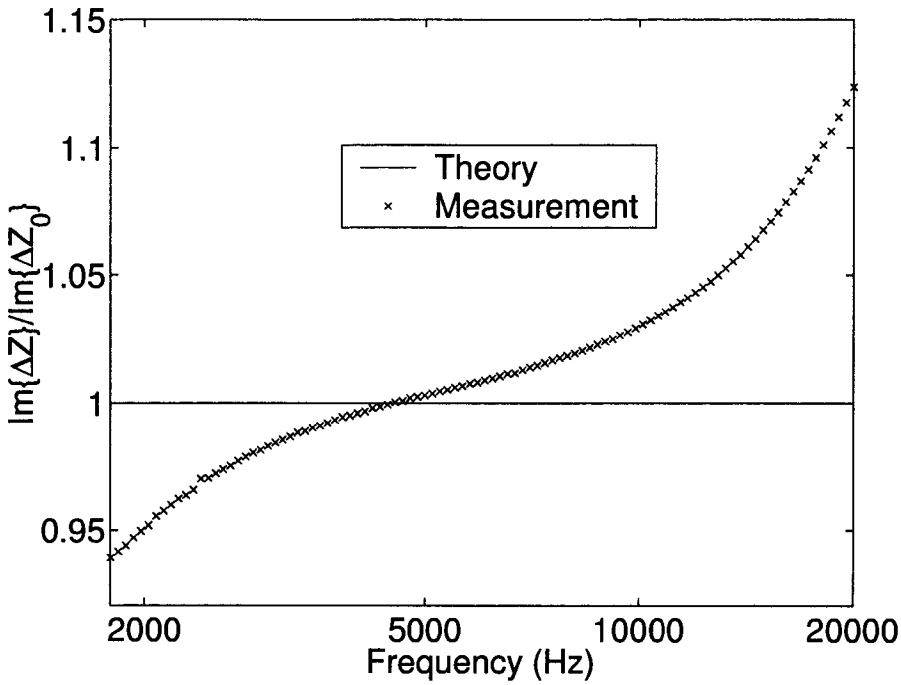

Figure 5.14 Imaginary part of the impedance change of the absolute coil on the stainless steel plate and in free space. The experiment data are normalized to the theoretical calculation value. The imaginary part of the impedance change data from 1.7 kHz to 20 kHz are used for data fitting. The parameters of this coil are given in Table 5.5.

this arrangement, but it is not guaranteed. Two separate plastic blocks are used to hold the two current probes respectively. One additional plastic block is used to hold the two potential drop probes. Four probes are fixed by three plastic blocks. One straight line is drawn on the plate surface. This straight line is determined by the two potential drop probe head points. Then the two current probe support blocks are put along this straight line. Here how accurate the current probes stay on the straight line is dependent on how accurate the current probes are put on this straight line, and how this line is marked on the metal plate surface. This kind of three support blocks arrangement is designed for scanning measurements. The two potential drop probes can move any way while the two current probes stay at fixed positions. For the stationary frequency measurement, one possible solution to this problem is to put all

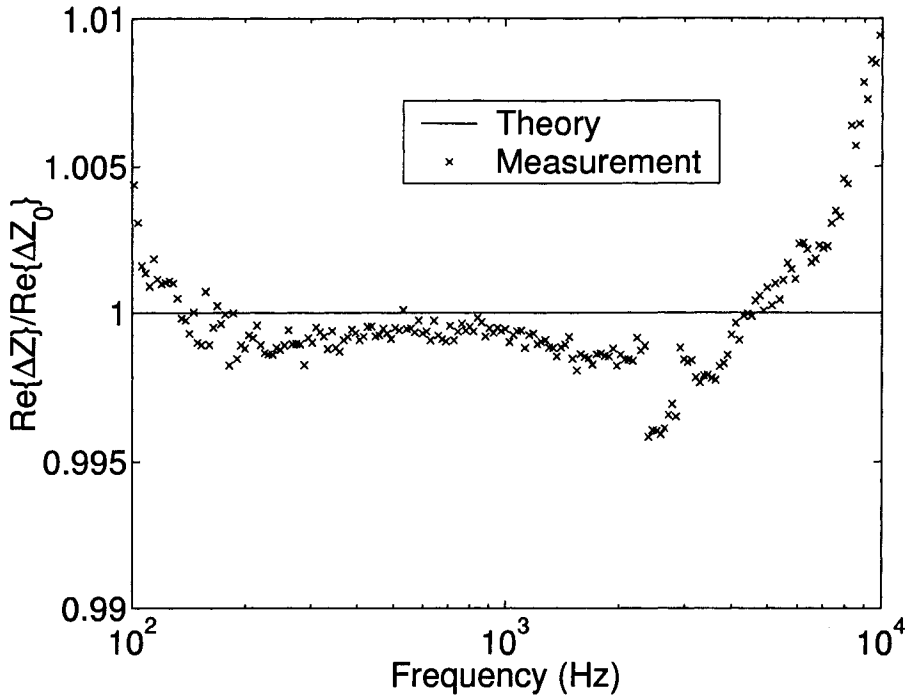

Figure 5.15 Real part of the impedance change of the absolute coil on the brass plate and in free space. The experiment data are normalized to the theoretical calculation value. The real part data are not used for data fitting. The parameters of this coil are given in Table 5.5.

four probes in one support plastic block. Then the four probes can be put on one straight line, and their separation can be measured more accurately. It is guaranteed if their receptacle holes stay on one straight line. Making one straight line from the bottom surface of one plastic block is much easier.

The high precision resistor is measured by using Agilent 4294A precision impedance analyzer from 40 Hz to 40 kHz. The resistance variation with frequency is less than 1%. The average of the measured resistance values is used for the actual resistance value. Its value is treated as constant in data analysis. SR830 DSP lock-in amplifier is used to measure the potential drop on the plate surface and voltage across the high precision resistor.

It is observed that the comparison between theory and experiment on the brass and aluminum plates are excellent. But the measurement result on carbon steel plate is not as good

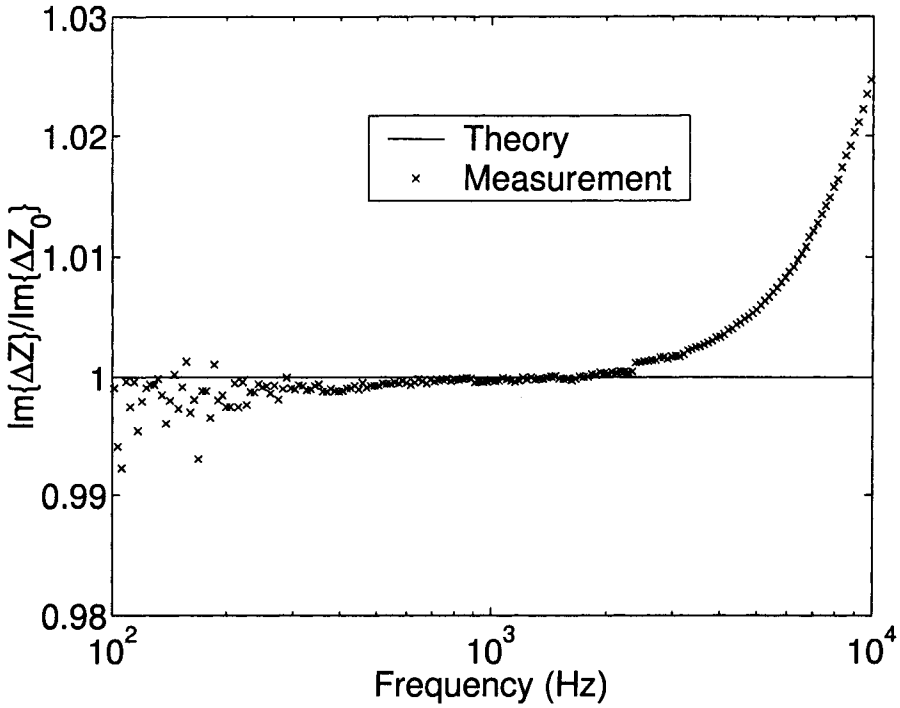

Figure 5.16 Imaginary part of the impedance change of the absolute coil on the brass plate and in free space. The experiment data are normalized to the theoretical calculation value. The imaginary part of the impedance change data from 100 Hz to 10 kHz are used for data fitting. The parameters of this coil are given in Table 5.5.

as the result on brass and aluminum plates. It is because the carbon steel plate is magnetic. It is not easy to measure its conductivity and permeability directly. For the brass and aluminum material, its relative permeability is known to be one. It is more simple. From the ACPD measurement on cylindrical rod, it is found that the carbon steel rod should be annealed and demagnetized before the ACPD measurements in order to get its conductivity and permeability more accurately. It is reasonable that the carbon steel plate should also be annealed and demagnetized. But it is not demagnetized because of its size. It is very tricky to demagnetize such big plate. Those available demagnetization system can not handle such size. One possible option is to demagnetize it locally and do it step by step at many different points. For the time being it is not annealed. Further work will be done to check the possibility to anneal it.

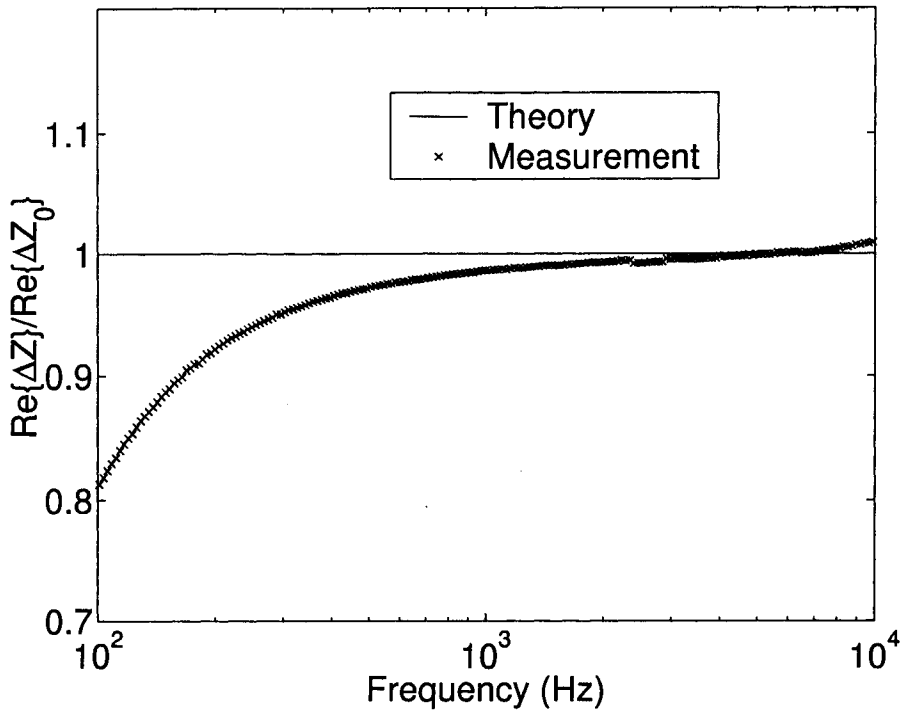

Figure 5.17 Real part of the impedance change of the absolute coil on the aluminum plate and in free space. The experiment data are normalized to the theoretical calculation value. The real part data are not used for data fitting. The parameters of this coil are given in Table 5.5.

5.5.2 Two Dimensional Scan

The two potential drop probes can be anywhere on the metal plate in the ACPD theory on metal plate. So it is interesting to see the two dimensional scan results.

Great care is given to avoid the scratch damage caused by the scan movement. Unfortunately it is found the tin head still leave scratch on the brass plate and its surface is damaged.

One possible solution is to change to three dimensional scan. The metal plate surface is in the XY coordinate plane. The two potential drop probe are also in the XY plane. From one scan point to the next scan point, the scratch damage can be completely avoided by three dimensional movement. The potential drop probes move in the Z direction first. Or they are lifted off from the metal plate surface. Then they move in the air to the next scan point. After

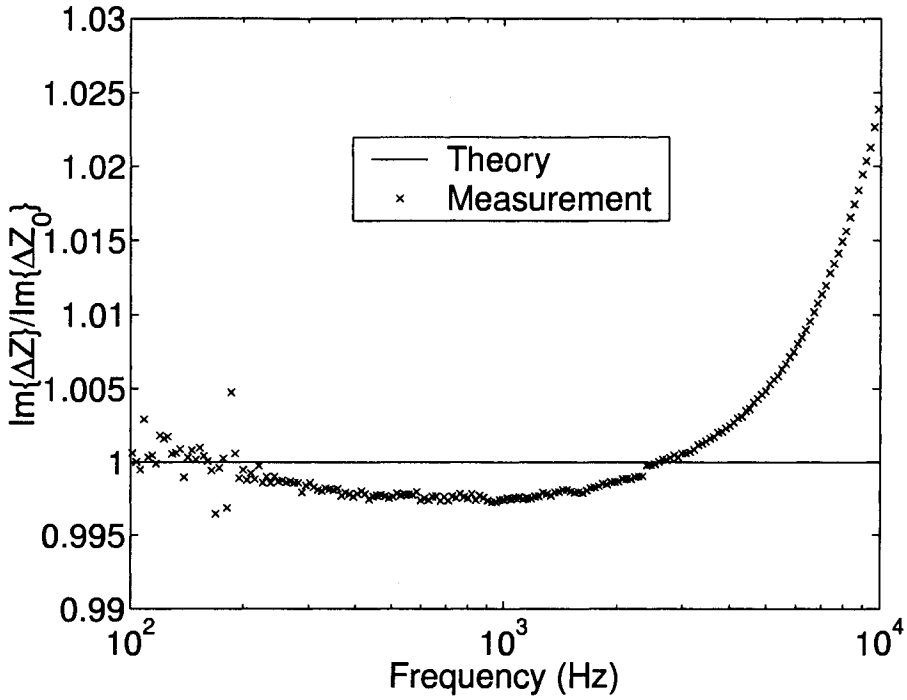

Figure 5.18 Imaginary part of the impedance change of the absolute coil on the aluminum plate and in free space. The experiment data are normalized to the theoretical calculation value. The imaginary part of the impedance change data from 100 Hz to 10 kHz are used for data fitting. The parameters of this coil are given in Table 5.5.

that they move in the Z direction to come back to the metal plate surface. Obviously it is more advanced than two dimensional scan. The hardware system will be more expensive. The computer control program will be more complicated.

CHAPTER 6. CONCLUSIONS AND FUTURE WORK

Alternating current potential drop method has been successfully developed and applied to nondestructive evaluation of case depth. Simple geometrical object is selected for the first step. Both alternating current potential drop and eddy current drive pickup coils induction methods are developed for cylindrical rod. Experiment measurements are made on homogeneous rods and case hardened rods with ACPD and eddy current methods. ACPD method is extended to the flat plate geometry. ACPD measurements are carried on different homogeneous metal plates.

6.1 Summary of Accomplishments

In this project, the contribution from the author is mainly focus on the experimental measurements part. Some computer code are developed to get numerical solution for theoretical model computation. The tasks that have been accomplished to-date include:

1. ACPD measurement system on cylindrical rods is designed and developed. Its accuracy is verified to within 2% by using alloy 101 oxygen-free (99.99% ultra-pure) copper rod.

2. Computer control program is developed to communicate with the SR830 DSP lock-in amplifier such that the ACPD measurements on cylindrical rods can be completed automatically and hand-free.

3. Multi-frequency ACPD measurements are performed on cylindrical homogeneous and case hardened steel rods. Very good data fitting is observed between the measured data and theoretical calculation. Reasonable agreement is achieved between the measured

case depth from ACPD method and effective case depth from the hardness profile on case hardened cylindrical rods.

4. Eddy current induction measurement system on cylindrical rods is designed and developed. Drive and pickup coils are carefully designed and developed. Random wiring is used to wire these two coils with accurate coil turns number. The eddy current measurement system is verified to be accurate within 2% by using alloy 101 oxygen-free (99.99% ultra-pure) copper rod.

5. The computer control program for ACPD measurements on cylindrical rods is modified to control the eddy current measurements on cylindrical rods such that it can be completed automatically and hand-free.

6. Multi-frequency eddy current driver pickup coils mutual impedance measurements are made on cylindrical homogeneous and case hardened steel rods. Good data fitting is observed between the measured data and theoretical calculation. Reasonable agreement is achieved between the measured case depth from eddy current method and effective case depth from the hardness profile on case hardened cylindrical rods.

7. ACPD measurement system on metal plate is designed and developed. Part of the two dimensional scanning system is redesigned for the ACPD metal plate measurement system.

8. Computer program is developed to control the SR830 DSP lock-in amplifier and Parker Automation 6K2 2-axis servo/stepper controller of the scan system such that two dimensional scanning ACPD measurements on metal plates can be completed automatically and hand-free.

9. Multi-frequency ACPD measurements with stationary probes are completed on brass, aluminum, low-carbon steel and stainless steel plates. Excellent agreement is observed between the measurement data and theoretical calculation for nonmagnetic materials.

10. Two dimensional scanning ACPD measurements with two fixed working frequency (10 Hz and 10 kHz) are completed on finite thickness brass plate. Good agreement is observed between the experiment and theory.

6.2 Future Work

For the eddy current induction method, a new theory is developed to take care of the finite length rod with coaxial encircling coil [66]. High precision experimental measurements will be made to check this theory. More measurements will be made on new cylindrical rods samples.

ACPD method on homogeneous metal plate will be extended to multi-layer metal plates. The theoretical calculation will be performed and high precision experiment measurements will be made.

For the case hardened cylindrical rods, reasonable agreement is achieved between the measured case depth and effective case depth from the hardness profile. But there are some errors between them. It is found that the basic assumption of the two-layer theoretical model is not very accurate. The electromagnetic properties do not track the hardness profile exactly. The hysteresis loss and initial permeability appear to lag significantly behind the hardness profile. Conversely the electrical conductivity appears to track hardness pretty well. Some anomalous values for surface conductivity and coercivity are observed. Some kind of modification or compensation should be made to this theoretical model in order to get better agreement between the measured case depth and effective case depth [64].

At the final stage of this research project, a prototype ACPD measurements system will be built for case depth measurements.

APPENDIX A. APPROXIMATE THEORY OF FOUR-POINT ALTERNATING CURRENT POTENTIAL DROP ON A FLAT METAL SURFACE

A paper accepted to publish in Electromagnetic Nondestructive Evaluation, Vol. **IX**

Nicola BOWLER Yongqiang HUANG

Iowa State University, Center for Nondestructive Evaluation,

Applied Sciences Complex II, 1915 Scholl Road, Ames, IA 50011, USA.

Abstract

An analytical expression for the voltage measured by a four-point alternating current potential drop (ACPD) method on a flat metal surface is derived. Far-field expressions for the electric field in a metal plate and in the region of the probe (air) are used to obtain contributions to the ACPD voltage from the metal plate and due to inductance in the pick-up circuit. The far-field approximation is accurate for a plate whose edges are several tens of skin depths from the probe, and for a probe whose pick-up points are several skin depths away from the current drive points. Comparison of the theory with experiment on a brass plate shows excellent agreement.

Introduction

The alternating current potential drop (ACPD) method measures the voltage, $\mathcal{V}$, between two pick-up points on the surface of a conductor. For the configuration shown in Figure A.1,

$$\mathcal{V} = V + \varepsilon = -\int_{(p,y,0)}^{(q,y,0)} \mathbf{E} \cdot d\mathbf{l} + \oint_C \mathbf{E} \cdot d\mathbf{l}, \tag{A.1}$$

where C is a closed loop [1]. ε is the rate of change of magnetic flux within the loop.

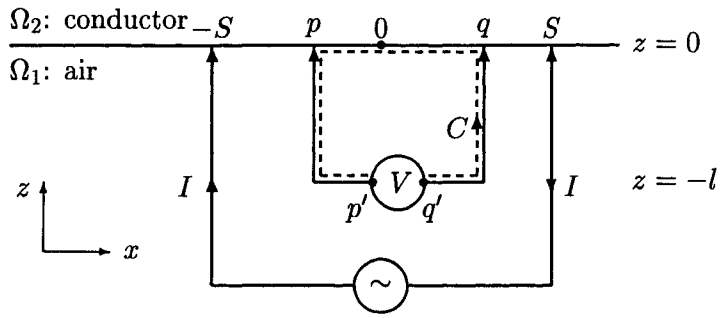

Figure A.1 Path of integration, C (- - -), may occupy any plane of constant y. Here the plane $y = 0$ is shown.

In direct current potential drop measurements there is no induction effect in the measurement circuit ($\varepsilon = 0$) since the current does not vary with time. The measured potential drop is almost exclusively due to the conductor. In ACPD measurements, the contribution to $\mathcal{V}$ from the conductor dominates when the frequency is sufficiently low, since the inductive contribution from the measurement circuit, $i\omega L$, is proportional to frequency ω. At sufficiently high frequency the inductive term dominates.

In this work, both contributions to $\mathcal{V}$ are evaluated. The far-field approximation for $\mathbf{E}$ is used in calculating $\mathcal{V}$. This approximation gives accurate results when pick-up points at $(p, y, 0)$ and $(q, y, 0)$ are sufficiently far from the source points at $(\pm S, 0, 0)$, in practice a few electromagnetic skin depths (δ) in the conductor.

Electric Field

For the configuration shown in Figure A.1, the electric field can be obtained by superposition of fields separately associated with the two current-carrying wires:

$$\mathbf{E}^T(\mathbf{r}) = \mathbf{E}(\mathbf{r}_+) - \mathbf{E}(\mathbf{r}_-), \tag{A.2}$$

where $r_\pm = \sqrt{(x \pm S)^2 + y^2 + z^2}$. In the following sections the far-field form of $\mathbf{E}$ is determined in the region of the pick-up circuit (air) and in the metal plate for a *single* current-carrying wire located on the axis of a cylindrical co-ordinate system.

Probe Region

For a single wire passing current I into, or out of, a conductive plate, there are two contributions to the electric field in air. One is from the current flowing in the wire, $\mathbf{E}^{\mathrm{w}}$, and the other is from the current density in the plate. In the far-field regime, for the closed loop C, only $\mathbf{E}^{\mathrm{w}}$ is important. Assuming that the wire is perpendicular to the surface of the plate and that the current has time-dependence $e^{-i\omega t}$, the integral form of Ampère's Law and then Faraday's Law yields

$$\mathbf{E}^{\mathrm{w}}(\rho, z) = \hat{z}\frac{i\omega\mu_0 I}{2\pi}\ln\rho, \qquad \rho \to \infty, z \leq 0, \tag{A.3}$$

where ρ is the radial co-ordinate of a cylindrical system centered on the wire and $\mathbf{E}^{\mathrm{w}}$ has the same direction as the current density in the wire, $\mathbf{J} = \hat{z}J_z$.

Plate

An expression for the electric field in the conductive plate is obtained in a manner similar to that given in reference [2] for a conductive half-space. For a current source oriented perpendicular to the surface of the plate, only the transverse magnetic (TM) potential, ψ'', is required to fully describe the electric field:

$$\mathbf{E}(\mathbf{r}) = -i\omega\mu\nabla\times\nabla\times\hat{z}\psi''(\mathbf{r}). \tag{A.4}$$

Define a modified TM potential

$$\Psi = \nabla_z^2\psi'', \tag{A.5}$$

where $\nabla_z \equiv \nabla - \hat{z}(\partial/\partial z)$ is the transverse differential operator. For a plate infinite in x and y, occupying $z \in [0, T]$, the governing equation is

$$(\nabla^2 + k^2)\Psi(\mathbf{r}) = 0, \qquad 0 \leq z \leq T, \tag{A.6}$$

where $k^2 = i\omega\mu\sigma$ with μ and σ being the permeability and conductivity of the plate, respectively. In the plate, only the horizontal component of the electric field, E_ρ, contributes to V. It is not convenient to express E_ρ in terms of Ψ. Rather, E_ρ will be obtained from the following

equation by means of relationship (A.5).

$$E_\rho(\mathbf{r}) = -i\omega\mu\frac{\partial^2\psi''(\mathbf{r})}{\partial\rho\partial z}, \tag{A.7}$$

where ρ and z are co-ordinates of the cylindrical system. Equation (A.6) is solved for Ψ subject to boundary conditions

$$\Psi(\rho,0) = C(\rho) \qquad \text{where} \qquad C(\rho) = \begin{cases} \frac{I}{\pi(ka)^2}, & \rho \le a, \\ 0, & \rho > a, \end{cases} \tag{A.8}$$

and

$$\Psi(\rho,T) = 0. \tag{A.9}$$

These derive from the fact that, at the surface of the plate, the normal component of current density is continuous - zero everywhere apart from at the point of contact with the current-carrying wire, radius a. Applying the zero-order Hankel transform to solve (A.6) and taking the limit $a \to 0$ yields

$$\Psi(\rho,z) = \frac{I}{2\pi k^2}\int_0^\infty e^{-\gamma z}\left[\frac{1-e^{2\gamma(z-T)}}{1-e^{-2\gamma T}}\right]J_0(\kappa\rho)\kappa d\kappa, \tag{A.10}$$

where $\gamma^2 = \kappa^2 - k^2$. If $T \to \infty$, the term in square brackets tends to unity and the resulting integral is identical to that obtained for a half-space conductor [2].

It is possible to evaluate the integral in (A.10) analytically by expanding the term in the denominator as a binomial series [4, 3.6.10]:

$$(1-e^{-2\gamma T})^{-1} = 1 + e^{-2\gamma T} + e^{-4\gamma T} + e^{-6\gamma T} + e^{-8\gamma T} + \ldots = \sum_{n=0}^{\infty} e^{-2n\gamma T}. \tag{A.11}$$

Multiplying the right-hand side of (A.11) by the factor $e^{-\gamma z}[1-e^{2\gamma(z-T)}]$, and substituting the result into (A.10), yields

$$\Psi(\rho,z) = \frac{I}{2\pi k^2}\sum_{n=0}^{\infty}\int_0^\infty \left\{e^{-\gamma(z+2nT)} - e^{\gamma[z-2(n+1)T]}\right\}J_0(\kappa\rho)\kappa d\kappa, \tag{A.12}$$

where the order of summation and integration has been reversed. The first term in braces in (A.12), $e^{-\gamma z}$, gives rise to the result for the TM potential in a half-space conductor. The second term, $-e^{\gamma(z-2T)}$, accounts for the primary reflection of the field from the surface of the

plate at $z = T$. Other terms deal with multiple reflections between the surfaces of the plate. By analogy with the result for the half-space conductor, reference [2], or by multiple use of the analytic result given in reference [5], result 8.2.23, the terms in (A.12) can be integrated. It is found that

$$\begin{aligned}\Psi(\rho,z) &= -\frac{I}{2\pi}\sum_{n=0}^{\infty}\left\{\frac{ik(z+2nT)}{(ikr_n)^3}e^{ikr_n}(1-ikr_n)\right. \\ &\left. + \frac{ik[z-2(n+1)T]}{(ikr'_n)^3}e^{ikr'_n}(1-ikr'_n)\right\}, \quad 0 \le z \le T, \end{aligned} \tag{A.13}$$

wherein $r_n = \sqrt{\rho^2+(z+2nT)^2}$ and $r'_n = \sqrt{\rho^2+[z-2(n+1)T]^2}$. To obtain E_ρ from Ψ as given in (A.13) via relations (A.7) and (A.5) requires some manipulation [2]. The result is

$$\begin{aligned}E_\rho(\mathbf{r}) &= -\frac{ikI}{2\pi\sigma\rho}\sum_{n=0}^{\infty}\left\{e^{ik(z+2nT)} - \frac{e^{ikr_n}}{ikr_n}\left[1+\frac{[ik(z+2nT)]^2}{ikr_n}\left(1-\frac{1}{ikr_n}\right)\right]\right. \\ &\left. + e^{-ik[z-(2n+1)T]} - \frac{e^{ikr'_n}}{ikr'_n}\left[1+\frac{\{ik[z-2(n+1)T]\}^2}{ikr'_n}\left(1-\frac{1}{ikr'_n}\right)\right]\right\}, \\ &\qquad 0 \le z \le T \end{aligned} \tag{A.14}$$

In the far field, the electric field is dominated by terms of the form e^{ikz}/ρ and

$$E_\rho(\mathbf{r}) = -\frac{ikI}{2\pi\sigma\rho}\sum_{n=0}^{\infty}\left\{e^{ik(z+2nT)} + e^{-ik[z-2(n+1)T]}\right\}, \qquad \rho\to\infty, 0\le z\le T. \tag{A.15}$$

If the far-field current density is integrated over a cylindrical surface of large radius extending from $z = 0$ to T, the result is $I[1+e^{ik(2N+1)T}]$ for a series truncated to N terms. This expression tends to I as $N \to \infty$, as it should. If $T \to \infty$ the far-field expression for the electric field in a half-space conductor is recovered [2]

$$E_\rho(\mathbf{r}) = -\hat{\rho}\frac{ikI}{2\pi\sigma\rho}e^{ikz}, \qquad \rho\to\infty, z\ge 0. \tag{A.16}$$

This expression was also given in reference [3] in the context of fatigue crack measurement.

Voltage calculation

Voltage is now calculated according to equation (A.1). For the configuration shown in Figure A.1 the contributions are

$$\mathcal{V} = V + \varepsilon = -\int_p^q E_x^T(x,y,0)dx + \int_0^{-l} E_z^T(p,y,z)dz + \int_{-l}^0 E_z^T(q,y,z)dz, \tag{A.17}$$

with $\mathbf{E}^T$ given by (A.2). It is a simple matter to evaluate the last two terms on the right-hand side of equation (A.17) with E_z given in equation (A.3). To neatly evaluate the first term on the right-hand side of (A.17) recognize that, at the surface defined by $z = 0$, equation (A.15) can be written

$$E_\rho(\rho, 0) = -\frac{ikI}{2\pi\sigma\rho}\left[\left(2\sum_{n=0}^{\infty} e^{2iknT}\right) - 1\right], \qquad \rho \to \infty. \tag{A.18}$$

Further [4, equation 3.6.10],

$$\sum_{n=0}^{\infty} e^{2iknT} = \frac{1}{1 - e^{2ikT}},$$

so that

$$E_\rho(\rho, 0) = \frac{ikI}{2\pi\sigma\rho}\coth(ikT), \qquad \rho \to \infty. \tag{A.19}$$

The final expression for $\mathcal{V}$ is

$$\mathcal{V} = \frac{I}{4\pi}\left[-\frac{ik}{\sigma}\coth(ikT) + i\omega\mu_0 l\right]\ln\left\{\left[\frac{(p-S)^2 + y^2}{(p+S)^2 + y^2}\right]\left[\frac{(q+S)^2 + y^2}{(q-S)^2 + y^2}\right]\right\}. \tag{A.20}$$

The first term in equation (A.20) is the contribution from the conductor and has approximately equal real and imaginary parts. The contribution from the measurement circuit is imaginary (inductive) and proportional to the dimension of the circuit perpendicular to the conductor surface, l. For a typical non-magnetic metal and $l \sim 1$ mm, the inductive term is practically negligible for frequencies up to about 10 Hz whereas at 10^4 Hz the terms are of similar magnitude. The logarithmic term represents the physical arrangement of the four probe points.

Experiment

ACPD measurements were made as a function of frequency on a brass plate whose conductivity and dimensions are given in Table A.1. The brass plate was precision ground to remove surface scratches and mounted on a two-inch thick plastic support plate. Electrical contact with the brass plate was made via sprung, point contacts, held perpendicular to the surface of the plate. In this experiment the four contact points were arranged in a straight line, with a common midpoint between the two current drive points and the two pick-up points. The dimensions of the probe are given in Table A.1.

Table A.1 Experimental parameters.

brass plate		probe (Figure A.1)	
conductivity, σ (MSm^{-1})	16.2 ± 0.3	S (mm)	38.2 ± 0.3
thickness, T (mm)	5.66 ± 0.01	p (mm)	-9.18 ± 0.01
horizontal dimensions (mm)	615 × 616	q (mm)	9.18 ± 0.01
		l (mm)	0.35 (fitted value)

The two current-carrying wires were held perpendicular to the plate surface for a distance of 16 inches, after which they were twisted together to reduce the effects of inter-wire capacitance. This distance was sufficient to remove any effect of motion of the current wires on the measured voltage. The two pick-up wires were arranged with the objective of minimizing l, lying as close to the plate surface as possible. They were twisted together at the midpoint between the pick-up points.

In the theoretical calculation, two measured values are needed. One is the current through the plate, the other is the voltage measured by the pick-up probe. To monitor the current in the plate, a high precision resistor was connected in series with the drive current circuit and the voltage across the resistor measured. The resistance maintains one percent accuracy over the range of frequency for which it could be measured with an Agilent 4294A precision impedance analyzer; 40 Hz to 40 kHz. The voltage across the resistor and that of the pick-up probe were both measured using a Stanford Research Systems SR830 DSP lock-in amplifier. In order to make both voltage measurements using the same lock-in amplifier, a switch was used activated by a control signal from the auxiliary analog output of the lock-in amplifier.

It was necessary to correct the experimental data for common-mode rejection (CMR) error in the lock-in amplifier. This systematic error shows itself in the fact that, when the pick-up terminals are reversed, the measured voltage changes by a few μV. The magnitude of the error is, therefore, similar to that of the voltage being measured, and a corrective procedure is essential. The CMR error was eliminated by taking two sets of measurements, reversing the pick-up terminals for the second. The two sets were then subtracted and the result divided by two.

The drive current was produced by a Kepco bipolar operational power supply/amplifier,

model number BOP 20-20M. The sine signal from the internal function generator of the lock-in amplifier was connected to the current programming input of the power supply, with the power supply working as a current drive.

The conductivity of the plate was measured using a MIZ-21A eddy current instrument. The error quoted in Table A.1 is estimated from the manufacturer's literature and derives from a combination of inaccuracy in the instrument, inaccuracy in the comparative standards and probe lift-off error.

In Figure A.2, ACPD measurements are compared with theory. The average of ten data sets (taken sequentially) is shown. The value of l was adjusted in the calculation to obtain the best fit to the high frequency part of the data, having negligible influence on the low-frequency data. The value $l = 0.35$ mm appears reasonable since the pick-up wire is AWG 32 with diameter 0.2 mm. The agreement between theory and experiment is excellent. There is no obvious error in the imaginary part of $\mathcal{V}$. The theory overestimates the low frequency real part of $\mathcal{V}$ by 3%. Applying standard error analysis to the low frequency limiting expression for $\mathcal{V}$, equation (A.22), shows that errors in the plate conductivity and in the relative positions of the probe points combine to give an experimental error which is also 3%.

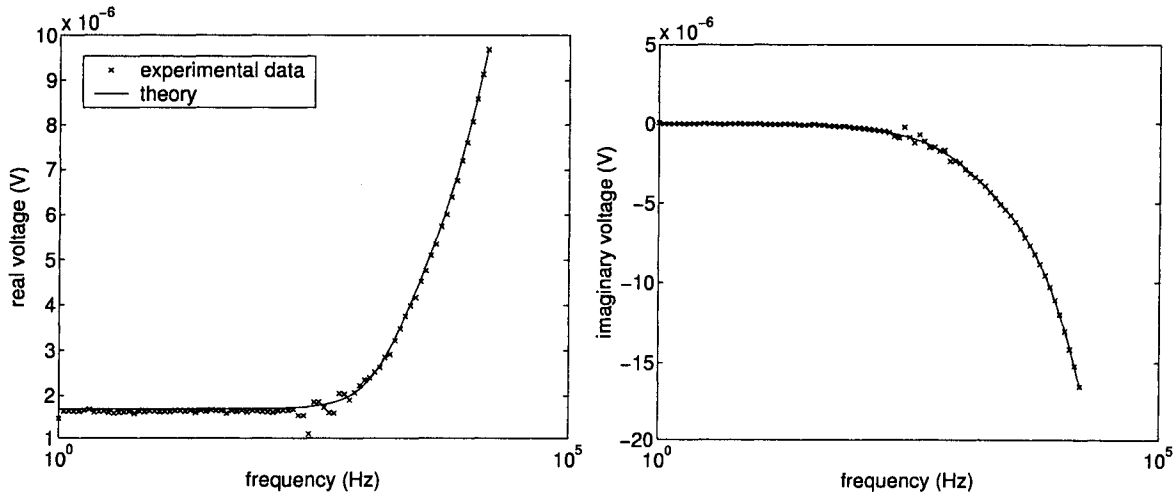

Figure A.2 ACPD measurements on a brass plate compared with theory, equation (A.20). Experimental parameters are given in Table A.1.

Limiting Cases

Half Space Conductor

If the limit $T \to \infty$ is taken in equation (A.20), $\coth(ikT) \to -1$ and $\mathcal{V}$ for a half-space conductor is given by

$$\mathcal{V} = \frac{I}{4\pi}\left(\frac{ik}{\sigma} + i\omega\mu_0 l\right) \ln\left\{\left[\frac{(p-S)^2+y^2}{(p+S)^2+y^2}\right]\left[\frac{(q+S)^2+y^2}{(q-S)^2+y^2}\right]\right\}. \tag{A.21}$$

Considering the behavior of $\coth(x)$, it can be shown that the plate thickness needs to be only twice the electromagnetic skin depth in order for the plate to behave as a half-space, to within 1% accuracy. In Figure A.3, $\mathcal{V}$ is plotted for a number of values of plate thickness, including a half-space. The calculations are made using equations (A.20) and (A.21). For the plate

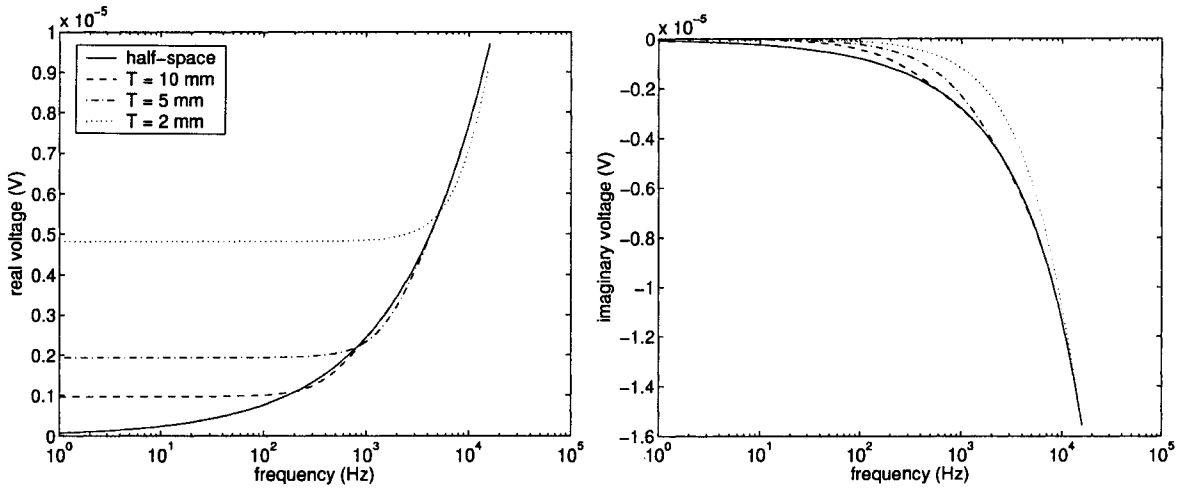

Figure A.3 Calculated values of $\mathcal{V}$ as a function of frequency and plate thickness. Other parameters are given in Table A.1.

with thickness 10 mm, the frequency at which $T = 2\delta$ is about 600 Hz. It can be seen from Figure A.3 that the theory for the half-space and the plate converge at this point, as expected.

Low Frequency

To take the limit $k \to 0$ in equation (A.20), note that $\lim_{k\to 0}[ikT/\sinh(ikT)] = 1$. Then

$$\mathcal{V} \to -\frac{I}{2\pi\sigma T} \ln\left\{\left[\frac{(p-S)^2+y^2}{(p+S)^2+y^2}\right]\left[\frac{(q+S)^2+y^2}{(q-S)^2+y^2}\right]\right\}, \qquad k \to 0. \tag{A.22}$$

It is seen that at low frequency the voltage is real, being inversely proportional to the plate thickness and conductivity. Formula (A.22) is consistent with one given by Yamashita and Masahiro for four-point DC measurements on a finite plate [6]. The inverse dependence of $\mathrm{Re}(\mathcal{V})$ on the plate thickness at low frequency, predicted by equation (A.22), can be clearly seen in Figure A.3.

High Frequency

At high frequency the voltage is dominated by the inductive term in equation (A.20). This term is proportional to l, the length of the pick-up wire perpendicular to the metal plate. Practically it is desirable to minimize the contribution of this term by making l as small as possible. In this way the contribution to $\mathcal{V}$ due to the plate, from which useful information may be derived, is not masked by induction in the measurement circuit. In Figure A.4, the effect on $\mathcal{V}$ of varying l is shown. Only $\mathrm{Im}(\mathcal{V})$ is shown since l has no influence on $\mathrm{Re}(\mathcal{V})$.

Conclusion

This simple analytic result, equation (A.20), gives useful insight into the primary contributors in ACPD measurements. It is accurate for a flat metal plate whose edges are several tens of skin depths from the probe, and for a probe whose pick-up points are several skin depths away from the current drive points. Near-field contributions to $\mathcal{V}$ and surface layers are subjects of future work.

Acknowledgment

This work was supported by the NSF Industry/University Cooperative Research program. The authors would like to thank Marcus Johnson and John Bowler for helpful comments

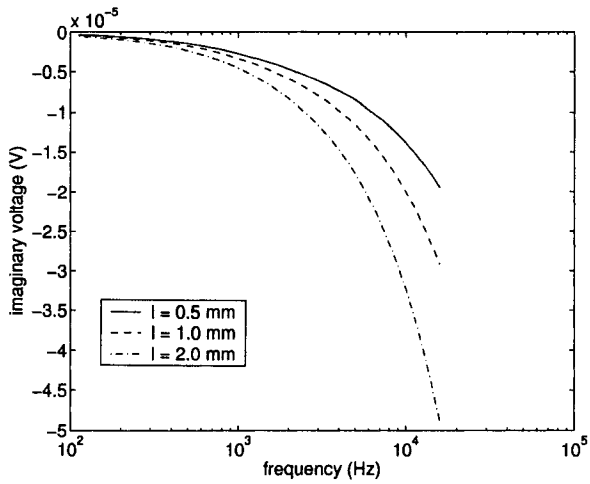

Figure A.4 Calculated values of $\mathrm{Im}(\mathcal{V})$ as a function of frequency and perpendicular length of the pick-up wire, l. Other parameters are given in Table A.1.

regarding the experiment.

Bibliography

[1] W. J. Duffin, *Electricity and magnetism*, McGraw-Hill, London, 1980. 3rd Edition.

[2] N. Bowler, "Analytical solution for the electric field in a half space conductor due to alternating current injected at the surface", *J. Appl. Phys.*, Vol. 95, no. 1, pp. 344-348 (2004)

[3] V. G. Gerasimov, A. D. Kovachev, Yu. V. Kulaev and A. D. Pokrovskii, "An analysis of the operation of a transducer with contact excitation in fatigue tests of flat samples", *Defektoskopiya*, No. 1, pp. 21-32 (1981)

[4] M. Abramowitz and I. A. Stegun (eds.), *Handbook of mathematical functions with formulas, graphs and mathematical tables* (Dover, New York, 1972)

[5] A. Erdélyi (ed.), *Tables of integral transforms* Vol. II (McGraw-Hill, New York, 1954)

[6] M. Yamashita and M. Agu, "Geometrical correction factor for semiconductor resistivity measurements by four-point probe method", *Japanese J. Appl. Phys.*, Vol. 23, no. 11, pp. 1499-1504 (1984)

APPENDIX B. EVALUATION OF CASE HARDENED STEEL RODS USING EDDY CURRENT AND ALTERNATING CURRENT POTENTIAL DROP MEASUREMENTS

A paper published in Electromagnetic Nondestructive Evaluation, Vol. **VII**

John BOWLER Yongqiang HUANG Haiyan SUN Marcus JOHNSON

Iowa State University, Center for Nondestructive Evaluation,

1915 Scholl Road, Ames, IA 50011, USA

Abstract

Eddy current measurements have been performed to determine the near-surface magnetic and electrical properties of case hardened steel rods. The measurements have been carried out over a range of frequencies using a coaxial encircling coil and the alternating current potential drop technique. A small excitation current used in the eddy current measurements ensures that the response is representative of linear material properties allowing the field in the rods to be determined using a linear theoretical model. In the linear regime, the steel is characterized by its initial permeability and electrical conductivity. Complementary measurements of alternating current potential drop provide information on the conductivity and permeability of the specimens. The measurements are used to estimate the linear material properties and the case depth with the aid of linear measurement models.

Introduction

Case hardening of steel components improves the resistance to wear by changing the carbon content and micro-structure of the surface region. In order to examine the results of case

hardening and quantify the effect on components non-destructively, a number of methods have been introduced. These methods usually require an extensive calibration procedure using samples of known properties. Here an alternative approach is presented in which the near surface material properties and the depth of penetration of the surface treatment is assessed using a model based approach.

The case-hardening process produces a change in the electromagnetic material properties of the steel in the near surface region. Consequently, the electrical conductivity and magnetic permeability have different values near the surface compared with the substrate values. The working hypothesis adopted in this study is that the conductivity and permeability variation with depth is indicative of the hardness profile allowing the depth of the case-hardened region to be estimated from electromagnetic measurements. In principle, one can also seek a correlation between the electromagnetic material properties and the hardness of the case hardened region but this relationship has not been studied in the present work.

Eddy-current impedance measurements are responsive to depth variations of the conductivity and permeability of steel components. The material properties can be evaluated by comparing experimental measurements of eddy-current coil impedance with predictions from an appropriate theoretical model and by adjusting the model parameters until agreement is obtained. Clearly the models are less complex if the component has an elementary geometry and simplifying assumptions are made concerning the nature of the case hardened layer. Although over simplification should be avoided, a reasonable strategy is to start with a basic model and progress to a more elaborate representation later if necessary. In this spirit, the cylindrical rod specimens are modelled as uniform in the axial direction having a homogeneous substrate surrounded by a homogeneous surface layer of uniform thickness. In general, the conductivity of the substrate differs from that of the surface layer and the same is true of the permeability. For a specimen modelled in this way, the eddy-current impedance of a co-axial coil is given by a closed form analytical expression [1]. By using this idealization of a case hardened rod, the objective is to estimate model parameters from eddy current coil impedance measurements and alternating current potential drop measurements.

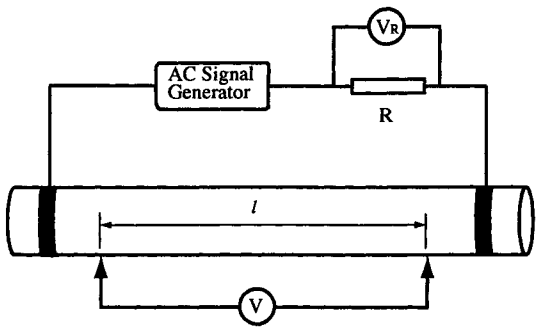

Figure B.1 Schematic diagram of the four-point conductivity measurement system.

Alternating current potential drop

Although electrical conductivity can be determined from eddy current measurements, independent estimates of the conductivity of the rods were obtained using alternating current potential drop (ACPD) measurements. At low frequencies, where the skin depth is much greater than the rod diameter, the ACPD is independent of the permeability of the rod. For a case hardened rod, the potential drop depends on the appropriate combination of the layer and substrate conductivity. At higher frequencies, however, the potential drop is dependent also on the permeability since the magnetic properties have an effect on the skin depth. As the frequency is increased, the skin depth decrease and the potential drop increases for a fixed total rod current. The variation of potential drop with frequency is easily predicted for a homogeneous rod as shown below.

A schematic diagram of the experimental arrangement for measuring the ACPD on rods is shown in Figure 1. Neglecting end effects, the electric field in a homogeneous rod of radius a is given by

$$E(\rho, k) = E_0(k) J_0(k\rho) / J_0(ka) \tag{B.1}$$

where E_0 is the electric field intensity on the rod surface, ρ is a radial coordinate and k is defined as $k = (1 - \jmath)/\delta$ where the skin depth δ is given by the usual formula $\delta = \sqrt{2/\omega\mu\sigma}$.

The total current passing through the rod can be expressed as

$$I = 2\pi\sigma \int_0^a E(\rho, k)\rho \, d\rho. \tag{B.2}$$

Using equation (B.1), gives

$$I = \frac{2\pi\sigma \, E_0(k)}{J_0(ka)} \int_0^a J_0(k\rho)\rho \, d\rho = \frac{2\pi\sigma \, aE_0(k)}{kJ_0(ka)} J_1(ka). \tag{B.3}$$

Hence the surface electric field is related to the total current by

$$E_0(k) = \frac{kIJ_0(ka)}{2\pi\sigma \, aJ_1(ka)}. \tag{B.4}$$

Letting l be the length measured along the rod between the two contact points of the voltage electrodes, the potential difference between these points is given by

$$V = E_0 l = \frac{klIJ_0(ka)}{2\pi\sigma \, aJ_1(ka)}. \tag{B.5}$$

The measured voltage includes a contribution from the electromotive force (emf) induced in the voltage measurement circuit due to changing of magnetic flux linking this circuit. Expressing the induced emf in terms of the self inductance L, the total voltage sensed across a length l of the rod is

$$V_T = \frac{klIJ_0(ka)}{2\pi\sigma \, aJ_1(ka)} + j\omega L, \tag{B.6}$$

where L is found from experimental data by fitting predictions of equation (B.6) to the high frequency ACPD measurements. Equation (B.6) can also be used to estimate both the conductivity and permeability of a homogeneous rod from multi-frequency measurements of potential drop.

A straightforward generalization of the above theory has been developed for a rod with a single homogeneous layer in order to predict ACPD measurements on case hardened rods and to fit the layer model parameters using experimental data.

Experimental results

The conductivity of a non-hardened steel rod, 40 cm long and 11 mm in diameter, measured at low frequency using ACPD, see Table 1, was found to be $\sigma = 3.90$ MS/m. By fitting

theoretical predictions [1] to impedance measurements made with an encircling coil, the relative permeability of the rod was found to be 70. The impedance data were acquired with an impedance analyzer having a low frequency measurement limit of 40 Hz. Note that the fitted theoretical curve, Figure B.2, determine using the permeability as a free parameter, did not precisely match the eddy current coil resistance measurements at low frequencies. This is due to the error in subtracting a substantial DC coil resistance which was subject to thermal drift.

Table B.1 Conductivity of a soft steel rod determine using the four-point alternating current measuring system shown in figure B.1

	Conductivity	
Frequency (Hz)	MS/m	% IACS
0.05	3.902	6.727
0.10	3.901	6.725
0.50	3.900	6.724

It is assumed that the process of case hardening does not change the material properties below the case hardened layer. Based on this assumption, the low frequency (less than 1 Hz) ACPD measurements on homogeneous non-hardened rods are used to fix the substrate conductivity, σ_1. Mono-static eddy current measurements on the same rods are used to determine the substrate relative permeability, μ_{r1}. Thus, the substrate properties are given by $\sigma_1 = 3.90$ MS/m and $\mu_{r1} = 70$.

As a check on the relative permeability estimate of the non-hardened rod, ACPD measurements were made in the frequency range up to 3 kHz and the ACPD predictions of the above theory fitted to the data by varying the relative permeability. The optimum fit was obtained with the relative permeability of 63.9. This is in reasonable agreement with the value of 70 obtained using mono-static eddy current data.

Finally, ACPD measurements in the frequency range 1 Hz to 3 kHz were made on a case hardened steel rod. With the substrate properties held fixed, the electrical conductivity, permeability and depth of the layer were varied to find an optimum least squares fit of ACPD model predictions to measurements. As a result of this fitting process, a layer conductivity

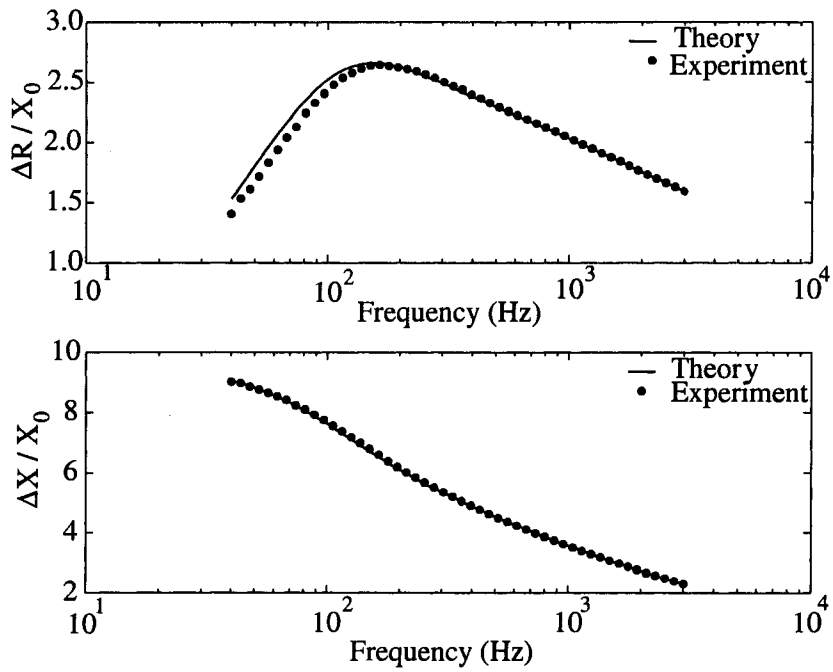

Figure B.2 Comparison between theory and experiment for eddy-current impedance measurements on a non-hardened steel rod with conductivity $\sigma = 3.9$ MS/m determined from ACPD measurements and relative permeability 70 determined by fitting the impedance data using a theoretical model [1]. Note that change in resistance ΔR and reactance ΔX of the coil due to the rod is plotted in normalized form by dividing by the free space reactance of the coil X_0.

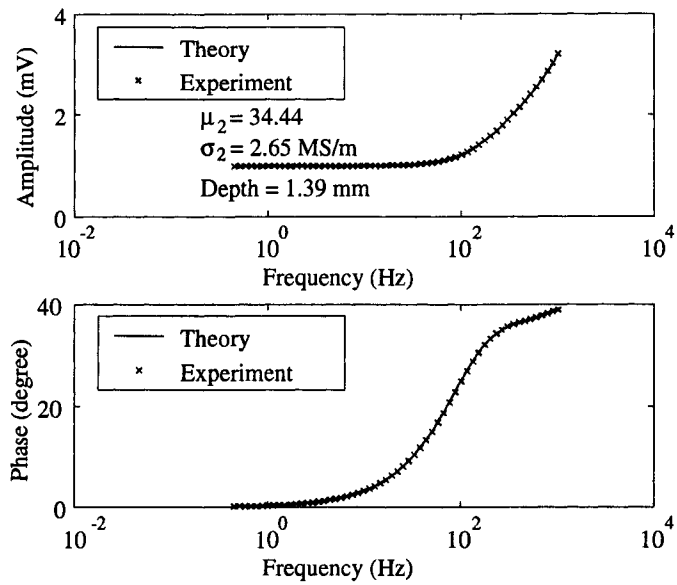

Figure B.3 Comparison between a theoretical fit using an ACPD model of a layered rod and ACPD measurements on a case hardened steel rod. The search for the layer parameters μ_{r2} and σ_2 and the layer depth was carried out with a conductivity and permeability of the substrate fixed: $\sigma_1 = 3.9$ MS/m and $\mu_{r1} = 70$.

$\sigma_2 = 2.65$ MS/m was found, the estimated layer permeability was $\mu_{r2} = 34$ and the layer depth was estimated to be 1.39 mm. The correspondence between experiment and the theoretic fit is shown in Figure B.3. Measurements of the hardness profile with depth showed that the transition region was roughly between 1 and 1.5 mm and therefore the case depth could be specified as approximately in the middle of this range at 1.25 mm.

Conclusion

The depth of a case-hardened layer on a steel rods has been estimated from ACPD measurements, having first establish the substrate material properties by making separate measurements on non-hardened rods using both low frequency ACPD and eddy currents. The case depth estimate is in reasonable agreement with the value found from measurements of the hardness profile. However, further work is required to establish the reliability of the approach.

The basic difficulty with parameter fitting is that the problem of finding an optimum result may be ill-posed. This difficulty manifests itself when large parameter error arises from relatively small measurements errors. In improving the model based approach it will be beneficial to carry out an analysis of the parameter errors.

Acknowledgement

This work was supported by the NSF Industry/University Cooperative Research Program at the Center for nondestructive Evaluation, Iowa State University.

Bibliography

[1] Dodd, C. V. and Deeds, W. E., J. Appl. Phys. **39**, 2829 (1968).

APPENDIX C. ALTERNATING CURRENT POTENTIAL DROP ON A CONDUCTING ROD AND ITS USE FOR EVALUATION OF CASE HARDENED STEEL RODS

A paper to be submitted to the Journal of Applied Physics

Haiyan Sun Yongqiang Huang John R. Bowler

Iowa State University, Center for Nondestructive Evaluation,

1915 Scholl Road, Ames, IA 50011, USA

Abstract

The case-hardening process modifies the near-surface permeability and conductivity of steel, as can be observed through changes in alternating current potential drop along a steel rod. In this work, a two-layer model is used approximating the case hardened rod as a homogeneous substrate with a single, uniformly thick, homogeneous surface layer, in which the conductivity and permeability values differ from those in the substrate. Analytical expressions showing the relationship between the alternating current potential drop along a homogeneous rod or a case hardened steel rod and its electrical and magnetic properties are provided. Potential drop measurements are performed on both homogeneous and case hardened steel rods over multi-frequency. By fitting model results to the experimental data, estimates of case depth and electromagnetic material properties are found. Case depth found by ACPD measurements are in reasonable agreement with the values obtained from hardness profile.

Introduction

Case hardening of steel components improves the resistance to wear by changing the carbon content and micro-structure of the surface region. In order to examine the results of case hardening and quantify the effect on components nondestructively, a number of methods have been developed [2–6]. These methods usually require an extensive calibration procedure using samples of known properties. Here an alternative approach, alternating current potential drop (ACPD) method, is presented in which the near surface material properties and the depth of penetration of the surface treatment is assessed using a model based approach. ACPD method and similarly, alternating current field measurement(ACFM), have already gained wide acceptance in crack measurements [7–12].

The case-hardening process produces a change in the electrical conductivity and magnetic permeability of the steel in the near surface region. Consequently, the electrical conductivity and magnetic permeability have different values near the surface compared with the substrate values. In this paper, the following assumptions are used. First, it is assumed that the conductivity and permeability variation with depth is indicative of the hardness profile allowing the case depth to be estimated from electromagnetic measurements. Second, cylindrical rod specimens are modelled as uniform in the axial direction having a homogeneous substrate surrounded by a homogeneous surface layer of uniform thickness. The transition zone between the two layers is neglected since it is very sharp (see Figure C.4). Third, it is assumed the process of case hardening does not modify the material properties below the case hardened layer. In other words, the conductivity and permeability of the substrate layer of a case hardened steel rod is the same as that of a non-hardened steel rod. Under these idealizations, the material properties can be evaluated by comparing alternating current potential drop (ACPD) measurements with theoretical prediction by adjusting the model parameters until their least-mean-square(LMS) errors are minimized. There are five unknown parameters in this model: the substrate conductivity σ_1 and relative permeability μ_{r1}, the surface conductivity σ_2 and relative permeability μ_{r2} and the surface layer depth (case depth) d. They are determined separately in two steps. The substrate layer conductivity and permeability are found from

non-hardened steel rod measurements. The surface layer conductivity, permeability and its layer depth are then estimated from case hardened steel rod measurements.

In this paper, analytical expressions for alternating current potential drop along a homogenous cylindrical rod and case hardened rod are derived. Then experimental results are given and material parameters are estimated based on the ACPD models and multi-frequency measurements.

Alternating current potential drop (ACPD) theory on conducting cylindrical rods

ACPD on a homogenous cylindrical rod

Suppose an alternating current is applied along an infinitely long cylindrical rod with a radius a. The current varies sinusoidally with time as the real part of $e^{\jmath\omega t}$.

The electromagnetic field inside the rod is governed by Maxwell's equations, which in the quasi-static limit,i.e., in the limit of negligible displacement current, can be written as:

$$\nabla \times \mathbf{H} = \mathbf{J} \tag{C.1}$$

$$\nabla \times \mathbf{E} = -\frac{\partial \mathbf{B}}{\partial t} \tag{C.2}$$

In addition Ohm's Law can be written as

$$\mathbf{J} = \sigma \mathbf{E} \tag{C.3}$$

It is assumed that there exist linear isotropic constitutive relations $\mathbf{D} = \epsilon\mathbf{E}$, $\mathbf{B} = \mu\mathbf{H}$. In these equations, ϵ,μ and σ are the permittivity, magnetic permeability and electrical conductivity of the metal rod. Equations (C.1),(C.2) and (C.3) can be used to give the following equation for $\mathbf{E}$

$$\nabla \times \nabla \times \mathbf{E} = -\mu\sigma\frac{\partial \mathbf{E}}{\partial t} \tag{C.4}$$

Note $\nabla \times \nabla \times \mathbf{E} = \nabla(\nabla \cdot \mathbf{E} - \nabla^2\mathbf{E})$. Since there's no free charges in the rod, $\nabla \cdot \mathbf{E} = 0$. Using the fact that $\mathbf{E}$ varies with time t as $e^{\jmath\omega t}$, (C.4) can be written as

$$\nabla^2\mathbf{E} = \jmath\omega\mu\sigma\mathbf{E} = -k^2\mathbf{E} \tag{C.5}$$

where $k^2 = -\jmath\omega\mu\sigma$, $k = (1-\jmath)/\delta$ and δ is the electromagnetic skin depth defined as $\delta = \sqrt{2/\omega\mu\sigma}$. Due to symmetry of the rod, $\mathbf{E}$ is a function of radial coordinate ρ only. Putting $\mathbf{E} = \hat{z}E(\rho, k)$, equation (C.5) gives

$$\frac{\partial^2 E}{\partial \rho^2} + \frac{1}{\rho}\frac{\partial E}{\partial \rho} + k^2 E = 0, \tag{C.6}$$

This is a modified form of the equation for the zeroth order Bessel function. On applying the boundary condition on the rod surface that $E = E_0$ where $\rho = a$, equation(C.6) has the following solution as:

$$E(\rho, k) = E_0 J_0(k\rho)/J_0(ka). \tag{C.7}$$

The total current passing through the rod can be expressed as

$$I = 2\pi\sigma \int_0^a E(\rho, k)\rho \, d\rho. \tag{C.8}$$

Using equation (C.7) and the following integration [1],

$$\int_0^a J_0(k\rho)\rho \, d\rho = \frac{a}{k} J_1(ka) \tag{C.9}$$

Equation (C.8) gives

$$I = \frac{2\pi\sigma \, aE_0}{kJ_0(ka)} J_1(ka). \tag{C.10}$$

Hence the surface electric field is related to the total current by

$$E_0(k) = \frac{kIJ_0(ka)}{2\pi\sigma \, aJ_1(ka)}. \tag{C.11}$$

Letting l be the length measured along the rod between the two contact points of the voltage electrodes(see Figure C.1), the potential drop between these two points is given by

$$V(k) = E_0(k)l = \frac{klIJ_0(ka)}{2\pi\sigma \, aJ_1(ka)}. \tag{C.12}$$

The measured voltage includes a contribution from the electromotive force(emf) induced in the voltage measurement circuit due to changing of magnetic flux linking this circuit. Express the induced emf in terms of the self inductance L, the total voltage, V_T, sensed across a length l of the rod is

$$V_T = \frac{klIJ_0(ka)}{2\pi\sigma \, aJ_1(ka)} + \jmath\omega LI. \tag{C.13}$$

The rod impedance is defined as

$$Z_{rod} = \frac{klJ_0(ka)}{2\pi\sigma\, aJ_1(ka)} + j\omega L. \tag{C.14}$$

Equation (C.14) can be used to estimate material properties of a homogeneous rod from multi-frequency potential drop measurements.

ACPD on a case hardened steel rod

A case hardened steel rod with radius of b has a conductivity of σ_1 and permeability of μ_1 in its inner core where $\rho \leq a$. In its outer layer where $a \leq \rho \leq b$, the conductivity and permeability are σ_2 and μ_2 respectively. Using a cylindrical polar coordinate system, put the axis of the rod in z direction, the coordinates of ρ and ϕ can be defined consequently.

When applying an alternating current down the axis of the case hardened steel rod (z direction), the electric field intensity in the rod should be governed by equations similar to (C.5), with different conductivity and permeability for the two regions:

$$\nabla^2\mathbf{E_1} = -k_1^2\mathbf{E_1} \qquad (0 \leq \rho \leq a) \tag{C.15}$$

$$\nabla^2\mathbf{E_2} = -k_2^2\mathbf{E_2} \qquad (a \leq \rho \leq b), \tag{C.16}$$

where k_1,k_2 satisfy $k_i^2 = -j\omega\mu_i\sigma_i$ for $i = 1, 2$. Note that the direction of $\mathbf{E_1}$ and $\mathbf{E_2}$ are both in the z direction. The solution to equation (C.15) can be borrowed from equation (C.7),

$$E_1(\rho, k) = E_0 A J_0(k_1\rho). \tag{C.17}$$

Because Bessel function $Y_0(k_2\rho)$ goes to infinity while ρ goes to zero, it's not included in the solution (C.17). But it should be added to give the solution to the equation (C.16) in the surface layer:

$$E_2(\rho, k) = E_0[BJ_0(k_2\rho) + CY_0(k_2\rho)]. \tag{C.18}$$

Note that A, B, C above are scaling factors to be determined by the following boundary conditions.

First, assuming the electric field intensity on the rod surface is E_0, i.e. $E_2 = E_0$ when $\rho = b$, gives

$$BJ_0(k_2b) + CY_0(k_2b) = 1. \tag{C.19}$$

Next, the tangential part of electric fields are continuous on $\rho = a$,so,

$$BJ_0(k_2a) + CY_0(k_2a) = AJ_0(k_1a). \tag{C.20}$$

Third, from

$$\nabla \times \mathbf{E} = -\frac{\partial E}{\partial \rho}\hat{\phi} \tag{C.21}$$

and

$$\nabla \times \mathbf{E} = -\jmath\omega\mu H_\phi\hat{\phi} \tag{C.22}$$

and the fact that the tangential part of magnetic field intensity is continuous at $\rho = a$, one can get

$$\frac{1}{\mu_1}\frac{\partial E_1}{\partial \rho} = \frac{1}{\mu_2}\frac{\partial E_2}{\partial \rho}. \tag{C.23}$$

From (C.17) and (C.18),

$$\frac{\partial E_1}{\partial \rho} = -E_0Ak_1J_1(k_1\rho) \tag{C.24}$$

and

$$\frac{\partial E_2}{\partial \rho} = -E_0k_2[BJ_1(k_2\rho) + CY_1(k_2\rho)], \tag{C.25}$$

thus the third condition is given by,

$$A\mu_2k_1J_1(k_1a) = B\mu_1k_2J_1(k_2a) + C\mu_1k_2Y_1(k_2a) \tag{C.26}$$

The scaling factors A, B, C can now be obtained from equations (C.19), (C.20),and (C.26) where

$$A = \Delta_A/\Delta, \qquad B = \Delta_B/\Delta, \qquad C = \Delta_C/\Delta. \tag{C.27}$$

$$\Delta_A = E_0\mu_1k_2[J_1(k_2a)Y_0(k_2a) - Y_1(k_2a)J_0(k_2a)] \tag{C.28}$$

$$\Delta_B = -E_0\mu_1k_2Y_1(k_2a)J_0(k_1a) + E_0\mu_2k_1J_1(k_1a)Y_0(k_2a) \tag{C.29}$$

$$\Delta_C = -E_0\mu_2k_1J_1(k_1a)J_0(k_2a) + E_0\mu_1k_2J_0(k_1a)J_1(k_2a) \tag{C.30}$$

$$\begin{aligned}\Delta &= -\mu_1 k_2 J_0(k_1 a) J_0(k_2 b) Y_1(k_2 a) - \mu_2 k_1 J_1(k_1 a) J_0(k_2 a) Y_0(k_2 b) \\ &\quad + \mu_2 k_1 J_1(k_1 a) J_0(k_2 b) Y_0(k_2 a) + \mu_1 k_2 J_1(k_2 a) Y_0(k_2 b) J_0(k_1 a) \qquad \text{(C.31)} \\ &= J_0(K_2 b)\Delta_B + Y_0(k_2 b)\Delta_C \qquad \text{(C.32)}\end{aligned}$$

Once the scaling factors A, B, and C are known, the electric field density inside the rod is also known from equations (C.17) and (C.18). Then the potential drop can be derived as follows. The current along the rod can be written as:

$$I = 2\pi\sigma_1 \int_0^a E_1(\rho)\rho\, d\rho + 2\pi\sigma_2 \int_a^b E_2(\rho)\rho\, d\rho \qquad \text{(C.33)}$$

By applying equations (C.17) and (C.18), (C.33) becomes

$$\frac{I}{E_0} = 2\pi\sigma_1 A \int_0^a J_0(k_1\rho)\rho\, d\rho + 2\pi\sigma_2 B \int_a^b J_0(k_2\rho)\rho\, d\rho + 2\pi\sigma_2 C \int_a^b Y_0(k_2\rho)\rho\, d\rho \qquad \text{(C.34)}$$

Use the result of the following integration [1],

$$\int_0^a x Y_0(x) dx = a Y_1(a) + \frac{2}{\pi} \qquad \text{(C.35)}$$

one can easily get

$$\int_0^a Y_0(k\rho)\rho\, d\rho = \frac{a Y_1(ka)}{k} + \frac{2}{k^2\pi}. \qquad \text{(C.36)}$$

After integration, equation (C.34) becomes

$$\frac{I}{E_0} = 2\pi\sigma_1 A a J_1(k_1 a)/k_1 + 2\pi\sigma_2 B[bJ_1(k_2 b) - aJ_1(k_2 a)]/k_2 + 2\pi\sigma_2 C[bY_1(k_2 b) - aY_1(k_2 a)]/k_2. \qquad \text{(C.37)}$$

Rearrange the above equation to give the electric field intensity on the surface of the rod:

$$E_0 = \frac{I}{2\pi\sigma_1 A a J_1(k_1 a)/k_1 + 2\pi\sigma_2 B[bJ_1(k_2 b) - aJ_1(k_2 a)]/k_2 + 2\pi\sigma_2 C[bY_1(k_2 b) - aY_1(k_2 a)]/k_2}. \qquad \text{(C.38)}$$

Thus the potential drop including emf is

$$V_T = E_0 l + j\omega L I \qquad \text{(C.39)}$$

where l is the length measured along the rod between the two contact points, and L is the self inductance of the measurement circuit. The rod impedance is defined as

$$Z_{rod} = \frac{E_0 l}{I} + j\omega L \qquad \text{(C.40)}$$

Experimental arrangement and results

ACPD measurement system

A Kepco bipolar operational power supply/amplifier, driven by the internal function generator of a SR830 DSP lock-in amplifier, is used to inject constant AC sinusoidal current into the cylindrical rod. The current is injected into the rod through copper loops which are kept tight contact with the rod surface. A high precision resistor is connected in serial with the rest of the circuit to detect the current by measuring the voltage (V_{res}) across it using the lock-in amplifier. To measure the potential drop along the cylindrical rod (V_{rod}), two GSS-8-7-G probes from Interconnect Devices Inc. are kept point contact with the rod surface. The distance between the two probes is l. The two probes are connected to the lock-in amplifier by very thin copper wire (0.13mm in diameter). To minimize the self inductance in the voltage measurement circuit, the two copper wires are twisted together and are kept as close to the rod surface as possible. Since both V_{res} and V_{rod} are measured by one lock-in amplifier, an electrical switch is added to switch between the two signals. ACPD measurements are taken in the frequency range of 1 Hz to 10 KHz. A control program is developed to control the lock-in amplifier and the electrical switch and acquire multi-frequency data automatically. Six cylindrical rod specimens are measured by the ACPD system: 1 copper rod, 1 non-hardened steel rod and 4 case hardened steel rods. Their dimensions are shown in Table C.1.

Cylindrical copper rod

The accuracy of the ACPD system is test by taking multi-frequency measurements on a pure copper rod with a known conductivity of 58MS/m or 100% IACS. Since the relative permeability of copper is 1, experimental data and equation (C.13) are used to fit the conductivity σ of the rod and self inductance L in the circuit. Results are shown in Figure C.2. The fit values are $\sigma = 58.4$MS/m or 100.70% IACS and L = 3.20nH. It is clear that the system is accurate within 2% and the self inductance in the measurement is very small.

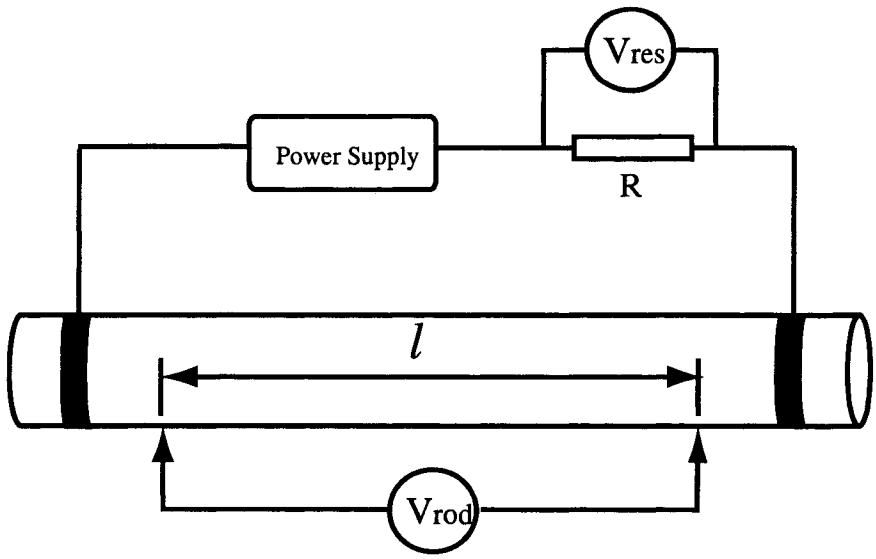

Figure C.1 Schematic diagram of the four-point ACPD measurement system.

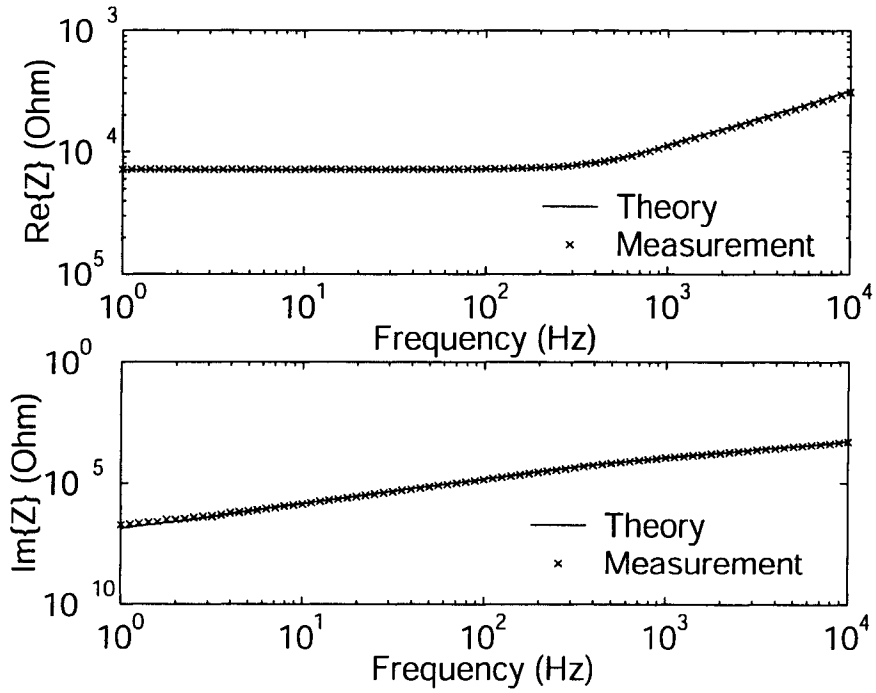

Figure C.2 Comparison between theory and the ACPD measurements on a copper rod with conductivity of 58.4MS/m.

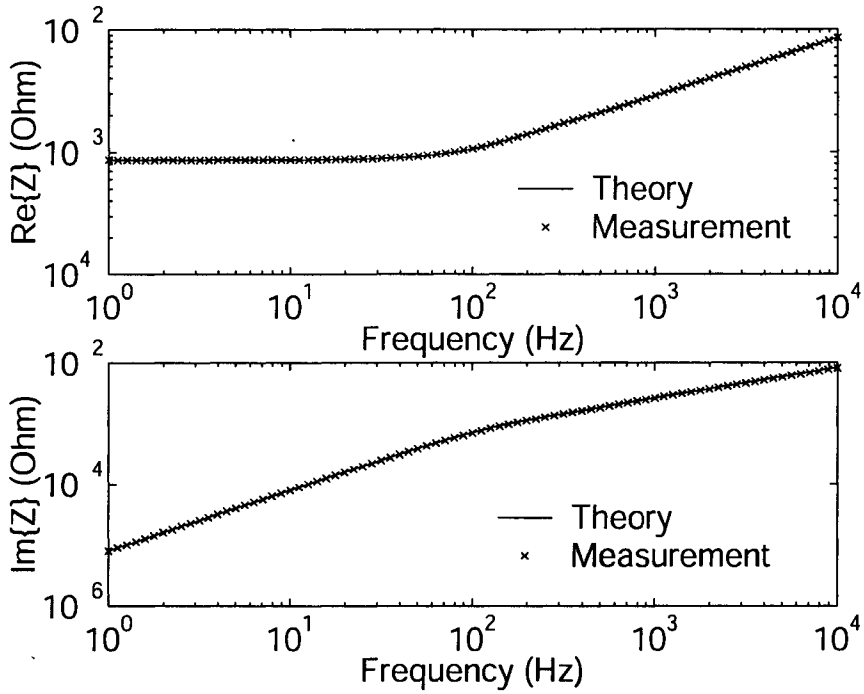

Figure C.3 Comparison between theory and the ACPD measurements on a homogeneous steel rod with $\sigma = 4.84$MS/m and $\mu_r = 70$ determined by data fitting between multi-frequency ACPD data and theoretical model.

Homogenous non-hardened cylindrical steel rod

The non-hardened cylindrical steel rod is assumed to be homogenous. Its conductivity and relative permeability are estimated by fitting the experimental data with theoretical model using equation (C.14). Self inductance L can vary in each measurement. Since it appears as a pure imaginary part in equation (C.14), to reduce error, only real part of the data are used to fit σ and μ_r. To give data in different frequencies the equal weight, the measured rod impedance is normalized by the theoretical rod impedance from the fitted parameters. Results are shown in Figure C.3. Fitted values are $\sigma = 4.84$MS/m, $\mu_{\mathrm{r}} = 64.2$.

Case hardened cylindrical steel rod

Four 1045 carbon steel rods from McMaster-Carr are heat treated by inductance hardening. They have a nominal case depth of 0.5mm, 1.0mm, 1.5mm, and 2.0mm respectively. Their hardness profile, shown in Figure C.4, is obtained through hardness measurements. The effective case depth is determined from the hardness profile. Consider the hardness range of the whole steel rod, one hardness number is selected to calculate the effective case depth. For the 1045 carbon steel that is used in this experiment, effective case depths are defined from surface to the 50 HRC point (shown in Figure C.4). Since this definition is different from the case depth defined in the ACPD model, it is acceptable that the ACPD measurement will give a different values for the case depth.

For the case hardened steel rods, it is assumed that substrate conductivity σ_1 and relative permeability μ_{r1} of the case hardened rod are the same as the non-hardened homogenous steel rod. Thus $\sigma_1 = 4.84$MS/m and $\mu_{r1} = 64.2$. ACPD measurements are taken on the case hardened steel rods to estimate the electrical conductivity σ_2, permeability μ_2 and case depth d of the outer layer by fitting experimental data to ACPD model using equation (C.14) and (C.40). Measured impedance data are normalized as $Z_n = Z/Z_0$ where Z is the measured data, and Z_0 is the theoretical rod impedance calculated using the σ and μ of the non-hardened steel rod and dimension of the case hardened steel rods. Again, only real part of the data are used for fitting. Fitted values are shown in Table C.2. Figures are in Figure C.5 and Figure C.6. The effective case depths d_e obtained from hardness profile are also shown. Reasonable agreement is observed between the case depth evaluated from ACPD measurements and the effective case depth from hardness profile.

Conclusion

The ACPD theory for cylindrical rod is developed for both homogenous and layered rod. By fitting experimental data with the theoretical model, material electromagnetic properties can be found. ACPD measurement system is set up and its accuracy is verified to be accurate within 2%. ACPD measurements are taken on a copper rod, a homogeneous non-hardened steel

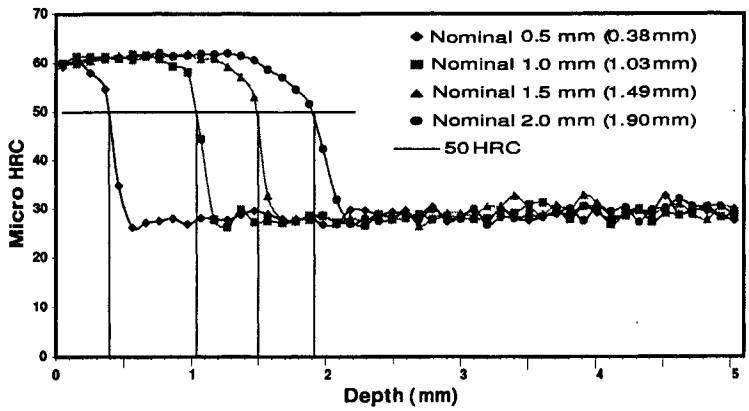

Figure C.4 Hardness profile of the four case hardened steel rods.

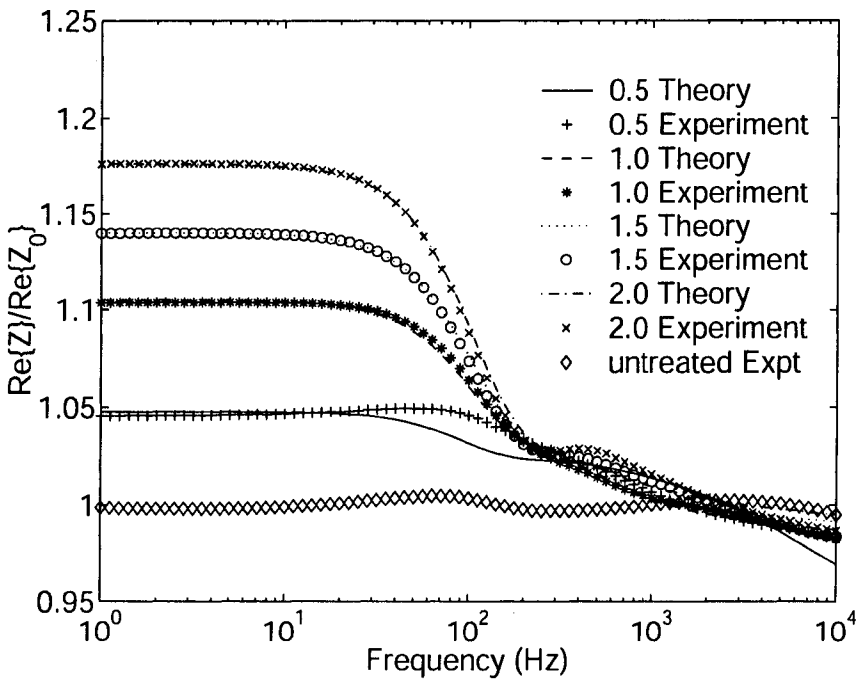

Figure C.5 Real part of experimental data and theoretical fit curve for case hardened steel rods. Numbers in the legend are the nominal case depth in mm.

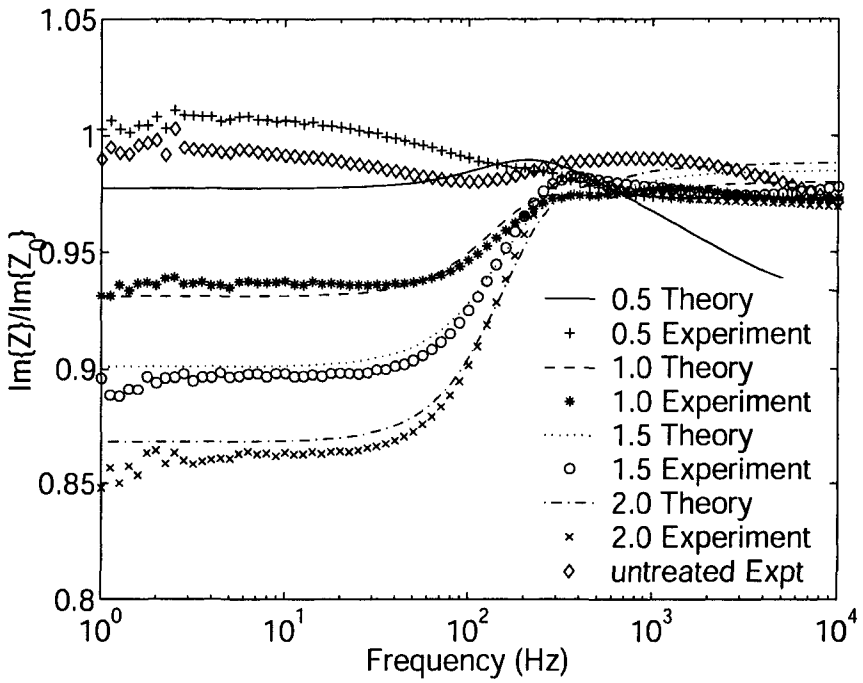

Figure C.6 Imaginary part of experimental data and theoretical curve fit by using real part of experimental data for case hardened steel rods. Numbers in the legend are the nominal case depth in mm.

Table C.1 Measured dimensions of six cylindrical rods. The last four rows are for case hardened steel rods with nominal case depth of 0.5mm, 1.0mm, 1.5mm and 2.0mm respectively.

Rod Specimens	Length (cm)	Diameter (mm)
Copper rod	50.9	11.06
untreated rod	50.3	11.02
nominal case depth 0.5mm rod	50.2	11.00
nominal case depth 1.0mm rod	50.3	11.02
nominal case depth 1.5mm rod	50.2	11.02
nominal case depth 2.0mm rod	50.1	11.02

Table C.2 Surface layer parameters found by data fitting between ACPD measurements and theoretical models. Their substrate parameters are fixed at $\sigma_1 = 4.84\text{MS/m}, \mu_{r1} = 64.2$. Effective case depth d_e is obtained from the hardness profile in Figure C.4.

Rod Specimens	μ_2	σ_2(Ms/m)	d(mm)	d_e(mm)
nominal case depth 0.5mm rod	37.1	3.14	0.37	0.38
nominal case depth 1.0mm rod	50.0	3.92	1.62	1.03
nominal case depth 1.5mm rod	50.6	3.93	2.27	1.49
nominal case depth 2.0mm rod	50.7	3.90	2.92	1.90

rod and four case hardened rods. Conductivity, permeability, and case depth are evaluated by fitting multi-frequency ACPD measurements with the theoretical model. The estimated case depth using this method is in reasonable agreement with the effective case depth obtained from hardness profile.

Bibliography

[1] Abramowitz, M., A. Stegun, I. A., *Handbook of Mathematical Functions With Formulas, Graphs, and Mathematical Tables* (1970)

[2] Mihaa, T., Obata, M., Carburized case depth estimation by Rayleigh-wave backscattering, *Materials Evaluation, 49*(6), 696–700, 1991

[3] Addison, R. C., Safaeinili, A., McKie, A. D. W., Ultrasonic determination of case depth and surface hardness in axles,*Nondestructive Characterization of Materials VIII*, Plenum publishing corp., 211–216, 1998

[4] Good, M., Schuster, G., Skorpik, J., Ultrasonic material hardness depth measurement, United States patent 5646351, 1997

[5] Dubois, M., Fiset, M., Evaluation of case depth on steels by Barkhausen noise measurement, *Materials Science and Technology,11*(3), 264–267, 1995

[6] Vaidyanathan, S., Moorthy, V., Jayakumar, T., Raj, B., Evaluation of induction hardened case depth through microstructural characterization using magnetic Barkhausen emission technique, *Materials Science and Technology,16*(2),202–208,2000

[7] Dover, W. D., Charlesworth, F. D., Tayler, K. A., Collins, R., and Michael, D. H.,The use of AC Field Measurements to Determine the Shape and Size of a Crack in a Metal, *ASTM Special Technical Publication 722*, American Society for Testing and Materials, 401–427, 1981

[8] Venkatasubramanian, T. V., Unvala, B. A., AC potential drop system for monitoring crack length, *Journal of physics E: scientific instruments*, *17*(9), 765–771, 1984

[9] Taylor, H., Kilpatrick, I. M., Jolley, G., Developments in AC potential drop crack sizing, *British Journal of nondestructive testing*, *27*(2), 88–90, 1985

[10] Frise, P. R., Bell, R., Improved probe array for ACPD crack measurements, *British journal of nondestructive testing*, *34*(1), 15–19, 1992

[11] Dai, Y., Marchand, N. J., Hongoh, M., Fatigue crack growth measurements in TMF testing of titanium alloys using an ACPD technique, *ASTM Special Technical Publication 1251*, American Society for Testing and materials, 17–32, 1995

[12] Tiku, S., Marchand, N. J., Unvala, B., An advanced multiple frequency ACPD system for crack detection and calibration, *ASTM Special Technical Publication 1318*, American Society for Testing and materials, 56–70, 1997

BIBLIOGRAPHY

[1] Methods of Measuring Case Depth, J423 (revised 1983), *SAE Handbook*, **1**, Society of Automotive Engineers, 1990

[2] ASM committee on gas carburizing, *Carburizing and Carbonitriding*, American Society for Metals, Metals Park, Ohio, 1977

[3] Klaren, C. M., Nelson J., Methods of Measuring Case Depth, *ASM Handbook*, **4**, Heating Treating, 451–461, ASM International, American Society for Metals, 1991

[4] Low, S. R., Rockwell Hardness Measurement of Metallic Materials. Special Publication 960-5. National Institute of Standards and Technology, 2001

[5] ASTM E 18, *Standard Test Methods for Rockwell Hardness and Rockwell Superficial Hardness of Metallic Materials*, West Conshohocken, PA, American Society for Testing and Materials 2000.

[6] Yee, R. and Lambert, S. B., A Reversing Direct Current Potential Drop System for Detecting and Sizing Fatigue Cracks along Weld Toes, *Journal of Testing and Evaluation*, **23** (4), 254–260, 1995

[7] Luukkonen, P. and Ericson, T., Robust Direct Current Potential Drop Method to Inspect Cold Pressed Green Bodies, *Powder Metallurgy*, **46** (4), 329–334, 2003

[8] ZUIDEMA, J. and KANAAR, M., Crack Closure Measurement Using a Pulsed Direct Current Potential Drop Method, *Proceedings of the Fifth International Conference on Fatigue and Fatigue Thresholds in the International Fatigue Series*, Montreal, Quebec, Canada, May 1993

[9] Matelect Products Main, DMC-2 DC Crack Growth Monitor, *www.matelect.com*, http://www.matelect.com/products_dcm2.html, 2003. (Last access date: June 12, 2004)

[10] Dover, W. D., Collins, R., Michael, D. H., Review of Developments in ACPD and ACFM, *British Journal of Nondestructive Testing*, **33** (3), 121–127, 1991

[11] Topp, D. A., Dover, W. D., Review of ACPD/ACFM Crack Measurement Systems, *Review of Progress in Quantitative Nondestructive Evaluation*, **10**, 301–308, 1991

[12] Dover, W. D., Monahan, C. C., The Measurements of Surface Breaking Cracks by The Electrical Systems ACPD/ACFM, *Fatigue and Fracture of Engineering Materials and Structures*, **17** (12), 1485–1492, 1994

[13] Merah, N., Detecting and Measuring Flaws Using Electric Potential Techniques, *Journal of Quality in Maintenance Engineering*, **9** (2), 160–175, 2003

[14] Raine, A., Cost Benefit Applications using the Alternating Current Field Measurement Inspection Technique. *Proceedings of 8th European Conference on Non-Destructive Testing*, Barcelona, Spain, June 2002

[15] Dover, W. D., Charlesworth, F. D., Tayler, K. A., Collins, R., and Michael, D. H., The Use of AC Field Measurements to Determine The Shape and Size of a Crack in a Metal, *ASTM Special Technical Publication*, **722**, American Society for Testing and Materials, 401–427, 1981

[16] Venkatasubramanian, T. V., Unvala, B. A., AC Potential Drop System for Monitoring Crack Length, *Journal of Physics E: Scientific Instruments*, **17** (9), 765–771, 1984

[17] Taylor, H., Kilpatrick, I. M., Jolley, G., Developments in AC Potential Drop Crack Sizing, *British Journal of Nondestructive Testing*, **27** (2), 88–90, 1985

[18] Lugg, M. C., Analysis of Sparse Data in ACPD Crack Growth Monitoring, *NDT International*, **21** (3), 153–158, 1988

[19] Livingstone, F., Kilpatrick, I. M., Online Fatigue Crack Growth Monitoring in Externally Pressurised Vessels Using the Alternating Current Potential Drop Technique, *Review of Progress in Quantitative Nondestructive Evaluation*, **7**, 1531–1539, 1988

[20] Lugg, M. C., Data Interpretation in ACPD Crack Inspection, *NDT International*, **22** (3), 149–154, 1989

[21] Collins, R., Michael, D. H., Clark R., Measurement of Crack Depth in a Transition Weld Using ACPD, *Review of Progress in Quantitative Nondestructive Evaluation*, **11**, 545–552, 1992

[22] Okada, H., Zhao, W., Atluri, S. N., A Computational Approach to Determining the Depth of Surface Flaws by the ACPD Technique, *Engineering Fracture Mechanics*, **43** (6), 911–921, 1992

[23] Frise, P. R., Bell, R., Improved Probe Array for ACPD Crack Measurements, *British Journal of Nondestructive Testing*, **34** (1), 15–19, 1992

[24] Dai, Y., Marchand, N. J., Hongoh, M., Fatigue Crack Growth Measurements in TMF Testing of Titanium Alloys Using an ACPD Technique, *ASTM Special Technical Publication*, **1251**, American Society for Testing and Materials, 17–32, 1995

[25] Tiku, S., Marchand, N. J., Unvala, B., An Advanced Multiple Frequency ACPD System for Crack Detection and Calibration, *ASTM Special Technical Publication*, **1318**, American Society for Testing and Materials, 56–70, 1997

[26] Matelect 4 Pin Hand Held ACPD Depth Probe Instruction Manual for MAT-2 Probes, copyright 2000, Version 10, Matelect Limited, London, U. K., 2000

[27] Mihaa, T., Obata, M., Carburized Case Depth Estimation by Rayleigh-wave Backscattering, *Materials Evaluation*, **49** (6), 696–700, 1991

[28] Singh, S., Mitra, R., Leeper, D., Fuquen, R., Ultrasonic Evaluation of Case Depth in Case-carburized Steel Components, *Review of Progress in Quantitative Nondestructive Evaluation*, **15**, 1589–1596, 1995

[29] Addison, R. C., Safaeinili, A., McKie, A. D. W., Ultrasonic Determination of Case Depth and Surface Hardness in Axles, *Nondestructive Characterization of Materials VIII*, Plenum publishing corp., 211–216, 1998

[30] Theiner, W., Kern, R., Stroh, M., Process Integrated Nondestructive Testing of Ground and Case Hardened Parts, *Proceedings of 8th European Conference on Non-Destructive Testing*, Barcelona, Spain, June 2002

[31] Ultrasonic Microstructural Analyzer Measures Case Depth, *Advanced Materials and Process*, **146** (6), 17, 1994

[32] Good, M., Schuster, G., Skorpik, J., Ultrasonic Material Hardness Depth Measurement, United States Patent 5646351, 1997

[33] Ultrasonic Analyzer Measures Case Depth of Hardened Parts, *Advanced Materials and Process*, **157** (6), 26, 2000

[34] Diaz, A., Good, M., Schuster, G., Ace, M., Kautzky, K., Advancements in NDE and Characterization of Metals, *Industrial Heating*, **69** (6), 47–50, 2002

[35] Ultrasonic Microstructural Analyzer (UMA): Breakthrough in Hardness Depth Measurement, *www.sonix.com*, http://www.sonix.com/learning/files/UMA_Breakthrough.pdf, 2003. (Last access date: May 24, 2004)

[36] Blitz, J., Electrical and Magnetic Methods of Nondestructive Testing, *Adam Hilger*, 1991

[37] Dubois, M., Fiset, M., Evaluation of Case Depth on Steels by Barkhausen Noise Measurement, *Materials Science and Technology*, **11** (3), 264–267, 1995

[38] Cao,H., Johnson,M. J., Fung, S., Jiles,D. C., Improved Measurements of Case Depth by the Application of Signal Processing Algorithms to Barkhausen Effect Data, *Review of Progress in Quantitative Nondestructive Evaluation*, **18**, 1725–1731, 1999

[39] Vaidyanathan, S., Moorthy, V., Jayakumar, T., Raj, B., Evaluation of Induction Hardened Case Depth Through Microstructural Characterisation Using Magnetic Barkhausen Emission Technique, *Materials Science and Technology*, **16** (2), 202–208, 2000

[40] Ruecker, D., Klein, K., Computer Aided Quality Sorting by Electromagnetic Methods, *International Committee on Nondestructive Testing*, 1787–1790, 1985

[41] Grotz, K., Steidinger, R., Magneto-inductive Materials Testing. An Effective Method of Quality Control in Production, *Wire*, **34** (3), 203–208, 1991

[42] Magneto Testing, Nondestructive Magneto-inductive Testing Instruments, *www.foerstergroup.com*, http://www.foerstergroup.com/eddycurrent/magnatest.html, 2003. (Last access date: May 24, 2004)

[43] Bowler, J. R., Review of Eddy Current Inversion with Application to Nondestructive Evaluation, *International Journal of Applied Electromagnetics and Mechanics*, **8** (1), 3–16, 1997

[44] Auld, B. A., Moulder, J. C., Review of Advances in Quantitative Eddy Current Nondestructive Evaluation, *Journal of Nondestructive Evaluation*, **18** (1), 3–36, 1999

[45] Sophian, A., Tian, G. Y., Taylor, D., Rudlin, J., Electromagnetic and Eddy Current NDT: a Review, *Insight Nondestructive Testing and Condition Monitoring*, **43** (5), 302–306, 2001

[46] Stephan, C. H., Chesney, H. L., Computer Aided Measurement of Case Depth and Surface Hardness in Automobile Axle Shafts, *Materials Evaluation*, **42** (13), 1612–1618, 1984

[47] McMaster, R. C., McIntire, P., Mester, M. L. (Editors), *Automotive Applications of Eddy Current Testing*, Nondestructive Testing Handbook, 2nd edition, Volume 4, Electromagnetic Tesing, 424–426, American Society of Nondestructive Tesing, 1986

[48] Palanisamy, R., Jackson, K. E., Eddy Current Sizing of Case Depth in Bearing Components, *Nondestructive Characterization of Metals Conference II*, Plenum Press, 363–372, 1987

[49] Keely, W. A., Check It Out: Using Eddy Current Profiling to Evaluate Part Quality, *Stamping Journal*, **11** (3), 22–27, 1999

[50] Theiner, W. A., Kern, R., Graus, M., Process Integrated Nondestructive Testing for Evaluation of Hardness, Case Depth and Grinding Defects, *Advanced Sensors for Metals Processing*, Canadian Institute of Mining, Metallurgy and Petroleum, 159–171, 1999

[51] Ricci, R. J., Pulses Electromagnetics for NDT of Heat Treated Components, *Heat Treating Progress*, **3** (6), 76–82, 2003

[52] Ricci, R. J., Pulsed Electromagnetics for Nondestructive Evaluation of Hardness and Case Depth in Heat Treating Operations, *Proceedings of The First ASM International Surface Engineering and the 13th IFHTSE Congress*, 250–257, 2003

[53] Verimet 7700, Verimet N7700/7710 Portable Eddy Current Test, *www.kjlaw.com*, http://www.kjlaw.com/verimet_7700-7710.htm, 2003. (Last access date: May 24, 2004)

[54] Nondestructive Testing and Inspection Equipment (NDT/NDE), Changing the Way You Inspect Metals and Metal Parts, *www.smarteddy.com*, http://www.smarteddy.com/benefits.html, 2003. (Last access date: May 24, 2004)

[55] Hub and Spindle, Just-in-time Zetec Hub and Spindle Inspection Systems Catch Defects Before They Cost You a Bundle, *www.zetec.com*, http://www.zetec.com/documents/hubspindle(3).pdf, 2003. (Last access date: May 24, 2004)

[56] Eddy Current Inspection, *www.milinc.com*, http://www.milinc.com/nondes.htm, 2003. (Last access date: May 24, 2004)

[57] Sun, H., Bowler, J. R., Bowler, N., Johnson, M. J., Eddy Current Measurements on Case Hardened Steel, *Review of Progress in Quantitative Nondestructive Evaluation*, **21**, 1561–1568, 2002

[58] Bowler, J. R., Huang, Y., Sun, H., Johnson, M. J., Evaluation of Case Hardened Steel Rods Using Eddy Current and Alternating Current Potential Drop Measurements, *Electromagnetic Nondestructive Evaluation*, **VII**, IOS Press. 2003

[59] Private communication with Dr. Douglas Rebinsky, Team Leader, Nondestructive Evaluation Advanced Materials Technology, Caterpillar Inc., Peoria, Illinois, USA. 2002–2004.

[60] Private communication with Haiyan Sun, Center for Nondestructive Evaluation, Iowa State University, Ames, Iowa, USA. 2002–2004

[61] Lampman, S. R., Zorc, T. B., Daquila, J. L. and Ronke, A. W. (Editors), *ASM Handbook*, revised version, Volume 4, Heat Treating, ASM International, 1991

[62] Dodd, C. V., Cheng, C. C. and Deeds, W. E., Induction Coils Coaxial with an Arbitrary Number of Cylindrical Conductors, *Journal of Applied Physics*, **45** (2), 638–647. 1974

[63] Dodd, C. V. and Deeds, W. E., Analytical Solutions to Eddy Current Probe Coil Problems. *Journal of Applied Physics*, **39** (6), 2829–2838. 1968

[64] Private communication with Dr. Marcus Johnson, Center for Nondestructive Evaluation, Iowa State University, Ames, Iowa, USA. 2002–2004

[65] Bowler, N., Analytical Solution for the Electric Field in a Half Space Conductor due to Alternating Current Injected at the Surface, *Journal of Applied Physics*, **95** (1), 344–348. 2004

[66] Bowler, J. R. and Theodoulidis, T. P., Eddy Currents Induced in a Conducting Rod of Finite Length by a Coaxial Encircling Coil. To be published. 2004

ACKNOWLEDGEMENTS

I would like to take this opportunity to express my sincere appreciation to those who encouraged and helped me with continual enthusiasm to complete this graduate study.

I would like to express my sincere gratitude to my major professor, Dr. John Bowler, for his guidance, patience and support throughout this research and the writing of this dissertation. His insights and words of encouragement have often inspired me and renewed my hopes for completing my graduate education.

I would like to thank Dr. Nicola Bowler and Dr. Marcus Johnson for many invaluable instructions and discussion during this research.

I would like to thank other committee members, Dr. Douglas Jacobson, Dr. Ronald Roberts and Dr. Jiming Song, for their willingness to serve in the committee and their valuable time and help to my research and dissertation work.

I would like to thank Haiyan Sun for many discussion and her work at the very beginning stage on this project. I would like to thank Shaun Lindsay, Fangwei Fu, Waqar Habib, Sanyi Zhan, Brent Eaton, Raza Ali in my research group for their help and they made the research work more enjoyable.

Finally I would like to thank my beloved family and so many friends for encouragement and help.

This work was supported by the NSF Industry/University Cooperative Research program.